Introduction

Although interference is intrinsically a classical-wave phenomenon, the superposition principle which underlies interference is at the heart of quantum physics. Feynman referred to interference as really "the only mystery" of quantum physics [FLS63]. Clearly interference confronts us with some basic questions of the interpretation of quantum physics. Despite its long history, going back to Thomas Young at the beginning of the 19th century, quantum optical interference still challenges our understanding. With the development of experimental techniques for fast and sensitive measurements of light, it has become possible to carry out many of the gedankenexperiments whose interpretations were widely debated in the course of the development of quantum physics [Whe84, SD82, SEW91, Per00]. The present thesis contains the experimental realization of three different gedankenexperiments: *a non-local quantum eraser*, *two-photon Hong-Ou-Mandel interference under Einstein locality conditions* and *delayed-choice entanglement swapping*.

The purpose of this thesis is to experimentally demonstrate some of the counter-intuitive features of quantum physics via various quantum phenomena. They dramatically underscore the different conceptions of space and time between classical and quantum physics. Such eyebrow-raising features of space and time in quantum physics have been described "as one of the most intriguing effects in quantum mechanics" [AZ05].

The "spooky action at a distance" (in Einstein's words) of an entangled system is illustrated in a striking way by Scully *et al.*'s quantum eraser [SD82, SEW91], in which one can choose whether or not to erase which-path information of one particle by performing suitable measurements on another particle entangled with it. Since quantum mechanics is indifferent to the spatial and temporal order of measurements on entangled particles, this choice can be arbitrarily delayed and spatially separated with respect to the interfering event of the first particle (see Chapter 3).

Wheeler illustrated the complementarity principle with single-photon interference in a delayed-choice gedankenexperiment [Whe84]. In contrast with single-photon interference (second-order interference), which has a classical analogue, two-photon Hong-Ou-Mandel (HOM) interference (fourth-order interference) stems from the bosonic nature of the photons and the unitary transformation of a beam splitter. As stressed by Mandel "this prediction has no classical analogue, and its confirmation would represent an interesting test of the quantum theory of the electromagnetic field" [Man83, Man99]. The realization of the two-photon HOM interference experiment under Einstein locality conditions (i.e. the relevant events are relativistically space-like separated) significantly extends Wheeler's delayed-choice gedankenexperiment's concept (see 4.2).

In quantum physics, present events can affect how we interpret the data obtained in the past. This phenomenon is illustrated in Peres' delayed-choice entanglement-swapping gedankenexperiment [Per00], where one chooses whether or not to entangle two particles after they have been detected and don't even exist anymore. The results show that the temporal order of the choice and the measurement events in such an experiment is irrelevant, as predicted by quantum physics (see 4.3).

The important features of the experiments presented in this thesis are: (1) High-speed electro-optical modulators controlled by a quantum random number generator, which together allow us to implement fast and random measurements of the photons. (2) The spatial and temporal relations of various events, which may be illustrated in space-time diagrams, are appropriately arranged to show non-classical and counter-intuitive features of quantum physics.

Xiao-song Ma, May 14th, 2010

Outline

This thesis is organized in the following way: In Chapter 1, I introduce a number of basic concepts and definitions. Although such an introduction can also be found in other works or even in textbooks, I would like to present them for completeness and as a reference of this thesis.

Wheeler's ingenious design of a delayed-choice gedankenexperiment elegantly illustrates the "spooky" nature of quantum physics. Naturally, it has drawn the attentions of other physicists and there have been a number of extensions of theoretical proposals (including the delayed-choice quantum eraser and delayed-choice entanglement swapping) and experimental demonstrations. In Chapter 2 I will review a selection of prior works, which directly relate to this thesis. On one hand, this should provide an introduction to the concept of delayed-choice and the motivation for my work. On the other hand, it is intended to differentiate the earlier demonstrations from the work presented in this thesis.

In Chapter 3, I report an experimental realization of a non-local quantum eraser. Firstly, the notion of hybrid entanglement is introduced and I show an experimental demonstration of hybrid entanglement between the polarization of a photon and the path of its twin. Then, by using this hybrid entanglement, we realize a non-local quantum eraser under Einstein locality conditions (i.e. under relativistic space-like separation) through an optical fibre link of 50 m and a free-space link of 144 km. We show that the decision whether or not to erase which-path information is decided by the space-like separated complementary polarization measurements of its *distant* twin photon. Moreover, a complementarity inequality is measured and fitted well the predictions of quantum mechanics even under Einstein locality conditions. Strictly guaranteeing the locality condition, our experiment represents the first conclusive demonstration of the quantum eraser concept.

A high-speed tunable beam splitter, whose reflectivity can be tuned from 0 to 1 rapidly, is employed in the experiments of two-photon Hong-Ou-Mandel

interference under Einstein locality conditions and delayed-choice entanglement swapping. We design, implement and characterize such a high-speed tunable beam splitter, as shown in Section 4.1. Using it and appropriate arrangements of spatial and temporal separations of the relevant events, we realize the two-photon HOM interference experiment under Einstein locality conditions, as shown in Section 4.2.

In Section 4.3, I report an ideal realization of Peres' delayed-choice entanglement-swapping gedankenexperiment, where two independent photons are first measured, and after the measurements we create entanglement between them via entanglement swapping with a high-speed bipartite state analyzer, which is adapted from the above mentioned tunable beam splitter. The choice between creating entanglement or not is made by a quantum random number generator, and the choice event is delayed until after the measurements.

The conclusion of and outlook for the presented work is given in Chapter 5.

In Chapter A.1 of the appendix, I discuss spontaneous parametric down conversion in detail. This includes the properties of the nonlinear crystal, phase matching conditions and walk-off compensation. Detailed information about the electro-optical modulators is presented in Chapter A.2 of the appendix.

Contents

1. The basics of quantum optics and quantum information.

In this chapter, I introduce the basic terminology used within this thesis and give a short overview of the relevant principles of quantum optics and quantum information. I begin by introducing the qubit and the superposition principle associated to it. One of the most counter-intuitive phenomena in quantum physics, wave-particle duality, will be described as an example of the complementarity principle. Then, entanglement between two particles and Bell's inequality will be introduced. At last, I discuss several quantum communication protocols, including quantum state teleportation and entanglement swapping. An excellent overview of quantum information and quantum computation is given in Ref. [NC00].

1.1. Qubits, superposition, wave-particle duality and complementarity.

1.1.1. Qubits and superposition

The classical bit, the fundamental element of classical computation, is defined to be either 0 or 1. A quantum bit or *qubit*, is the quantum analogue of the classical bit. However, unlike a classical bit, a qubit can be in a superposition of the states of $|0\rangle$ and $|1\rangle$, where the states $|0\rangle$ and $|1\rangle$ are the computational basis states and form an orthonormal basis. The state of a qubit can be represented as a vector

in a two-dimensional *Hilbert space* and any normalized linear combination of them is, according to the superposition principle, a valid pure quantum state. This superposition, $|Q\rangle$, can be written as:

$$|Q\rangle = \alpha|0\rangle + \beta|1\rangle, \tag{1.1}$$

where α, β are complex numbers and $|\alpha|^2 + |\beta|^2 = 1$. When we measure a qubit in its computational basis, we obtain a probabilistic result, either '0' or '1', with the probabilities of $|\alpha|^2$ and $|\beta|^2$ respectively. This is different from the measurement of a classical pure bit, where the outcome is deterministic.

The qubit $|Q\rangle$ has been realized physically utilizing different degrees of freedom (DOF) of many different particles and systems. For instance, qubits can be encoded in the internal energy states of a single atom, or the spin directions of an electron in a quantum dot. In this thesis, I mainly focus on qubits encoded in the polarization and path DOF of photons. For a polarization qubit, I assign

$$\begin{aligned} |0\rangle &= |H\rangle \\ |1\rangle &= |V\rangle, \end{aligned} \tag{1.2}$$

where $|H\rangle$ and $|V\rangle$ are quantum states of photons with horizontal and vertical polarizations respectively. Therefore, a polarization-encoded qubit $|Q\rangle$ can be represented as:

$$|Q\rangle = \alpha|0\rangle + \beta|1\rangle = \alpha|H\rangle + \beta|V\rangle. \tag{1.3}$$

The Hilbert space of one qubit can be represented graphically by the so-called Bloch sphere. There is a one-to-one mapping between the Bloch sphere and the Poincaré sphere, which is widely used in polarimetry. A pure qubit state may be rewritten as:

$$|Q\rangle = \cos\frac{\theta}{2}|H\rangle + e^{i\varphi}\sin\frac{\theta}{2}|V\rangle, \tag{1.4}$$

where θ and φ are the angles of the three-dimensional polar coordinate system shown in Figure 1.1. In Table 1.1, I list the mapping from the qubit states to

polarization states and their Jones matrix representations.

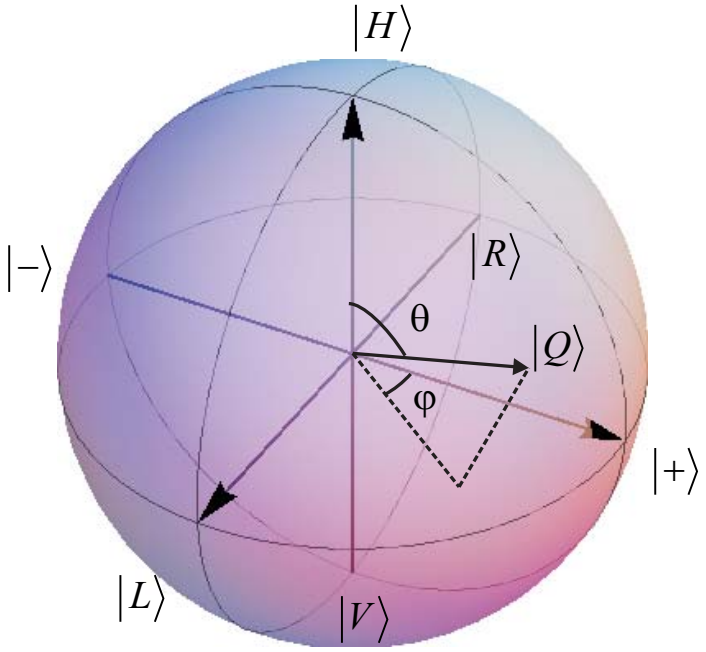

Figure 1.1.: Bloch sphere of a polarization qubit. A pure qubit state, as in Equation 1.4, is a point on the surface of the Bloch sphere. $|H\rangle$ and $|V\rangle$ lie on the poles of the sphere while $|+\rangle$ and $|-\rangle$, and $|L\rangle$ and $|R\rangle$ (refer to Table 1.1) are located on the equatorial plane. These states lie on the mutually orthogonal axes. θ and φ uniquely define a point on the surface of the Bloch sphere.

In order to manipulate and measure polarization-encoded qubits, one can use a half-wave plate (HWP), a quarter-wave plate (QWP) and a polarizing beam splitter (PBS). The unitary operation of a HWP oriented along θ can be represented as:

$$\mathrm{U}_{HWP}(\theta) = \begin{pmatrix} -\cos 2\theta & -\sin 2\theta \\ -\sin 2\theta & \cos 2\theta \end{pmatrix}. \tag{1.5}$$

The operation of a QWP oriented along θ can be represented as:

$$\mathrm{U}_{QWP}(\theta) = \begin{pmatrix} 1-(1+i)\cos^2\theta & -(1+i)\sin\theta\cos\theta \\ -(1+i)\sin\theta\cos\theta & 1-(1+i)\sin^2\theta \end{pmatrix}. \tag{1.6}$$

A PBS is a device which transmits horizontally polarized light and reflects

Qubit State	Polarization State	Jones Matrix	Polarization Name
$\|0\rangle$	$\|H\rangle$	$\begin{pmatrix} 1 \\ 0 \end{pmatrix}$	Horizontal Linear
$\|1\rangle$	$\|V\rangle$	$\begin{pmatrix} 0 \\ 1 \end{pmatrix}$	Vertical Linear
$\frac{1}{\sqrt{2}}(\|0\rangle + \|1\rangle)$	$\frac{1}{\sqrt{2}}(\|H\rangle + \|V\rangle) = \|+\rangle$	$\frac{1}{\sqrt{2}}\begin{pmatrix} 1 \\ 1 \end{pmatrix}$	$+45°$ Linear
$\frac{1}{\sqrt{2}}(\|0\rangle - \|1\rangle)$	$\frac{1}{\sqrt{2}}(\|H\rangle - \|V\rangle) = \|-\rangle$	$\frac{1}{\sqrt{2}}\begin{pmatrix} 1 \\ -1 \end{pmatrix}$	$-45°$ Linear
$\frac{1}{\sqrt{2}}(\|0\rangle + i\|1\rangle)$	$\frac{1}{\sqrt{2}}(\|H\rangle + i\|V\rangle) = \|L\rangle$	$\frac{1}{\sqrt{2}}\begin{pmatrix} 1 \\ i \end{pmatrix}$	Left-handed Circular
$\frac{1}{\sqrt{2}}(\|0\rangle - i\|1\rangle)$	$\frac{1}{\sqrt{2}}(\|H\rangle - i\|V\rangle) = \|R\rangle$	$\frac{1}{\sqrt{2}}\begin{pmatrix} 1 \\ -i \end{pmatrix}$	Right-handed Circular

Table 1.1.: A list of some qubit states that correspond to polarization states of photons and their Jones Matrix representation. These states will be used throughout this thesis.

vertically polarized light. The combination of a PBS, a HWP and a QWP is able to measure the polarization state of a photon in an arbitrary basis.

Path or spatial mode of a photon can also be used to encode quantum information when only two possible states exist. This forms a qubit, commonly called a path qubit. A general path qubit can be represented as:

$$|Q\rangle = \alpha|a\rangle + \beta|b\rangle, \tag{1.7}$$

where $|a\rangle$ and $|b\rangle$ are the orthogonal path states. Beam splitters and phase shifters are two essential elements used to manipulate path states. A $50:50$ (BS) beam splitter is equivalent to a Hadamard gate for a path qubit. In general,

the operation of a 50 : 50 BS can be represented as:

$$\begin{aligned} |a\rangle &\xrightarrow{\text{BS}} \frac{|a\rangle + e^{i\chi}|b\rangle}{\sqrt{2}} \\ |b\rangle &\xrightarrow{\text{BS}} \frac{|b\rangle + e^{i(\pi-\chi)}|a\rangle}{\sqrt{2}}, \end{aligned} \tag{1.8}$$

where $\chi = \frac{\pi}{2}$ for a symmetric beam splitter [Zei81]. A phase shifter (PS) on spatial mode $|a\rangle$ can be represented as:

$$\begin{aligned} |a\rangle &\xrightarrow{\text{PS}} e^{i\phi}|a\rangle, \\ |b\rangle &\xrightarrow{\text{PS}} |b\rangle, \end{aligned} \tag{1.9}$$

where ϕ is the amount of the phase shift.

1.1.2. Complementarity and wave-particle duality

Complementarity is one of the fundamental principles of quantum physics. We say that two observables are complementary if precise knowledge of one of them implies that all possible outcomes of measuring the other one are equally probable. Practically speaking, no matter how the system is prepared, there is always a measurement whose outcome is completely unpredictable [SEW91].

One classic example used to illustrate the complementarity principle is the Mach-Zehnder interferometer (MZI) with a single quantum as input. The single quantum propagates through a MZI, which is composed of two beam splitters (BS1 and BS2), two mirrors (M1 and M2), and one phase shifter (PS) on path b'. There are two experimental configurations: with BS2 inserted at the output or without BS2, as shown in Figure 1.2A and B respectively. For the configuration in Figure 1.2A, the state evolution of the single quantum in the MZI can be derived as following:

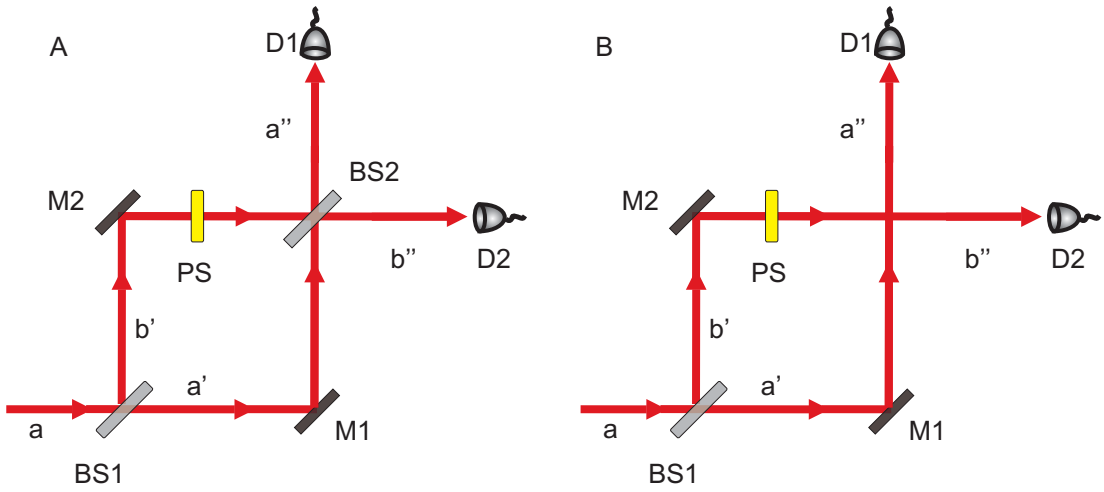

Figure 1.2.: A single quantum propagates through a Mach-Zehnder interferometer, which is composed of two beam splitters (BS1 and BS2), two mirrors (M1 and M2), and one phase shifter (PS) on path b'. With the setup in **A**, one can observe phase-dependent oppositely-modulated sinusoidal interference fringes from the counts detected by D1 and D2. See text for details. This reveals the wave nature of the single quantum. On the contrary, with the setup in **B**, where BS2 is removed, one can obtain phase-independent counts detected by D1 and D2.

$$
\begin{aligned}
|a\rangle \xrightarrow{\text{BS1}} & \frac{1}{\sqrt{2}}(|a'\rangle + i|b'\rangle) \\
\xrightarrow{\text{PS}} & \frac{1}{\sqrt{2}}(|a'\rangle + ie^{i\phi}|b'\rangle) \\
\xrightarrow{\text{BS2}} & \sin\frac{\phi}{2}e^{i(\frac{\pi-\phi}{2})}|a''\rangle + \cos\frac{\phi}{2}e^{\frac{i\phi}{2}}|b''\rangle.
\end{aligned} \tag{1.10}
$$

Therefore, the probabilities of this particle to be detected by D1 placed on path a" and D2 on path b" are respectively:

$$
\begin{aligned}
P(D1) &= \sin^2\frac{\phi}{2} \\
P(D2) &= \cos^2\frac{\phi}{2}.
\end{aligned} \tag{1.11}
$$

These *phase-dependent* oppositely-modulated sinusoidal interference fringes detected by D1 and D2 are the signatures of the wave nature of the single particle. This is because which-path information of the quantum (i.e. the information of through which path the quantum propagates) has been erased, made available by inserting BS2.

For the configuration shown in Figure 1.2B, the state evolution of the single particle can be derived as following:

$$\begin{aligned} |a\rangle &\xrightarrow{\text{BS1}} \frac{1}{\sqrt{2}}(|a'\rangle + i|b'\rangle) \\ &\xrightarrow{\text{PS}} \frac{1}{\sqrt{2}}(|a'\rangle + ie^{i\phi}|b'\rangle). \end{aligned} \tag{1.12}$$

Therefore the probabilities of this particle detected by D1 and D2 in this configuration are respectively:

$$\begin{aligned} P(D1) &= \frac{1}{2} \\ P(D2) &= \frac{1}{2}. \end{aligned} \tag{1.13}$$

These *phase-independent* constant detection probabilities of D1 and D2 are the consequence of revealing which-path information, made available by removing BS2.

Therefore, on one hand, the superposition of two probability amplitudes for different but indistinguishable processes, leads to interference patterns. On the other hand, distinguishability of these processes reduces the interference visibility. Hence, complementary measurements allow us to demonstrate mutually exclusive properties of a single quantum.

These facts have been confirmed by previous experiments with single photons [Cla74, GRA86, BZKW03], neutrons [ZGS+88, Zei99], and even large

molecules [ANVA+99]. I will discuss the details in Chapter 3.

1.2. Entanglement and Bell's inequality.

Entanglement [Sch35] is a unique property of quantum systems, where the quantum state of a *multipartite* system cannot be represented as a product state of individual parts, i.e. the multipartite quantum state cannot be factorized. Physically, this means that the correlations of the overall system are well defined, but the properties of the individual particles are not. This counter-intuitive feature of quantum physics is at the heart of one of the famous debates between Einstein [EPR35] and Bohr [Boh35]. After many years Bell developed the so-called Bell's inequality [Bel64], which shows a quantitative difference between predictions for the correlations of a bipartite entangled state given by quantum physics and by local realistic theories. Two important assumptions of local realistic theories are as follows. (1) Realism: if the outcome of a measurement can be predicted with a probability equal to unity, there must exist a corresponding element of reality. (2) Locality: if two systems no longer interact, no real change can take place in the second system in consequence of anything that may be done to the first system [EPR35, Bel64]. While local realistic theories predict the bound of Bell's inequality to be 2, quantum physics predicts the bound of Bell's inequality to be $2\sqrt{2}$.

Later on, Clauser, Horne, Shimony and Holt derived the CHSH inequality, which is an experimentally realizable version of Bell's inequality [CHSH69]. They also proposed a scheme to test Bell's inequality with polarization-entangled photon pairs. The CHSH inequality has the form of:

$$S = |E(a,b) - E(a,b')| + |E(a',b) + E(a',b')| \leq 2. \tag{1.14}$$

The correlation function $E(a,b)$ of particles 1 and 2 measured with the respec-

tive settings of a and b is defined as:

$$E(a,b) = \frac{C(a,b) + C(a^{\perp},b^{\perp}) - C(a^{\perp},b) - C(a,b^{\perp})}{C(a,b) + C(a^{\perp},b^{\perp}) + C(a^{\perp},b) + C(a,b^{\perp})}, \tag{1.15}$$

where $C(a,b)$, $C(a^{\perp},b^{\perp})$, $C(a^{\perp},b)$, and $C(a,b^{\perp})$ are the coincidence counts of particles 1 and 2 with the respective settings of a and b, $a^{\perp}$ and $b^{\perp}$, $a^{\perp}$ and b, and a and $b^{\perp}$. Note that $a^{\perp}$ and $b^{\perp}$ are the orthogonal settings of a and b, respectively.

I will introduce Bell states and show how a Bell state falsifies local realism via a violation of the CHSH inequality. The four Bell states are:

$$|\Psi^{-}\rangle = \frac{1}{\sqrt{2}}(|01\rangle - |10\rangle), \tag{1.16}$$

$$|\Psi^{+}\rangle = \frac{1}{\sqrt{2}}(|01\rangle + |10\rangle), \tag{1.17}$$

$$|\Phi^{-}\rangle = \frac{1}{\sqrt{2}}(|00\rangle - |11\rangle), \tag{1.18}$$

$$|\Phi^{+}\rangle = \frac{1}{\sqrt{2}}(|00\rangle + |11\rangle). \tag{1.19}$$

Quantum physics predicts the correlation function for the entangled state $|\Psi^{-}\rangle$, shown in Equation 1.17, to be $E(a,b) = -\cos 2(a-b)$. For the settings $a, a' = 0°, 45°$ and $b, b' = 22.5°, 67.5°$, a maximal violation of the CHSH inequality can be obtained as:

$$S = |-cos(-45°) + cos(-135°)| + |-cos(45°) - cos(-45°)| = 2\sqrt{2}. \tag{1.20}$$

Alternatively, if two particles are in $|\Psi^{+}\rangle$, their correlation function is $E(a,b) = -\cos 2(a+b)$. With the same settings of $|\Psi^{-}\rangle$, a maximal violation of the CHSH inequality can also be obtained as:

$$S = |-cos(45°) + cos(135°)| + |-cos(135°) - cos(-135°)| = 2\sqrt{2}. \tag{1.21}$$

Hence the value of S predicted by quantum physics clearly violates the limit of 2, given by local realistic theories.

Many experiments based on polarization-entangled photons have been performed that verified the predictions of quantum physics [FC72, ADR82, WJS+98]. Besides using the polarization of photons, there have been theoretical proposals to test Bell's inequality with other degrees of freedom, e.g. using the momentum [HZ85, HSZ89, ZP88] or the emission time [Fra89] of entangled photon pairs. The experimental violation of Bell's inequality based on the momentum and phase was demonstrated by Rarity and Tapster [RT90], while time-bin entanglement has been employed in fiber-based quantum cryptography and communication [GRTZ02]. In Chapter 3.1.1, I introduce a new type of entanglement, hybrid entanglement, where a pair of photons are entangled in different degrees of freedom.

Practically, there arise some imperfections in the preparation of Bell states. Therefore, the experimentally measured state, ρ, will be different from the expected Bell state, $|\Psi\rangle$. State fidelity, $F(\Psi, \rho)$, is a parameter used to measure the difference between ρ and $|\Psi\rangle$ [JWPZ02]. It is defined as:

$$F(\Psi, \rho) = \langle\Psi|\rho|\Psi\rangle. \tag{1.22}$$

For the singlet $|\Psi^-\rangle$, we assume the experimentally measured state to be: $\rho = V|\Psi^-\rangle\langle\Psi^-| + (1 - V)\hat{I}/4$, where $\hat{I}$ is the identity operator. This state is a Werner state [Wer89] and the white noise degrades the state fidelity. Note that the visibility, V, is defined as $V = (C_{max} - C_{min})/(C_{max} + C_{min})$, where C_{max} and C_{min} are the maximum and minimum coincidence counts. One can thus connect the state fidelity $F(|\Psi^-\rangle, \rho)$ and the visibility V (average of all three mutually unbiased bases) in the following form:

$$F(|\Psi^-\rangle, \rho) = \frac{3}{4}V + \frac{1}{4}. \tag{1.23}$$

One can also connect the state fidelity to the so-called entanglement witness

operator $\mathcal{W}$ via

$$Tr(\rho\mathcal{W}) = \frac{1}{2} - F(|\Psi^-\rangle, \rho). \tag{1.24}$$

When the expectation value of the entanglement witness operator is negative, the measured state is entangled [ZGW+06]. This is a sufficient condition for proving entanglement.

1.3. Quantum communication protocols

1.3.1. No-cloning theorem for qubits

The security of quantum cryptography stems from the so-called no-cloning theorem. It also prevents us from using classical teleportation to faithfully transmit a qubit. The no-cloning theorem, first given by Wooters and Zurek [WZ82], states that a single qubit in an unknown state cannot be copied onto a different qubit while leaving the original qubit undisturbed. To prove the no-cloning theorem, imagine we have a copy machine, which can copy the state of an input qubit to a separate blank qubit without disturbing the original qubit. This operation can be written as:

$$|0\rangle|0\rangle \rightarrow |0\rangle|0\rangle \tag{1.25}$$

$$|1\rangle|0\rangle \rightarrow |1\rangle|1\rangle \tag{1.26}$$

If the input qubit is in a superposition state $\frac{1}{\sqrt{2}}(|0\rangle + |1\rangle)$ then this copy machine will produce the following output because of the linearity of quantum physics:

$$\frac{1}{\sqrt{2}}\Big(|0\rangle + |1\rangle\Big)|0\rangle \rightarrow \frac{1}{\sqrt{2}}\Big(|0\rangle|0\rangle + |1\rangle|1\rangle\Big) \tag{1.27}$$

However, the desired output of a copy machine should rather be:

$$\frac{1}{\sqrt{2}}\Big(|0\rangle + |1\rangle\Big)|0\rangle \;\rightarrow\; \frac{1}{\sqrt{2}}\Big(|0\rangle + |1\rangle\Big)\frac{1}{\sqrt{2}}\Big(|0\rangle + |1\rangle\Big) \tag{1.28}$$

$$= \frac{1}{2}\Big(|0\rangle|0\rangle + |0\rangle|1\rangle + |1\rangle|0\rangle + |1\rangle|1\rangle\Big) \tag{1.29}$$

which is different from expression (1.27). Therefore a quantum cloning machine cannot exist.

1.3.2. Quantum state teleportation and entanglement swapping

Quantum state teleportation (QST) was proposed by Bennett *et al.* in 1993 [BBC+93]. It circumvents the no-cloning theorem and teleports the quantum state of a qubit with a unity fidelity by using an entanglement channel (EPR channel) and a classical channel.

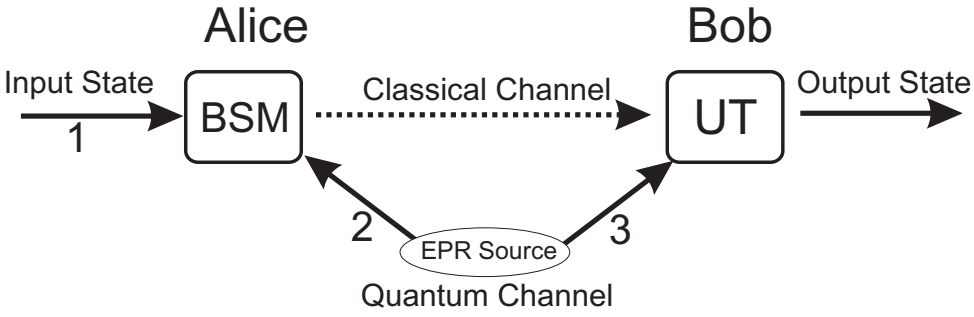

Figure 1.3.: Scheme of quantum state teleportation. The task is to teleport the input state of photon 1 from Alice to Bob by using entangled photons 2 and 3 from a quantum channel, and a classical channel. Alice performs a Bell-state measurement (BSM) on photons 1 and 2 and then sends her result to Bob via the classical channel. Bob can finally convert photon 3 into a perfect copy of photon 1 via a unitary transformation (UT) based on the classical information.

The scheme of quantum state teleportation is shown in Figure 1.3. Alice

wants to teleport an arbitrary and unknown input state,

$$|\chi\rangle_1 = \alpha|0\rangle_1 + \beta|1\rangle_1, \tag{1.30}$$

of photon 1 to Bob. They share a pair of photons, 2 and 3, which are in the maximally entangled state $|\psi^-\rangle_{23}$. This is one of the four Bell states that I introduced earlier. So the overall state of the three photons is:

$$|\Psi\rangle_{123} \;=\; |\chi\rangle_1 \otimes |\psi^-\rangle_{23}. \tag{1.31}$$

The state of the three photons can be written by expressing photons 1 and 2 in the basis of Bell states:

$$\begin{aligned} |\Psi\rangle_{123} &= |\chi\rangle_1 \otimes |\psi^-\rangle_{23} \\ &= \frac{1}{2}\left[|\phi^+\rangle_{12}\left(-\beta|0\rangle_3 + \alpha|1\rangle_3\right) + |\phi^-\rangle_{12}\left(\beta|0\rangle_3 + \alpha|1\rangle_3\right)\right. \\ &\quad \left. + \; |\psi^+\rangle_{12}\left(-\alpha|0\rangle_3 + \beta|1\rangle_3\right) + |\psi^-\rangle_{12}\left(-\alpha|0\rangle_3 - \beta|1\rangle_3\right)\right]. \end{aligned} \tag{1.32}$$

Alice projects photons 1 and 2 into the Bell states basis, i.e. perform a *Bell-state measurement* (BSM) on photons 1 and 2. She then obtains one of the four Bell states, each with equal probability of $\frac{1}{4}$. Depending on which Bell state she obtained, photon 3 will be in one of the following states (according to Equation 1.32):

$$\begin{aligned} |\psi^-\rangle_{12} &\;\Rightarrow\; \alpha|0\rangle_3 + \beta|1\rangle_3 = I_3|\chi\rangle_3 \\ |\psi^+\rangle_{12} &\;\Rightarrow\; \alpha|0\rangle_3 - \beta|1\rangle_3 = \sigma_3^{(z)}|\chi\rangle_3 \\ |\phi^-\rangle_{12} &\;\Rightarrow\; \beta|0\rangle_3 + \alpha|1\rangle_3 = \sigma_3^{(x)}|\chi\rangle_3 \\ |\phi^+\rangle_{12} &\;\Rightarrow\; \beta|0\rangle_3 - \alpha|1\rangle_3 = -i\sigma_3^{(y)}|\chi\rangle_3. \end{aligned} \tag{1.33}$$

Hence the quantum state of photon 3 is equivalent to that of photon 1 up to

one of the four local unitary transformations (UT):

$$I = \begin{pmatrix} 1 & 0 \\ 0 & 1 \end{pmatrix}, \quad \sigma^{(z)} = \begin{pmatrix} 1 & 0 \\ 0 & -1 \end{pmatrix}, \quad \sigma^{(x)} = \begin{pmatrix} 0 & 1 \\ 1 & 0 \end{pmatrix}, \quad -i\sigma^{(y)} = \begin{pmatrix} 0 & -1 \\ 1 & 0 \end{pmatrix}. \tag{1.34}$$

Alice can tell Bob which Bell state she obtained via the classical channel and then Bob can perform one of the four unitary transformations to photon 3. After this correction, Bob receives the identical copy of photon 1, i.e. QST is completed.

One remarkable feature of QST is that the quantum state of the teleported qubit does not have to be well defined. It can be entangled with other particles. An example of this is the so-called entanglement swapping [ZZHE93]. The scheme used for entanglement swapping is shown in Figure 1.4. Suppose that we have two pairs of entangled photons, 1&2 and 3&4, which are produced from two different sources, EPR source I and II. One can establish entanglement between photons 1 and 4 via a BSM on photons 2 and 3, although photons 1 and 4 never interact nor share any common past. The procedure is as follows: Victor performs a BSM on photons 2 and 3 with his Bell-state analyzer. Alice and Bob perform polarization measurements on photons 1 and 4 and send the results to Victor. Victor then divides and sorts Alice's and Bob's results into subsets according to his results of the BSM , and checks each subset for entanglement.

Two polarization-entangled photon pairs of photons 1&2 and 3&4 are generated in the state:

$$|\Psi\rangle_{1234} = |\Psi^-\rangle_{12}|\Psi^-\rangle_{34}, \tag{1.35}$$

Rewriting Equation 1.35 in the basis of Bell states of photons 2 and 3 leads to:

$$|\Psi\rangle_{1234} = \frac{1}{2}(|\Psi^+\rangle_{14}|\Psi^+\rangle_{23} - |\Psi^-\rangle_{14}|\Psi^-\rangle_{23} - |\Phi^+\rangle_{14}|\Phi^+\rangle_{23} + |\Phi^-\rangle_{14}|\Phi^-\rangle_{23}). \tag{1.36}$$

If photons 2 and 3 are projected into the state $|\Phi^-\rangle_{23}$, according to Equa-

tion 1.36, photons 1 and 4 are projected into $|\Phi^-\rangle_{14}$. Hence in this case the entanglement between photons 1 & 2 and photons 3 & 4 can be swapped to photons 2 & 3 and photons 1 & 4, with a probability of 0.25. Refer to Chapter 4 for details of entanglement swapping.

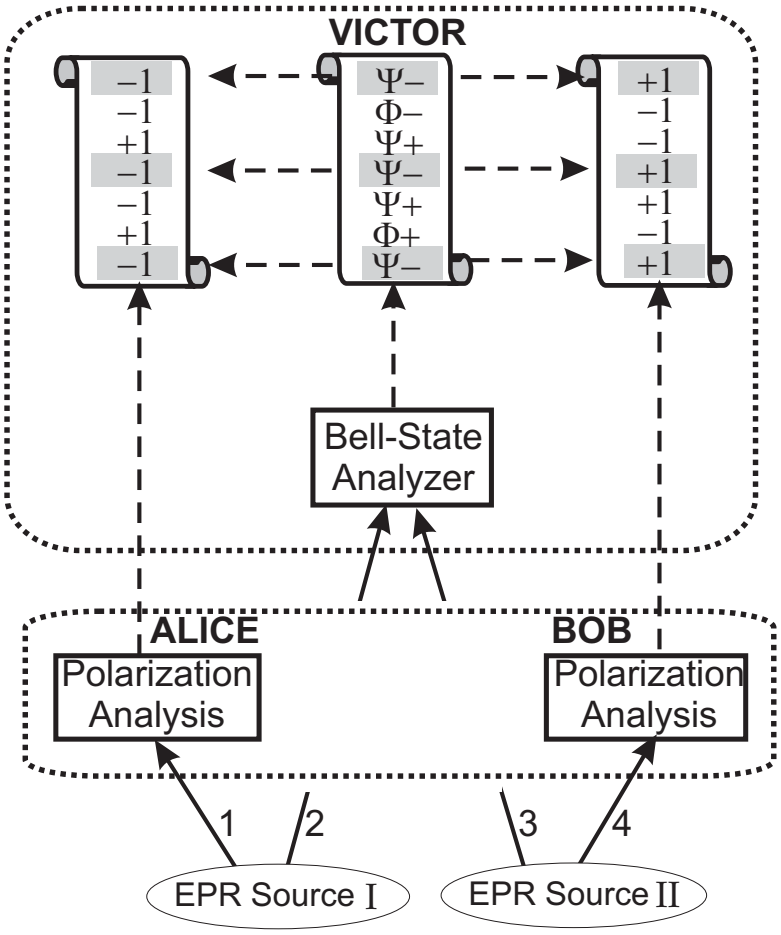

Figure 1.4.: Scheme for entanglement swapping. Two entangled pairs of photons 1&2, and 3&4 are generated from the EPR sources I and II respectively. Photons 2 and 3 are sent to Victor who can project them into a Bell state with his Bell-state analyzer. Alice and Bob perform polarization measurements on photons 1 and 4. They record the results and send them to Victor. Victor then sorts Alice's and Bob's results into subsets according to the results of his BSM, and checks each subset for a violation of Bells inequality. This will show that photons 1 and 4 became entangled although they never interacted in the past. (Figure taken from [JWPZ02].)

2. Delayed-choice gedankenexperiments: theory and previous realizations

In this chapter, I review three kinds of delayed-choice gedankenexperiments, which include the delayed-choice wave-particle duality experiment proposed by Wheeler [Whe84], the delayed-choice quantum eraser proposed by Scully *et al.* [SD82] and the delayed-choice entanglement swapping proposed by Peres [Per00]. Some earlier realizations of these proposals will be summarized.

2.1. Wheeler's delayed-choice gedankenexperiment

Wave-particle duality was one of the themes of the debates between Einstein and Bohr. Until today, it is still under discussion among physicists, as well as philosophers, and many interpretations have been proposed. The Copenhagen interpretation stands out from the others due to its consistency and austerity. One of the essential ideas of the Copenhagen interpretation is that the result of an experiment to test complementarity should depend on the experimental configuration; according to Bohr, rephrased by Wheeler: "No elementary phenomenon is a phenomenon until it is a registered (observed) phenomenon" [Boh28, Whe84].

To translate this into a wave-particle duality experiment, imagine a setup as shown in Figure 2.1A, where we have a Mach-Zehnder interferometer and a single-photon wave packet as input. Depending on the choice made by the observer, different properties of the single-photon wave packet can be demon-

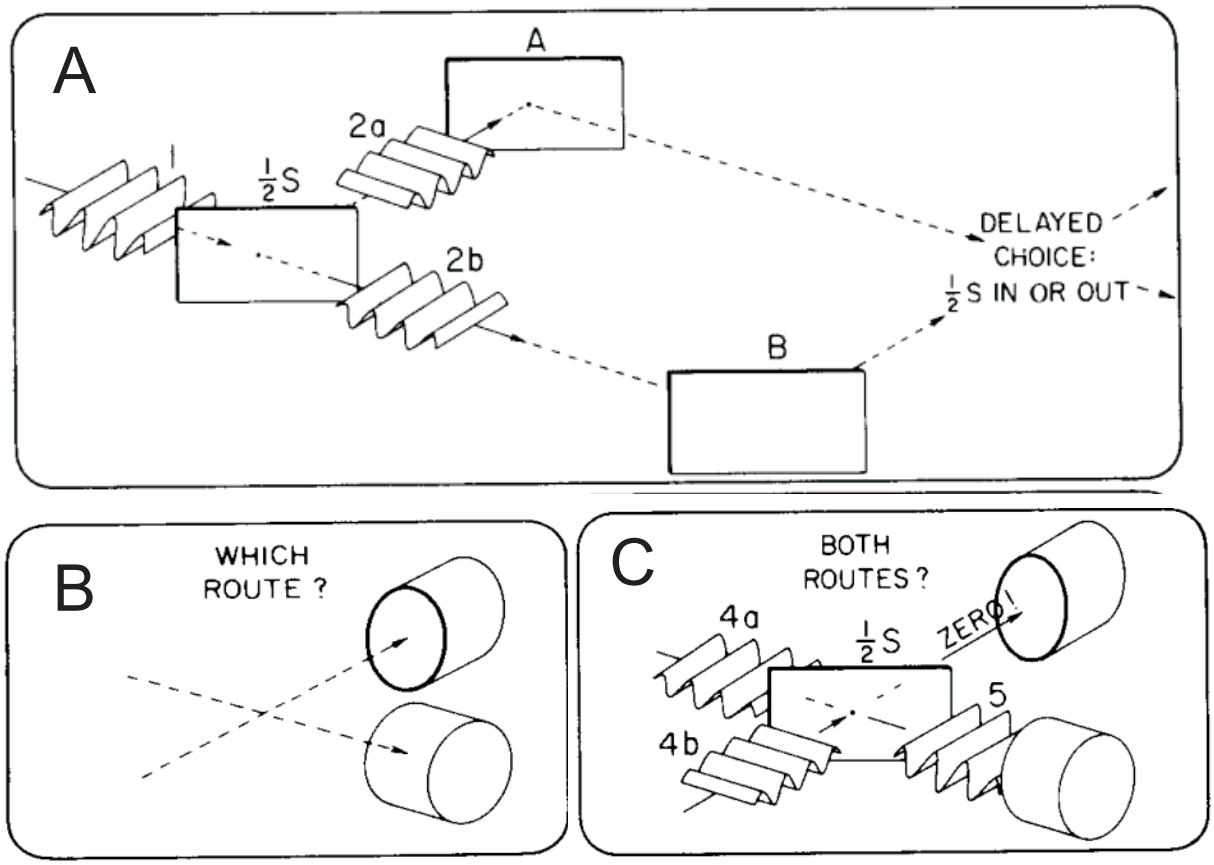

Figure 2.1.: Wheeler's delayed-choice gedankenexperiment with a single photon wave packet in a Mach-Zehnder interferometer. **A**. The output half-silvered mirror ($\frac{1}{2}$s) of the interferometer can be inserted or removed at will. When it is removed, as in **B**, the detectors allow one to determine which path has been followed by the photon. When it is inserted, as in **C**, detection probabilities of the two detectors depend on the length difference between the two arms. When the difference is zero, only one detector will fire. The choice to insert or remove the output half-silvered mirror is made only after the passage of the photon through the input half-silvered mirror, so that the photon entering the interferometer "cannot know" which experimental configuration will be arranged at the output. (Figure taken from p183 of [Whe84].)

strated, as shown in Section 1.1.2. If the observer chooses to demonstrate the particle nature of the single-photon wave packet, he should remove the output half-silvered mirror ($\frac{1}{2}$s), which acts as a beam splitter, as shown in Figure 2.1B. Both detectors will fire with equal probabilities but not at the same time. As

Wheeler pointed out, "[...] one counter goes off, or the other. Thus the photon has traveled only one route" [Whe84].

On the other hand, if the observer chooses to demonstrate the wave nature of the single-photon wave packet, he inserts the output half-silvered mirror ($\frac{1}{2}$s) as shown in Figure 2.1C. In this experimental configuration, only the detector on path 5 will fire and the other detector will never fire, if the path lengths of the interferometer are equal. As Wheeler pointed out, "This is evidence of interference . . . that each arriving light quantum has arrived by both routes" [Whe84]. This shows that whether the single-photon wave packet travels one route or both routes depends on whether the output half-silvered mirror is removed or inserted. This is counter-intuitive as it seems that we could change the propagation history of the single-photon wave packet just by changing the setting of the experimental apparatus.

Furthermore, in order to rule out some naive interpretations of these phenomena, Wheeler proposed a "delayed-choice" version of this experiment, in which the choice of which property will be observed is made after the photon has passed the first beam splitter. "Thus one decides the photon 'shall have come by one route or by both routes' after it has *already done* its travel" [Whe84].

As show in Figure 2.2, in Wheeler's "delayed-choice gedankenexperiment at the cosmological scale" proposal [Whe84], he stated "When night comes and the telescope is at last usable we leave the half-silvered mirror out or put it in, according to our choice [...] we discover 'by which route' it came with one arrangement; or by the other, what the relative phase is of the waves associated with the passage of the photon from source to receptor 'by both routes'–perhaps 50,000 light years apart as they pass the lensing galaxy G-1. But the photon has already *passed* that galaxy billions of years before we made our decision". Given the distance between the quasar and the receptor (billions of light years), the choice can be made long after the light's entry into the interferometer, an extreme case of the delayed-choice gedankenexperiment.

Moreover, inspired by Wheeler's proposals, one could expect that even if the

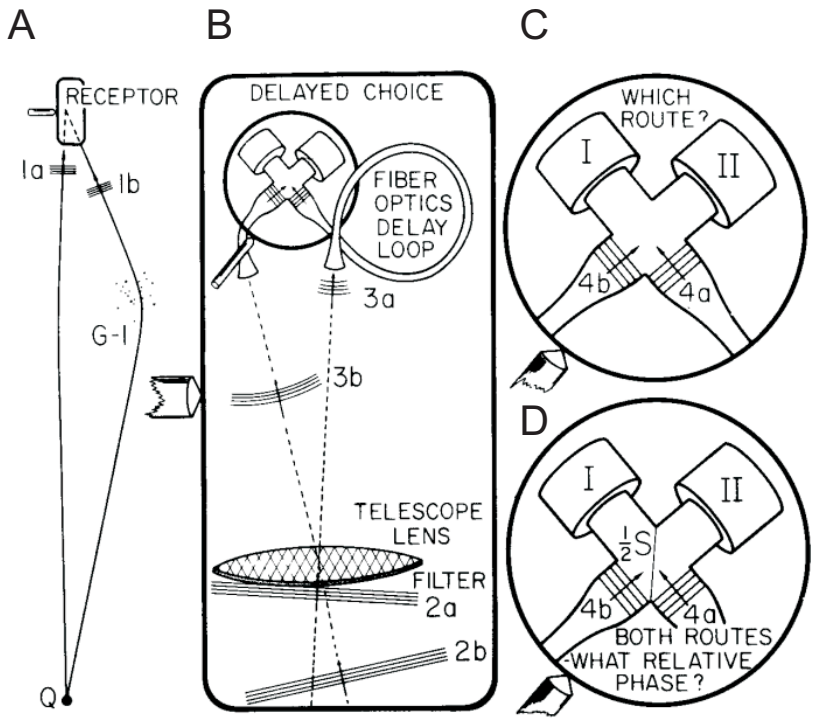

Figure 2.2.: Delayed-choice gedankenexperiment at the cosmological scale. **A**. Due to the gravitational lens action of galaxy G-1, light generated from a quasar has two possible paths to reach the receptor. This mimics the setup in Figure 2.1. **B**. The receptor setup. Filters are used to increase the coherence length of the light and thus allow us to perform the interference experiment. A fiber optics delay loop is used to adjust the phase of the interferometer. **C, D**. The choices to remove or insert the output half-silvered mirror, allow one to measure which route the light traveled or what the relative phase of the two routes was (thus it traveled both routes). Given the distance between the quasar and the receptor (billions of light years), the choice can be made long after the light's entry into the interferometer, an extreme example of the delayed-choice gedanken experiment. (Figure taken from p193 of [Whe84].)

choice is space-like separated from the photon's entry into the interferometer, the same result will be obtained. This shows the fact that the complementarity principle is independent of the space-time arrangement of the above mentioned events.

2.2. Earlier realizations of Wheeler's delayed-choice gedankenexperiment

Following the proposal of Wheeler, there are several experimental demonstrations. In this section, I review three experiments performed with photons.

Hellmuth, Walther, Zajonc, and Schleich

The layout of this delayed-choice experiment is shown in Figure 2.3A [HWZS87]. An attenuated picosecond laser (less than 0.2 photon per pulse) was used as the light source for a Mach-Zehnder interferometer (MZI). Two 5 m (20 ns) glass fibers were used to delay the input photon. The transit time of the photon through the whole interferometer was about 24 ns. The combination of a Pockels cell (PC) and a polarizer (POL) was placed in the upper arm of the MZI as a PC shutter. When a half-wave voltage was applied on the PC, the PC shutter became closed. Hence the photon propagating in the upper arm would be directed out from the MZI and one only obtained the interference pattern if the PC shutter was open when the photon met it. The PC shutter was kept closed when there was no input photon. The photons were detected with two photomultipliers (PM1 and PM2). In Figure 2.3B, the time diagram of the delayed-choice mode is illustrated. In the laboratory reference frame, the input photon meets Beam splitter 1 first and then is kept in the fiber for 20 ns. During the photon propagating in the fiber, the PC shutter opens after 4 ns PC rise time and is kept open until after the photon meets Beam splitter 2. Then the photon exits from the fibers, and meets the opened shutter and Beam splitter 2. Therefore, in this case, opening of PC shutter is delayed until after the input photon meets Beam splitter 1 and is well inside of the interferometer. With this experimental arrangement, the delayed-choice condition was fulfilled because the photon's entry into MZI lies in the past light cone of opening the PC shutter.

In Figure 2.3C, the time diagram of the normal mode is illustrated. In the laboratory reference frame, the PC shutter is open first and is kept open until

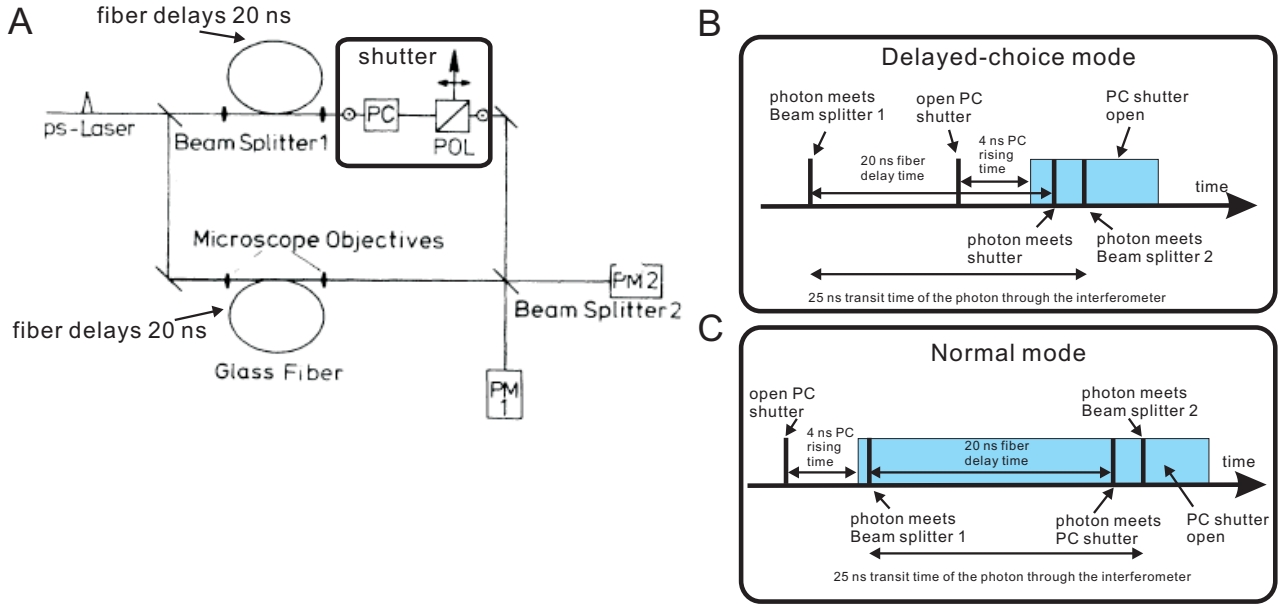

Figure 2.3.: The delayed-choice experiment realized in Walther's group. **A**: The layout of the setup. An attenuated picosecond laser was used as the light source for a Mach-Zehnder interferometer (MZI). Two 5 m "Glass fibers" were used as optical delays (20ns each) for the photon. The transit time of the photon through the whole interferometer was about 24 ns. The combination of a Pockels cell (PC) and a polarizer (POL) was placed in the upper arm of the MZI as a PC shutter. With this configuration, one could only obtain the interference pattern if the PC shutter was open when the photon met it. The photons were detected with two photomultipliers (PM1 and PM2). **B**: Time diagram of the delayed-choice mode. In the laboratory reference frame, the input photon meets Beam splitter 1 first and then is kept in the fiber for 20 ns. During the photon's propagation through the fiber, the PC shutter is open after 4 ns PC rise time and is kept open until after the photon meets Beam splitter 2. Then the photon exits from the fibers, and meets the opened shutter and Beam splitter 2. Therefore, in this case, opening of PC shutter is delayed until after the input photon meets Beam splitter 1 and is well inside of the interferometer. With this experimental arrangement, the delayed-choice condition was fulfilled. **C**: Time diagram of the normal mode. In the laboratory reference frame, the PC shutter is open first and is kept open until after the photon meets Beam splitter 2. Then the input photon meets Beam splitter 1 and is kept in the fiber for 20 ns. Later the photon exits from the fibers, and meets the shutter and Beam splitter 2. Therefore, in this case, opening of PC shutter is earlier than the input photon meeting Beam splitter 1. Hence, contrary to the delayed-choice mode, this experimental configuration corresponds to the normal-choice mode. (Figure **A** taken from [HWZS87].)

after the photon meets Beam splitter 2. Then the input photon meets Beam splitter 1 and is kept in the fiber for 20 ns. Later the photon exits from the fibers, and meets the shutter and then Beam splitter 2. Therefore, in this case, opening of PC shutter is earlier than the input photon meeting Beam splitter 1. Hence, contrary to the delayed-choice mode, this experimental configuration corresponds to the normal-choice mode.

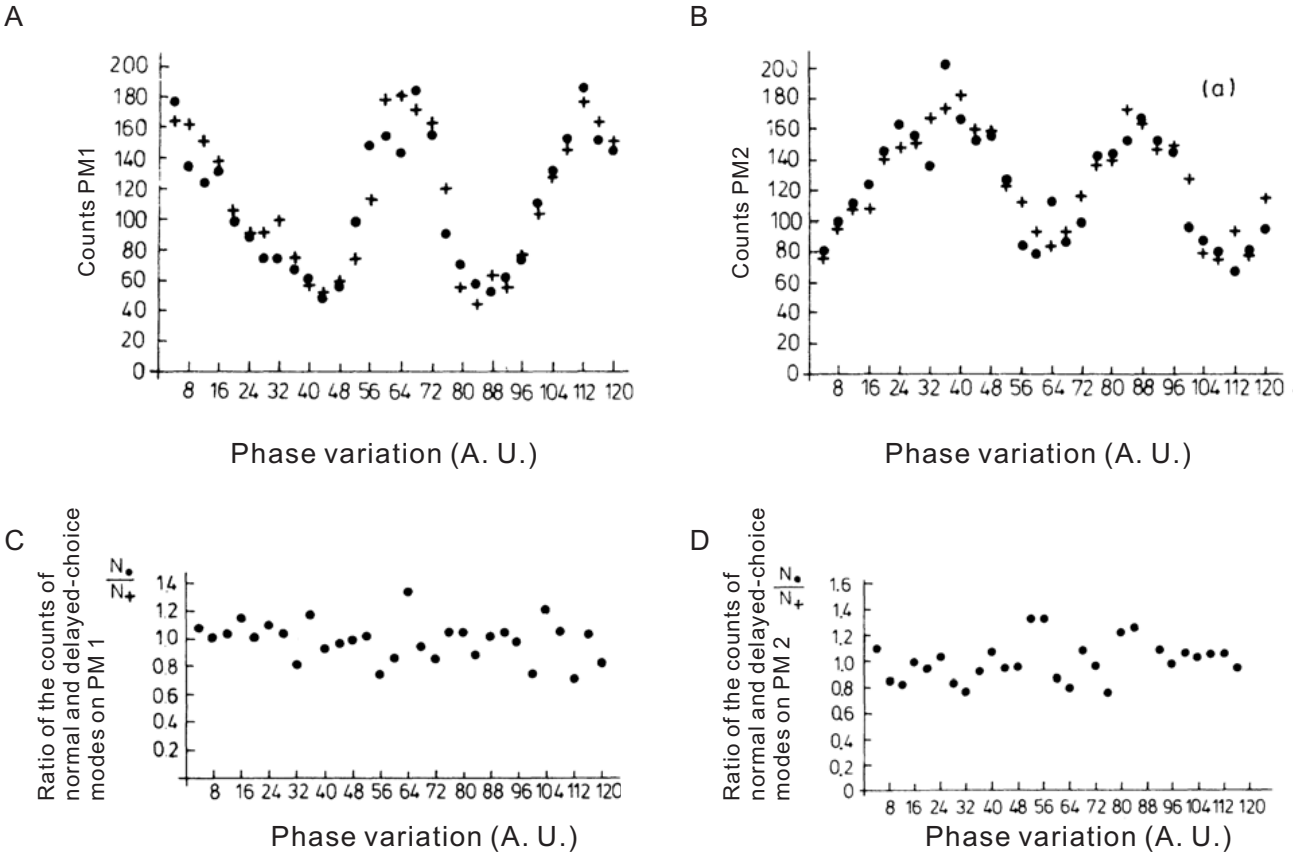

Figure 2.4.: The experimental results of the delayed-choice experiment realized in Walther's group. **A** and **B**: Comparison of interference patterns for normal mode (dots) and delayed-choice mode (crosses). Complementary interference fringes were recorded by photomultipliers 1 (PM 1) and 2 (PM 2), respectively. **C** and **D**: Ratio of the counts of normal and delayed-choice modes on PM 1 and PM 2, respectively. Quantum physics predicts the ratios to be unity. (Figure taken from [HWZS87].)

Having the delayed-choice and normal operating modes in mind, the authors

alternated experimental arrangement from the normal mode (open the PC shutter *before* the photon passing through Beam Splitter 1) to the delayed-choice mode (open the PC shutter *after* the light passing through Beam Splitter 1) for each successive light pulse, while kept all the other experimental configurations to be the same, e.g. the phase of MZI. The corresponding results are presented in Figure 2.4A (detected by PM 1) and B (detected by PM 2).

A more quantitative comparison between the data for delayed-choice and normal modes was obtained by taking the ratio of the corresponding counts. These ratios for PM 1 and PM 2 are shown in Figure 2.4C and D and yield a mean value 1.00 ± 0.02 and 0.99 ± 0.02, respectively. This is in agreement with quantum physics, which predicts the ratio to be unity.

This experiment was a pioneering work in the realization of Wheeler's gedanken-experiment, although true single photons were not used and space-like separation between the choice and the photon passing through Beam splitter 1 was not achieved.

Baldzuhn, Mohler, and Martienssen

The layout of the setup of the delayed-choice experiment performed in Martienssen's group [BMM89] is shown in Figure 2.5A. The light source was a heralded single-photon source from spontaneous parametric down conversion (SPDC) and thus it met the requirement of using a single-particle quantum state. The detection signal of one photon (trigger photon) was used to trigger a Pockels cell (P) in a Sagnac interferometer through which the other (signal) photon propagated.

As shown in Figure 2.5B and C, the signal photon passed through P first and then I (reference point) in the clockwise path. On the other hand, the signal photon met I first and then P in the counter-clockwise path, shown in Figure 2.5D and E. Therefore, if the Pockels cell is off during the photon's propagation through the whole interferometer, the polarization of signal photon will not be rotated and remain the same for both paths. If the Pockels cell is on during the photon propagating through the whole interferometer, the

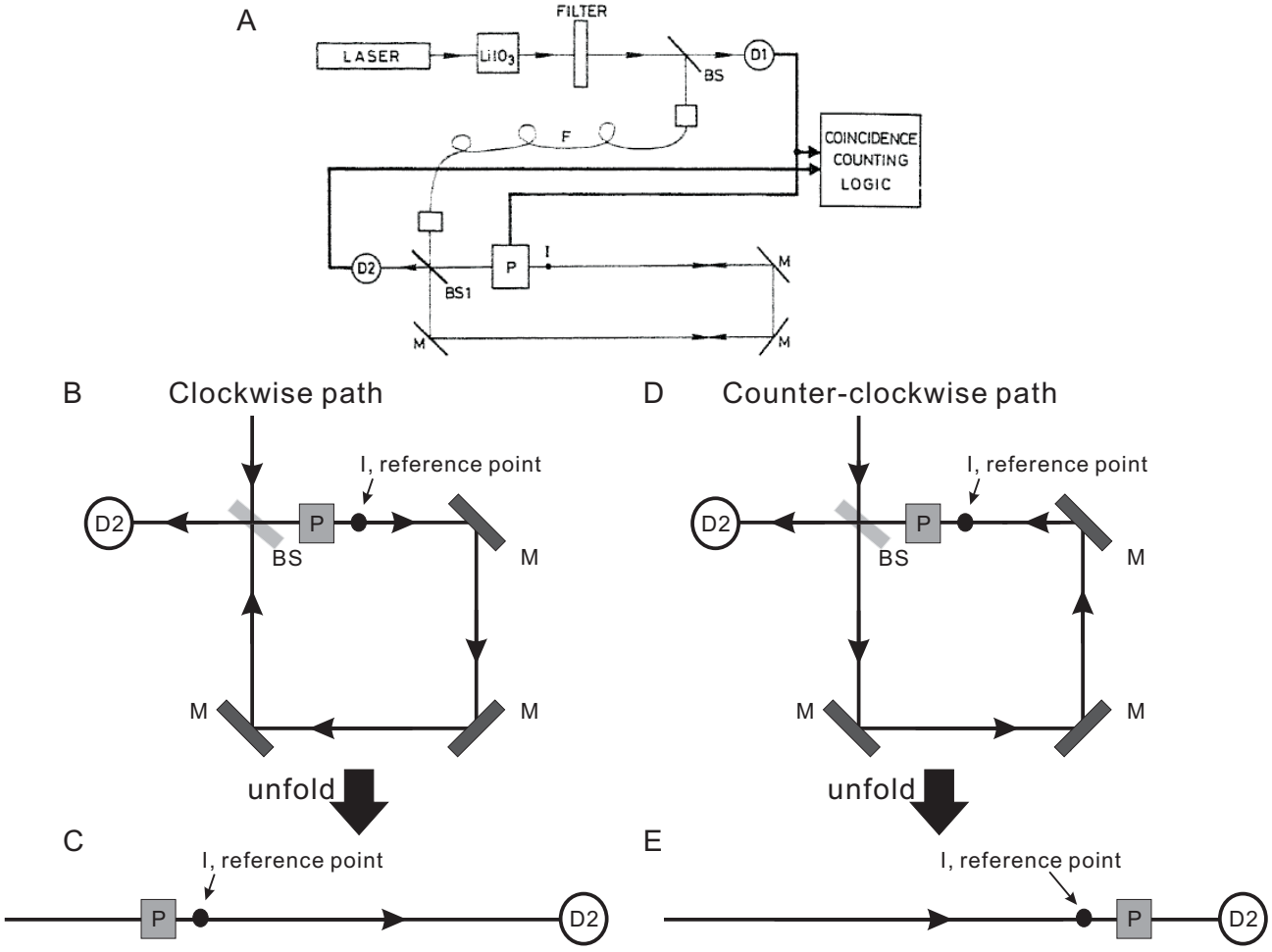

Figure 2.5.: The delayed-choice experiment realized in Martienssen's group. **A**: The layout of the setup. A heralded single-photon from spontaneous parametric down conversion was used as the photon source. The detection signals of one photon were used to trigger a Pockels cell (P) in a Sagnac interferometer through which the other photon propagated. The Pockels cell could rotate the polarization of the photon passing though it if one applied voltage to it. With this experimental configuration, one could choose to detect photon's particle-like behavior or wave-like behavior by using the Pockels cell. See text for details. **B** Schematic diagram of the photon propagating through the clockwise path. The photon meets beam splitter (BS), Pockels cell (P), reference point (I), mirrors (M) and BS again, sequentially. The unfolded diagram is shown in **C**, illustrating that the photon meets P first and then I. **D** Schematic diagram of the photon propagating through the counter-clockwise path. The photon meets beam splitter (BS), mirrors (M), reference point (I), Pockels cell (P), and BS again, sequentially. The unfolded diagram is shown in **E**, illustrating that the photon meets I first and then P. (Figure **A** taken from [BMM89].)

polarization of signal photon will also not be rotated and remain the same for both paths. But if the Pockels cell is switched on at the time when the signal photon arrives at I (the reference point) and is kept on until after the photon meets beam splitter again, no interference will be observed. This is because that the polarization of the clockwise path will remain, but polarization of the clockwise path will be rotated. This introduces distinguishability between two paths and hence destroys interference.

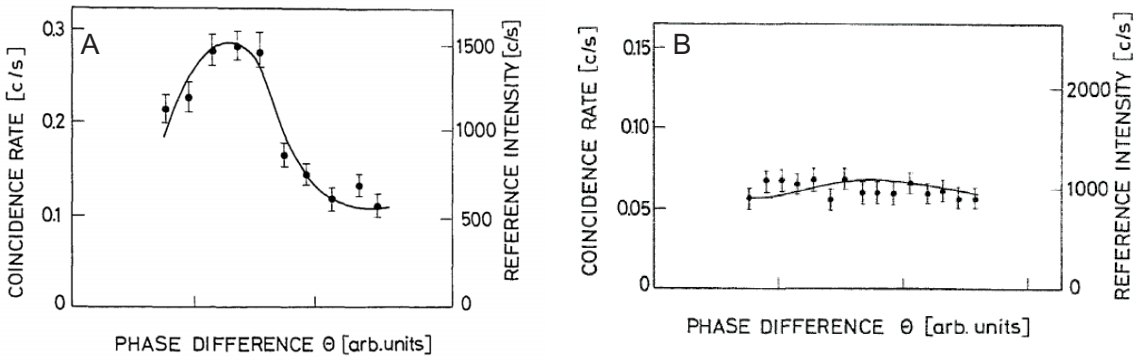

Figure 2.6.: The delayed-choice experiment realized in Martienssen's group. **A**: If the Pockels cell was continuously on or off, one observed an interference pattern. But if it was switched on at the reference point (I), indicated in Figure 2.5, no interference showed up, as illustrated in **B** (Figure taken from [BMM89].)

The experimental results are presented in Figure 2.6. If the Pockels cell was continuously on or off, one observed an interference pattern (Figure 2.6A). This corresponds to the wave-like behavior of the photon. On the other hand, if the Pockels cell was switched on at the time when photon passed through the reference point (I), one couldn't observed any interference pattern (Figure 2.6B). This corresponds to the particle-like behavior of the photon.

To introduce the delayed-choice aspect into this experiment, the signal photon was delayed by an optical fiber (F), one could vary the time of the application of the voltage on the Pockels cell via electronic delays. This allowed for demonstrating a delayed-choice experiment with time-like separation. Space-like sep-

aration between the choice of the performed measurement and the entering of the photon into the interferometer was not been fulfilled in this experiment.

Jacques, Wu, Grosshans, Treussart, Grangier, Aspect and Roch

Recently, two important requirements of Wheeler's delayed-choice gedankenexperiment, namely, use of a single-particle quantum state and space-like separation between the choice of the performed measurement and the entering of the particle into the interferometer, have been fulfilled simultaneously. In [JWG+07, JWG+08] NV color centers in diamonds were used as a single-photon source. As shown in Figure 2.7A, a 48-meter-long polarization interferometer and a fast electro-optical modulator (EOM) controlled by a quantum random number generator (QRNG) were used to fulfill the relativistic space-like separation requirement. The space-time diagram of this experiment is shown in Figure 2.7B. The measurement applied to photon "n" was synchronized on clock pulse "*n-1*" which triggered the emission of photon "*n-1*". The sequence for the measurement applied to photon "n" constituted three steps. First, the binary random number (in blue), which determines the interferometer configuration, was generated by the QRNG simultaneously with the trigger of single photon "n" emission. Then, this binary random number (equal to 0 for photon "n") drove the EOM voltage between $V = 0$ and $V = V_\pi$ within 40 ns, as shown in the Figure 2.7B in red. Finally, the single-photon pulse was detected at the outputs by D1 or D2, after its time of flight τ_{interf} in the interferometer. The blue zone, in Figure 2.7B, represents the future light cone of the choice. The event of "entering of photon 'n' into the interferometer" was space-like separated from the choice. If the EOM was on with voltage of $V = V_\pi$, one erased the polarization distinguishability of the two paths and thus could observe interference pattern, as shown in Figure 2.7C. But if the EOM was switched off, due to the polarization distinguishability of the two path, no interference showed up, as shown in Figure 2.7D.

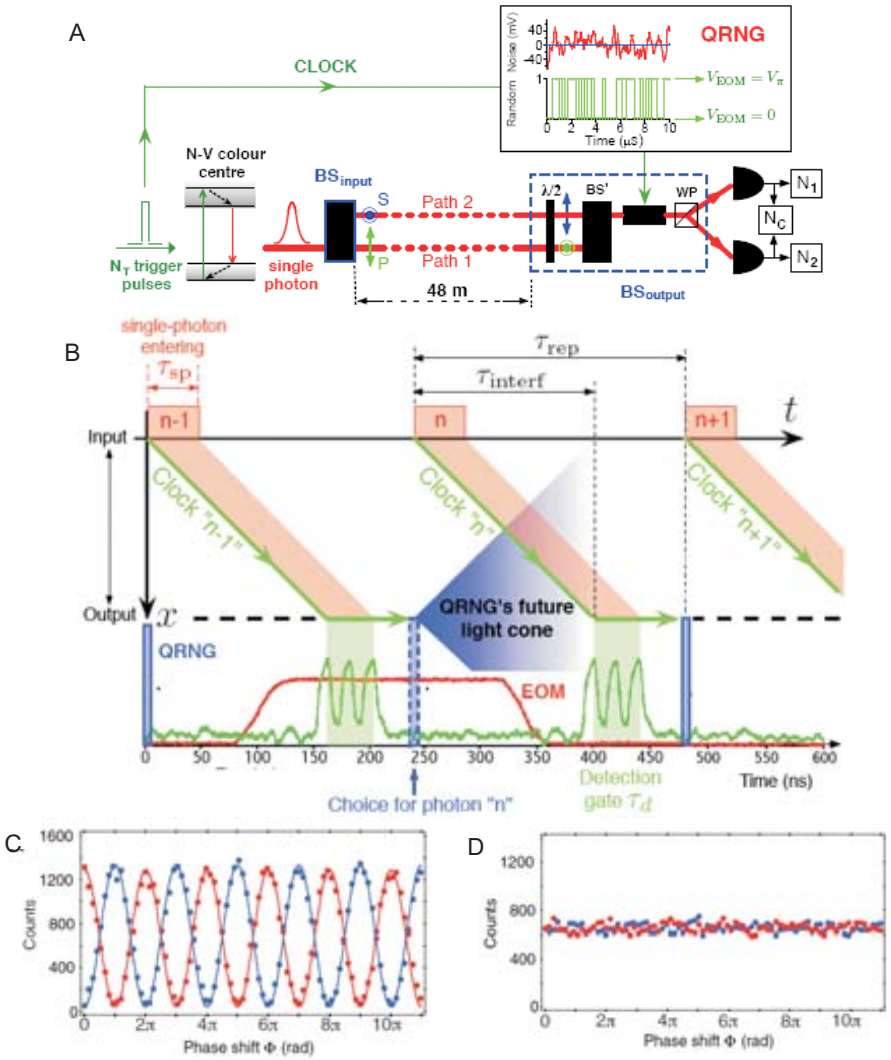

Figure 2.7.: The delayed-choice experiment realized in Roch's group. **A**: The layout of the setup. Single photons generated from NV color centers in diamond were used as the input. A 48-meter-long polarization interferometer and a fast electro-optical modulator (EOM), controlled by a quantum random number generator (QRNG), were used to fulfil the relativistic space-like separation condition. The space-time diagram is shown in **B**. The choice was space-like separated from the entry of the photon into the interferometer. If the EOM was on, one erased the polarization distinguishability of the two paths and thus could observe interference pattern, as shown in **C**. But if the EOM was switched off, due to the polarization distinguishability of the two path, no interference showed up, as illustrated in **D**. (Figure taken from [JWG+07].)

2.3. Delayed-choice quantum eraser

Heisenberg and von Weizsäcker

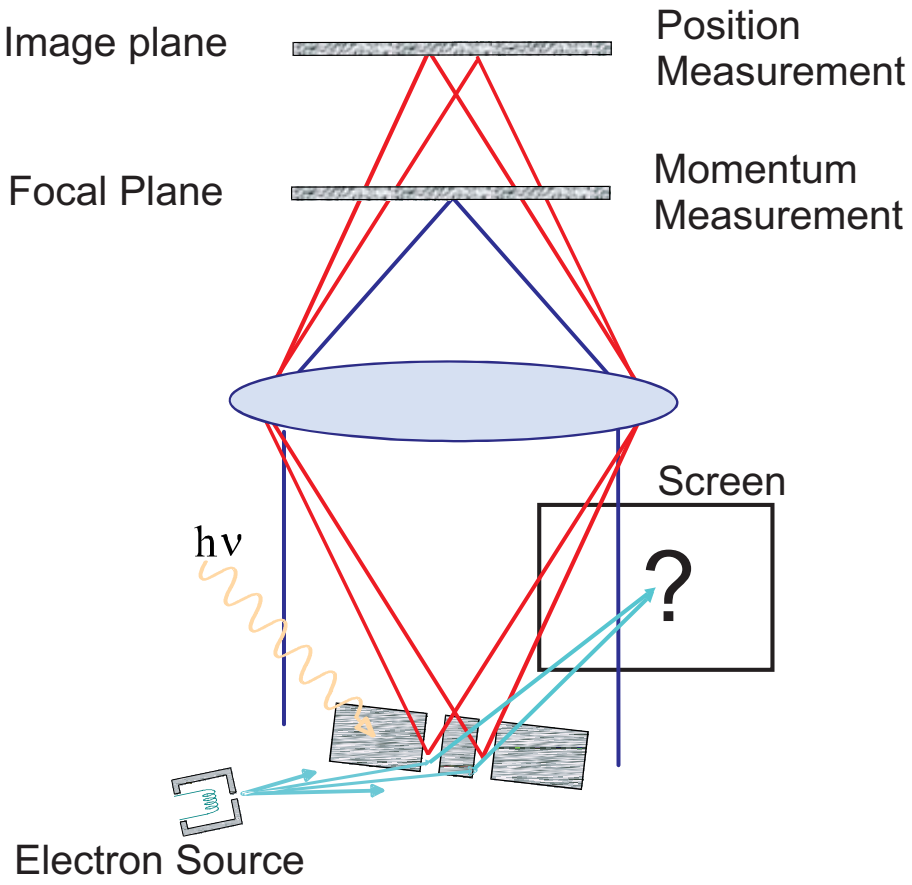

Figure 2.8.: Heisenberg microscope gedankenexperiment. The photon and the electron are correlated in momentum and in position. Different measurements on the photon, whether to observe it in the focal or image plane, allow choosing whether to exactly determine the momentum or the position of the electron. When the position of the electron is determined, one can not observe any interference pattern on the screen. When the electron's momentum is determined, one can observe interference. See text for details. (Figure taken from [Dop98].)

The Heisenberg microscope gedankenexperiment is an experiment whose pur-

pose is to measure the position of an electron with high resolution [Hei27]. Due to the wave nature of light, there is a limitation on how close two regions can be seen as two minimally spaced distinguishable separate regions. This limitation is the so-called diffraction limit and the distance between two regions is of the order of the wavelength of light. Therefore, the purpose of this gedankenexperiment is equivalent to distinguish the region (or slit in the language of double-slit experiment) through which the electron propagates, as shown in Figure 2.8.

If the electron is assumed to be initially stationary, its momentum is exactly zero. To observe where the electron is, one of the incident photons from left must hit the electron and then be scattered into the microscope. When the photon hits the electron, it transfers momentum to the electron. Due to the conservation of momentum, the momentums of the photon and the electron are correlated. The sum of their momentums is constant and equals to the initial momentum of the photon. Basing on the concept of the Heisenberg microscope [Hei27], von Weizsäcker [Wei31, Wei41] discussed the gedankenexperiment in detail. The photon and the electron are not only correlated in momentum but also in position. As shown in Figure 2.8, there are two extreme situations:

- We can obtain the exact momentums of the photon and the electron but no information whatsoever about their positions. Experimentally, if the photon is detected in the focal plane of the objective of the microscope, we obtain the full momentum information of the photon and no position information. Due to the correlation of the momentums of the electron and the photon, we also obtain the full momentum information and no position information of the electron itself. Hence, on the screen for detecting electron, one can obtain interference pattern after integration.

- On the other hand, if we detect the photon in the image plane, we obtain the full position information of the photon and no momentum information. Because of the position-correlation of the electron and the photon, we also

obtain the full position information and no momentum information of the electron. Hence, on the screen for detecting electron, one can't obtain interference pattern.

In between these two cases, there is a trade-off of the information we can obtain about the position and momentum of the electron via the measurement of the photon, as restricted by the uncertainty relation.

Scully and Drühl

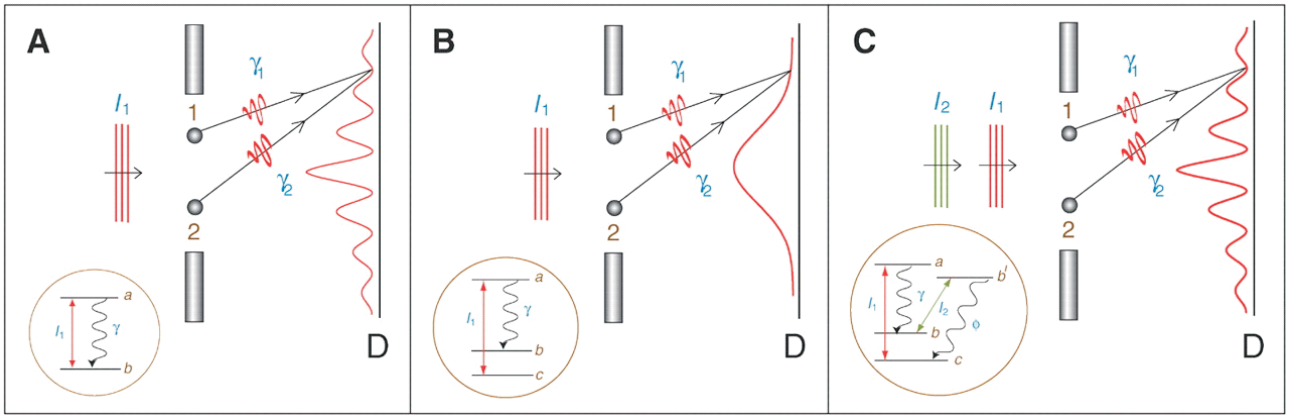

Figure 2.9.: The delayed-choice quantum eraser proposed by Scully and Drühl in [SD82]. In **A**, two two-level atoms are initially in the state b. The incident pulse l_1 excites one of the two atoms to state a from where it decays to state b, emitting a γ photon. Because the final states of both atoms are identical, one can observe the interference of the photons. In **B**, two atoms are initially in the ground state c and one of them is excited by the pulse l_1 to state a from where it decays to state b. Because the final states of both atoms are different, one can not observe the interference of the photons. In **C** a fourth level is added. A pulse l_2 excites the atom to state b' from state b. The atom in the state b' emits a γ photon and ends up in state c. If one can detect the ϕ photon in a way that the which-path information is erased, interference can be recovered. See text for details. (Figure taken from [AZ05].)

Scully *et al.* proposed the so-called quantum eraser [SD82, SEW91], in which an entangled atom-photon system was studied. The authors considered the scattering of light from two atoms located at sites 1 and 2 and analyzed three

different cases:

1. Resonant light impinges on two two-level atoms (Figure 2.9A) located at sites 1 and 2. One of the two atoms is excited to level a and emits a γ photon. But we don't know which atom contributed this γ photon, because both atoms are finally in the state b after the emission of this γ photon. Then we are able to obtain the interference of these photons at the detector. This is an analog of Youngs double-slit experiment.

2. In the case where the atoms have three levels (Figure 2.9B), the driving field excites the atoms from a ground state c to the excited state a. The atom in state a can then emit a γ photon and end up in state b. Therefore, the atom contributing the γ photon is in level b, whereas the other atom remains in level c. Thus, this distinguishability of the atoms' internal states provides us the which-path information of the photon and no interference can be observed.

3. As shown in Figure 2.9C, imagine we drive the atom by another field l_2 that takes the atom from level b to b'. Then a ϕ photon will be emitted at the b' to c transition and the atom ends up in level c. Now the final state of both the atoms is c, and thus the atoms' internal states can't provide us any which-path information. If one can detect the ϕ photon in a way that the which-path information is erased, interference can be recovered. Note that in this case, there are two photons: One is γ photon for interference; The other one is ϕ photon, acting as a which-path information carrier.

As shown in Figure 2.10, Scully and Drühl designed a device based on an electro-optic shutter, a photon detector and two elliptical cavities to achieve the above mentioned experimental configuration. A delayed-choice configuration could be arranged in this experiment: one could choose to reveal or erase the which-path information long after the γ photon had been generated.

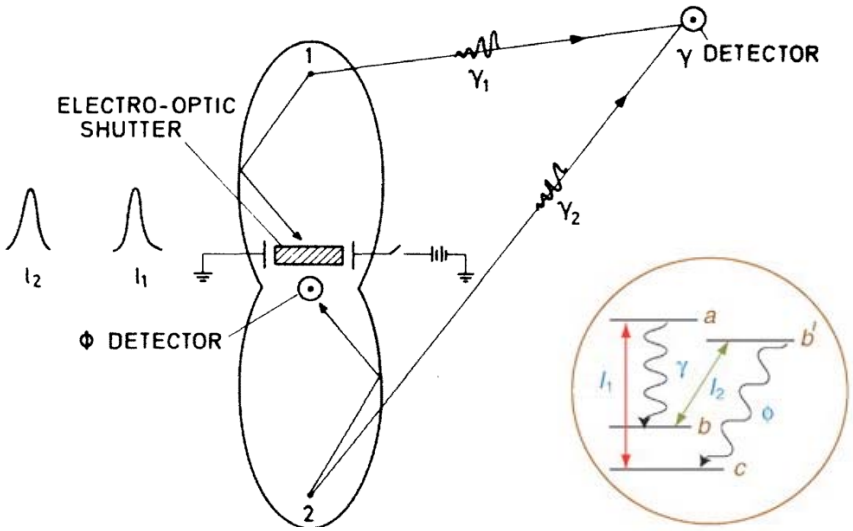

Figure 2.10.: Proposed delayed-choice quantum-eraser setup from [SD82]: Laser pulses l_1 and l_2 incident on atoms at sites 1 and 2. Scattered photons γ_1 and γ_2 are generated from $a \rightarrow b$ atomic transition. Decay of atoms from $b' \rightarrow c$ transition produces ϕ photon. This corresponds to the situation depicted in the inset. In order to operate this experiment in a delayed-choice mode, two elliptical cavities and an electro-optical shutter are employed. Two elliptical cavities reflect ϕ photon onto a common detector (ϕ DETECTOR). Electro-optical shutter transmits ϕ photons only when switch is open. Choice of open electro-optical shutter or not determines whether one can observe wave or particle nature of γ photons and can be delayed with respect to the γ photons' generations. (Figure taken from [SD82].)

Scully, Englert and Walther

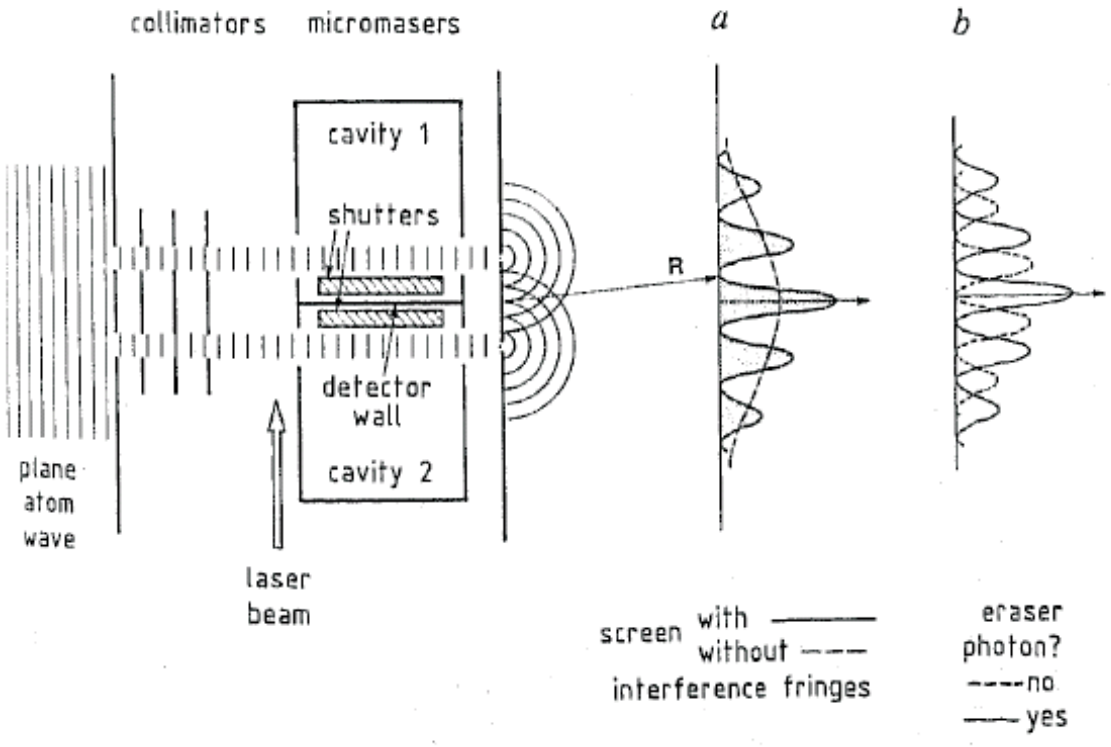

Figure 2.11.: Proposed quantum-eraser setup from [SEW91]: A detector wall, separating two cavities for microwave photons, is sandwiched by two electro-optic shutters. **a**: To open one and only one shutter will reveal which-path information and destroy interference. To open both shutters will erase which-path information and retrieve interference. **b**: The authors assumed that the detector wall had unity quantum efficiency and could only be excited by the symmetric photonic state $|+\rangle_{12} = \frac{|10\rangle_{12}+|01\rangle_{12}}{\sqrt{2}}$. Hence conditionally on the shutters were open and only one photon was emitted from the atom, if the detector was not excited, the photon was in the antisymmetric state $|-\rangle_{12} = \frac{|10\rangle_{12}-|01\rangle_{12}}{\sqrt{2}}$. Since the internal energy state of the atom was entangled with photon number state, the detections of the symmetric and antisymmetric photonic state gave rise to the oppositely-modulating interference fringes (solid and dashed curves), respectively. (Figure taken from [SEW91].)

In another proposal [SEW91] the interfering system is an atomic beam propagating through two cavities coherently. The internal energy state of the atom is

$\frac{1}{\sqrt{2}}(|e\rangle_1 + |e\rangle_2)$, where $|e\rangle_i$ denotes the excited state of the atom passing through cavity i, as shown in Figure 2.11. Two cavities (cavity 1 and cavity 2), separated with a photon detector wall, are used to trap photons emitted from the atoms. At t_0, the initial state of the atom and photon is $|\Phi(t_0)\rangle_{ap} = \frac{1}{\sqrt{2}}(|e\rangle_1 + |e\rangle_2)|00\rangle_{12}$, where $|00\rangle_{12}$, $|10\rangle_{12}$, and $|01\rangle_{12}$ denote the photon number state with no photon in both cavities, one photon in cavity 1 and no photon cavity 2, and no photon in cavity 1 and one photon cavity 2, respectively. The atom can decay to the ground state, $|g\rangle$, and emit one photon. At time t, conditional on the emission of one and only one photon from the atom in one of the cavities, the state becomes:

$$|\Phi(t)\rangle_{ap} = \frac{1}{2}((|g\rangle_1 + |e\rangle_2)|10\rangle_{12} + (|g\rangle_2 + |e\rangle_1)|01\rangle_{12}). \tag{2.1}$$

This can also be rewritten as:

$$|\Phi(t)\rangle_{ap} = \frac{1}{2\sqrt{2}}[(|g\rangle_1 + |e\rangle_1 + |g\rangle_2 + |e\rangle_2)|+\rangle_{12} + (|g\rangle_1 - |e\rangle_1 - |g\rangle_2 + |e\rangle_2)|-\rangle_{12}], \tag{2.2}$$

where $|+\rangle_{12} = \frac{|10\rangle_{12}+|01\rangle_{12}}{\sqrt{2}}$ and $|-\rangle_{12} = \frac{|10\rangle_{12}-|01\rangle_{12}}{\sqrt{2}}$. If one detects one photon in cavity 1 and no photon in cavity 2 by only opening the shutter of cavity 1, $|10\rangle_{12}$, defined as measurement **I**, the atomic internal state would be:

$$|\Phi(t)\rangle_{a\mathbf{I}} = \frac{|g\rangle_1 + |e\rangle_2}{\sqrt{2}}. \tag{2.3}$$

From Equation 2.3, upon measurement **I**, one acquires the which-path information of the atom. Since the final internal states of the atom propagating through cavity 1 and 2 are different, no interference shows up. If one detects a superposition of the photon states, say $|+\rangle_{12}$ by opening both shutters, defined as measurement **II+**, the atomic internal state is:

$$|\Phi(t)\rangle_{a\mathbf{II}+} = \frac{1}{2}[(|g\rangle_1 + |e\rangle_1) + (|g\rangle_2 + |e\rangle_2)] \equiv \frac{1}{\sqrt{2}}(|u\rangle_1 + |u\rangle_2), \tag{2.4}$$

where $|u\rangle_1 = \frac{|g\rangle_1+|e\rangle_1}{\sqrt{2}}$ and $|u\rangle_2 = \frac{|g\rangle_2+|e\rangle_2}{\sqrt{2}}$. Therefore, upon measurement **II+**, because the final states of the atom propagating through cavity 1 and 2 are identical, one can not in principle distinguish which cavity the atom propagated through. Therefore, interference shows up again (solid curve in Figure 2.11b). If one detects the antisymmetric state of the photon states, $|-\rangle_{12}$, the atomic internal state is:

$$|\Phi(t)\rangle_{a\textbf{II-}} = \frac{1}{2}(|g\rangle_1 - |e\rangle_1 - |g\rangle_2 + |e\rangle_2) \equiv \frac{1}{\sqrt{2}}(|d\rangle_1 - |d\rangle_2), \tag{2.5}$$

where $|d\rangle_1 = \frac{|g\rangle_1-|e\rangle_1}{\sqrt{2}}$ and $|d\rangle_2 = \frac{|g\rangle_2-|e\rangle_2}{\sqrt{2}}$. Therefore, upon measurement **II-**, the final states of the atom propagating through cavity 1 and 2 are also identical. Again, one could not in principle distinguish which cavity the atom propagated through and interference shows up (dashed curve in Figure 2.11b). Note that there is a π phase difference between measurements **II+** and **II-**, which gives rise to the oppositely-modulating interference fringes. A delayed-choice configuration can be arranged in this experiment: one can choose to reveal or erase the which-path information of the atoms (by performing measurement **I** or **II** on the photon) after the atoms finishes the propagation through the two cavities.

2.4. An earlier delayed-choice quantum-eraser experiment.

Several quantum-eraser experiments have been performed in the past [HKWZ95, Zei99, ZWJA05, KYK+00, WTCPM02] which used photon pairs created from SPDC. No which-path measurements need to be performed on the interfering photon itself to destroy interference. Instead specific measurements of the other photon can introduce distinguishability, which consequently destroys interference. However, a suitable measurement can erase this distinguishability and interference may be recovered. In the following, I discuss a quantum-eraser

experiment with the delayed-choice configuration.

Kim, Yu, Kulik, Shih and Scully

In [KYK+00], a pair of entangled photons were used to mimic the entangled atom-photon system proposed in [SEW91]. The layout of the experimental setup is shown in Figure 2.12A. The photon pair could be generated either from region A or region B of a BBO crystal via SPDC. Photon 1, simulating the atom, propagating to the right was first focused by a lens and then detected by D0. D0 was mounted on a step motor which could change the lateral position of D0 allowing for scanning the interference pattern.

Photon 2, propagating to the left, passed through one or two of three beam splitters. If the pair was generated in region A, photon 2 would propagate through path a and meet beam splitter 1 (BS1). At BS1 it has a 50% chance of being reflected or transmitted. If the pair was generated in region B, photon 2 would follow path b and meet beam splitter 2 (BS2), again with a 50% chance of being reflected or transmitted. In the case that photon 2 transmitted at either BS1 or BS2, it was detected by either detector D3 or D4. The detection of D3 or D4 provided the which-path information (path a or path b) for photon 2, thus also providing the which-path information for photon 1 due to the linear momentum entanglement of the photon pair. Therefore, there was no interference, as shown in Figure 2.12B.

Given a reflection at both BS1 and BS2, photon 2 continued its path to meet another 50:50 beam splitter BS3 and then was detected by either D1 or D2. The detection by D1 or D2 erased the which-path information of photon 1 and interference showed up (Figure 2.12B). The choice of observing interference or not was made randomly by photon 2 by being either reflected or transmitted at BS1 or BS2. This "delayed-choice" was about 7.7 ns after the detection of photon 1. However, this choice was situated in the future light cone of both the emission of the photon pair and the measurement event of photon 1. Therefore, it is in principle conceivable that the emission event and photon 1's measurement event could influence the choice, which then only appears to be free or random.

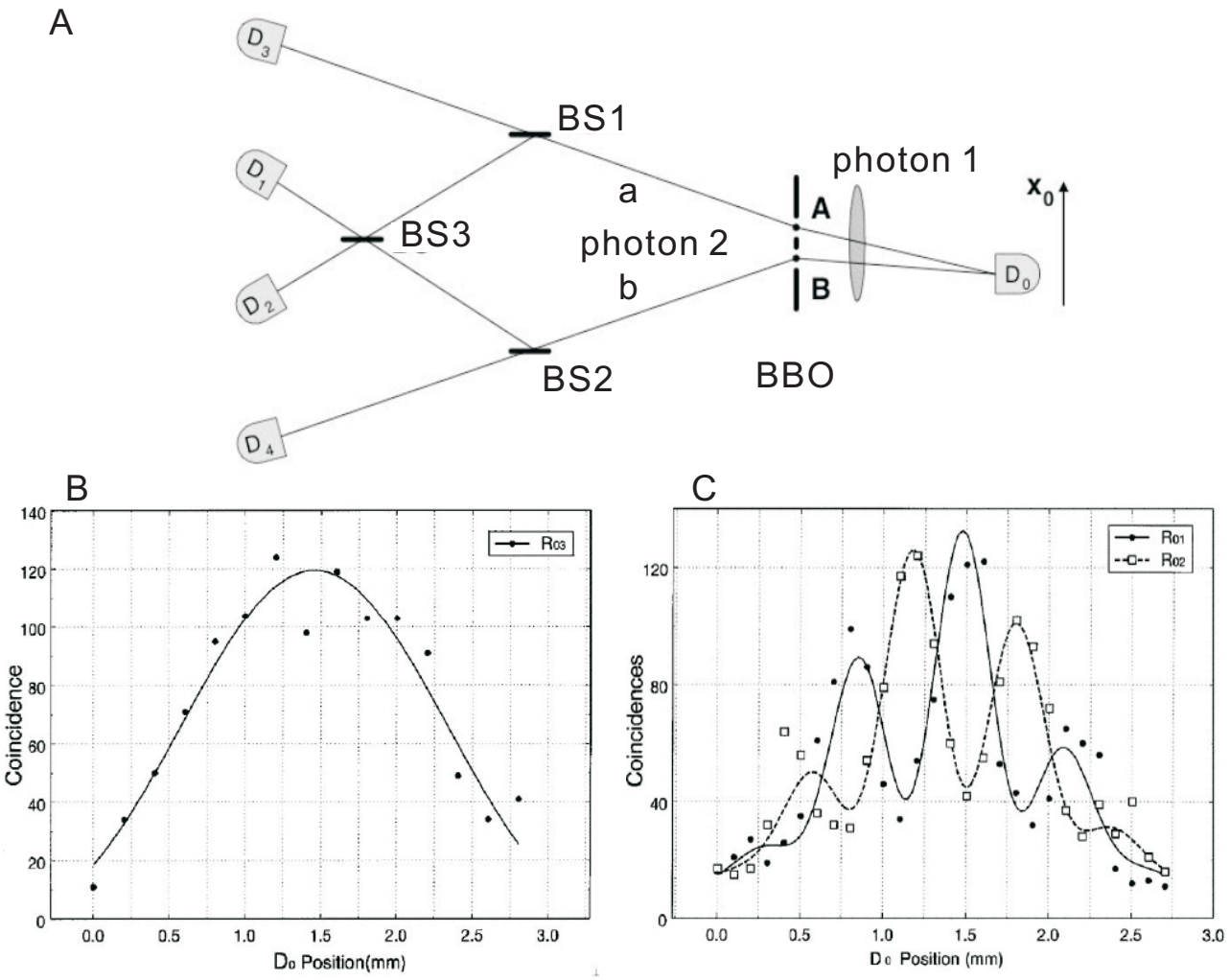

Figure 2.12.: The delayed-choice quantum-eraser experiment realized in Shih's group [KYK+00]. **A**. The experimental scheme. One and only one pair of entangled photons was emitted from either region A or region B of a BBO crystal via spontaneous parametric down conversion. These two emission processes are coherent. Detections at D3 or D4 provided the which-path information and detections at D1 or D2 erased the which-path information. **B**. Coincidence counts between D0 and D3, as a function of the lateral position of the D0, were shown. Absence of interference was demonstrated. **C**. Coincidence counts between D0 and D1, D0 and D2 were plotted as a function of the lateral position of the D0. Interference fringes were obtained. See text for details. (Figure taken from [KYK+00].)

2.5. Delayed-choice entanglement swapping

Two particles in a quantum system can be in an entangled state, where the correlations of the overall system are well defined but not the properties of the individual particles [Sch35, EPR35], regardless of their spatial separation [UTSM+07] and life time [FUH+09]. Peres raised the question of whether it is possible to produce entanglement between two particles even after they do not exist anymore [Per00]. Surprisingly, quantum mechanics allows this via entanglement swapping [ZZHE93]. Two pairs of entangled particles, 1&2 and 3&4, are produced from two different sources. One can establish entanglement between particles 1 and 4 via Bell-state measurement on particles 2 and 3, although particles 1 and 4 never interact nor share any common past. Note that after the entanglement swapping, particles 1&2 and 3&4 are no longer entangled, following the monogamy of entanglement [CKW00].

Peres suggested another addition to an entanglement-swapping experiment by combining it with the delayed-choice paradigm [Whe84]. He proposed that the correlations of photons 1 and 4 can be defined even after they have been detected via a *later* projection of photons 2 and 3 into an entangled state. This leads to a seemingly paradoxical situation, that "entanglement is produced *a posteriori*, after the entangled particles have been measured and may even no longer exist" [Per00].

In [JWPZ02], a delayed-choice experiment was performed by including two 10 m optical fiber delays for both outputs of the Bell-state analyzer. Thus in this case the detection of photons 2 and 3 was delayed by about 50 ns. Alice's and Bob's detectors were located next to each other. The time travel of photons 1 and 4 from the source to these detectors was about 20 ns. Victor and Alice and Bob were separated by about 2.5 m, corresponding to luminal traveling time of 8 ns between them. The space-time diagram for this is shown in Figure 2.14. The observed fidelity of the entanglement state of photon 1 and photon 4 matches the fidelity in the non-delayed case to within experimental error. Remarkably, this

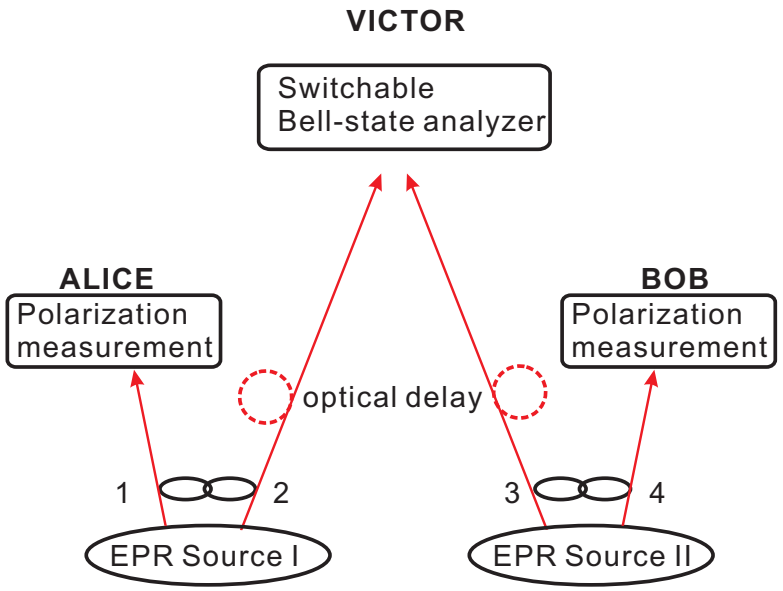

Figure 2.13.: The concept of entanglement swapping with the delayed-choice configuration. Photons 1 and 2 are generated from EPR source I in a polarization-entangled state; photons 3 and 4 are generated from EPR source II in the same entangled state. Firstly, Alice and Bob measure the polarization states of photons 1 and 4 respectively. Photons 2 and 3 are delayed with optical fibers and sent to Victor. Victor chooses to swap the entanglement or not with a switchable Bell-state analyzer. If he choose to perform Bell-state measurement on photons 2 and 3, photons 2 and 3 become entangled. Hence photons 1 and 4 are also entangled, although they have been previously measured and thus already destroyed.

is the first attempt of the realization of delayed-choice entanglement swapping, although a switchable Bell-state analyzer was not implemented.

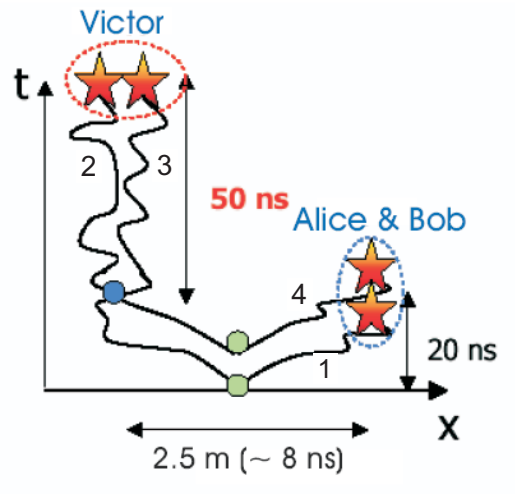

Figure 2.14.: Space-time diagram for delayed-choice entanglement-swapping experiment reported in [JWPZ02]. (Figure taken from [BAZ05].)

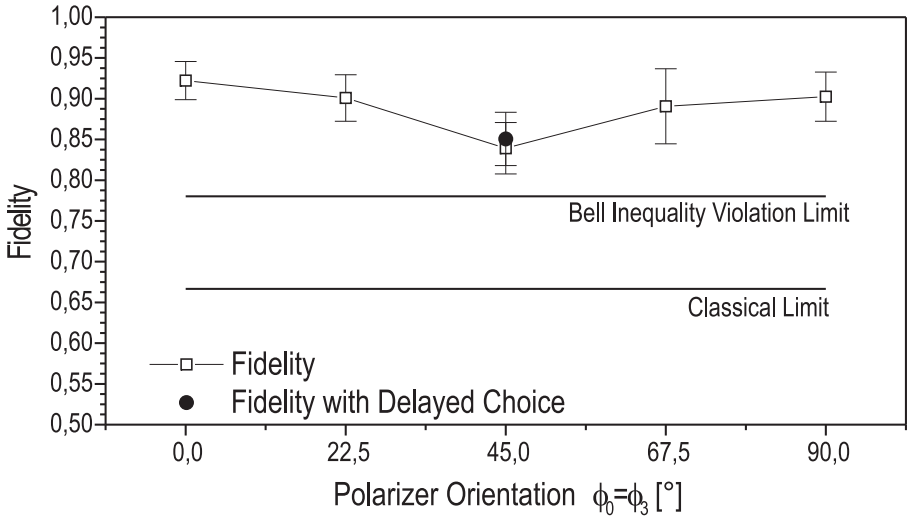

Figure 2.15.: Observed entangled state fidelity obtained via correlation measurements between photons 1 and 4 in [JWPZ02]. ϕ_0, ϕ_3 are the settings of the polarization analyzer for photon 1 and photon 4, and are always equal ($\phi_0 = \phi_3$). The minimum fidelity, F, of 0.84 is well above the classical limit of 2/3 and also above the limit of 0.79 necessary for violating Bell's inequality (see Chapter 1). Note that fidelity is related to the visibility via $F = \frac{3}{4}V + \frac{1}{4}$. Therefore, $F = 0.79$ corresponds to $V = 0.72$. The square dots represent the fidelity for the case that Alice's, Bob's and Victor's detection events are space-like separated. The circular dot is the fidelity for the case, that Victor's detections are delayed by 50 ns with respect to Alice's and Bob's detections. That is Victor's measurement projects photon 1 and 4 into an entangled state, at a time after they have already been registered. (Figure taken from [JWPZ02].)

3. A non-local quantum eraser

As reviewed in Chapter 2, Scully *et al.* proposed a so-called *quantum eraser* with examples of atom-photon entangled states [SD82, SEW91]. The atom, which is denoted as the "system", is sent through a double slit. The photon, which can be regarded as the "environment", carries which-path information of the atom. Scully *et al.* suggested: First, no atomic interference pattern will be obtained if one ignores the detection events of the photon since the atom's path states are not in a coherent superposition due to the atom-photon entanglement. Second, and more importantly, when the photon is measured in a way that reveals the which-path information of the atom, the atom does not show interference. If, however, the photon is measured such that it cannot, not even in principle, reveal the atom's which-path information, the spatial coherence of the atom can be retrieved and interference can be observed. These illustrate another different example of the complementarity principle, in addition to the wave-particle duality experiment. There is a trade-off between acquiring the system's which-path information or its interference pattern via complementary measurements on the environment and not on the system itself.

With that in mind, and combining the delayed-choice paradigm with the quantum eraser, Scully *et al.* further suggested that, since which-path information of the atom was carried by the photon, the decision of whether to erase or read out this information could be delayed until after the atom exit from the cavities [SEW91]. Thus, this later detection of the photon "decides" whether the atom interfered or not.

More dramatically, according to quantum physics, the quantum eraser will

work even when the choice for the measurement of the photon (environment) is delayed not only until after the atom (system) has passed the photon detector but even until after is has been detected. Moreover, it should also work under enforced Einstein locality for the experimental configuration. The locality condition imposes that if "two systems no longer interact, no real change can take place in the second system in consequence of anything that may be done to the first system" [EPR35]. Operationally, the erasure of which-path information event has to be relativistically space-like separated from the measurement of the interfering system event. This means that no subluminal or luminal physical signal can travel from one event to the other and causally influence it. Locality is much stronger than the delayed-choice condition, as the latter usually means that the erasure takes place in the future light cone of (i.e. is time-like separated from) the measurement of the interfering system. Hence, under the delayed-choice condition there could be a causal influence of the first measurement event to the second. Under space-like separation (Einstein locality), however, such an influence is impossible in any and all reference frames and therefore would be a conclusive demonstration of the quantum eraser concept. This seemingly counter-intuitive situation comes from the fact that in a bipartite quantum state the observed correlations are independent of the space-time arrangement of the measurements on the individual systems.

In this chapter, I firstly introduce a specific type of entanglement: hybrid entanglement. This allows us to perform a quantum eraser experiment under various space-time configurations. Secondly, I present a conclusive demonstration of the quantum eraser concept: a non-local quantum eraser.

3.1. Hybrid Entanglement

3.1.1. The proposal and theory.

Before presenting the non-local quantum eraser, we introduce a special type of entanglement: *hybrid entanglement*. It is the entanglement between *different* degrees of freedom (DOF) of a particle *pair*. Here we follow the proposal in [ZZ91] and experimentally demonstrate the hybrid entanglement between the polarization of one photon from a photon pair and the path (momentum) of its twin. *A hybrid entangled state cannot be factorized into states of individual DOF.* The defined joint properties are such that they link one DOF of one particle with another DOF of the other particle, where those degrees of freedom may even be defined in Hilbert spaces of different dimensionalities. For instance, in a hybrid-entangled state of photon A and B, their polarization and linear momentum are entangled as $|\Phi^+_{\text{hybrid}}\rangle = \frac{1}{\sqrt{2}}(|b\rangle_{\text{A}}|V\rangle_{\text{B}} + |a\rangle_{\text{A}}|H\rangle_{\text{B}})$. $|H\rangle$ and $|V\rangle$ denote the horizontal and vertical linearly polarized quantum states respectively, and $|a\rangle$ and $|b\rangle$ denote two orthogonal momentum quantum states. While the Hilbert space structure of quantum mechanics demands the existence of such hybrid entangled states, they have not been realized experimentally until now. We want to stress that hybrid entanglement is fundamentally different from the so-called hyper-entanglement [BLPK05]. A hyper-entangled state is a tensor product of states entangled in each *individual* DOF and there is no entanglement between different DOF. For instance, in a hyper-entangled state of photon A and B, $|\Phi^+_{\text{hyper}}\rangle = \frac{1}{2}(|H\rangle_{\text{A}}|V\rangle_{\text{B}}+|V\rangle_{\text{A}}|H\rangle_{\text{B}})\otimes(|a\rangle_{\text{A}}|b\rangle_{\text{B}}+|b\rangle_{\text{A}}|a\rangle_{\text{B}})$, their polarization states are entangled and their momentum states are also entangled, but there is no entanglement between the polarization states of one photon and momentum states of the other photon. In a hyper-entangled state of two particles joint properties of the same DOF are well-defined but not individual properties. The joint properties allow us to make predictions for experimental situations where both particles are measured in one and the same degree of freedom. This is fundamentally different from the hybrid entanglement as stated above.

The entanglement between the polarization and the momentum degrees of freedoms [BBDM+98, MWidZ00] as well as between the polarization and the orbital angular momentum DOF [BWK08] of a *single* photon, and between the spatial and spin DOF of a *single* neutron [HLB+03] has been demonstrated experimentally. The idea to convert the polarization entanglement to path entanglement of a photon pair was proposed [ZP88] and realized in [SPS+96]. There have also been experimental realizations of two-photon four-qubit cluster states with entanglement between both path and polarization [VPM+07, CLZ+07]. On the other hand, entanglement between the same degree of freedom of different physical systems has also been realized. In many atom-photon experiments entanglement has been demonstrated between the spin of the atom state and the spin (i.e. polarization) of the photon [RBH01].

In the following section, we demonstrate hybrid entanglement of photon pairs between two different degrees of freedom, namely path and polarization, via the experimental violation of the CHSH inequality. In the case of the polarization entanglement of a photon pair, the maximum violation of the CHSH inequality is established with the polarizers oriented at $(-22.5°, 22.5°)$ at Bob's side and $(0°, 45°)$ at Alice's side, while in the case of path entanglement it is established with the phase shift at $(-45°, 45°)$ at Bob's side and $(0°, 90°)$ at Alice's side. In order to maximally violate the CHSH inequality for the hybrid entanglement, the polarizer at Bob's side is oriented at the *angles* of $(-22.5°, 22.5°)$ and the phase shifter at Alice's side is adjusted at the *phase* to $(0°, 90°)$. This shows the hybrid nature of our entangled photon pairs.

3.1.2. Experiment and results.

The scheme for the experiment is shown in Figure 3.1. Firstly, the polarization-entangled state $|\Phi^+\rangle = \frac{1}{\sqrt{2}}(|H\rangle_A |V\rangle_B + |V\rangle_A |H\rangle_B)$ [KMW+95] is created, where A and B index the photons. We use a picosecond pulsed Nd:Vanadate laser emitting light at the wavelength of 355 nm after frequency tripling (repetition

rate of 76 MHz and average power of 200 mW) to pump a β-Barium-Borate (BBO) crystal in a cross rings type-II phase-matching scheme of spontaneous parametric down conversion SPDC [KMW+95]. Refer to the appendix for the details of the generation of the polarization-entangled photon pairs.

Secondly, I will show how the quantum state $|\Phi^+\rangle$ evolved in the setup. A polarizing beam splitter (PBS) transmits the horizontal and reflects the vertical polarization state of photon A. Thus, this PBS acts as a deterministic polarization-path converter. Two fiber polarization controllers (FPCs) are used to rotate the orthogonal polarization states of photon A in path a and b ($|H\rangle_{\mathrm{a}}$ and $|V\rangle_{\mathrm{b}}$) to an identical one ($|\theta,\gamma\rangle_{\mathrm{a}}$ and $|\theta,\gamma\rangle_{\mathrm{b}}$, where $|\theta,\gamma\rangle_{\mathrm{a}} = |\theta,\gamma\rangle_{\mathrm{b}} = \cos\theta\,|H\rangle + \exp(i\gamma)\sin\theta\,|V\rangle$, thus eliminate the polarization distinguishability of the two paths. From now on I will ignore the polarization of photon A and label photon A with its path quantum states, where $|a\rangle_{\mathrm{A}} \equiv |\theta,\gamma\rangle_{\mathrm{a}}$ and $|b\rangle_{\mathrm{A}} \equiv |\theta,\gamma\rangle_{\mathrm{b}}$. Hence, the source creates the hybrid entangled state between the path of photon A and the polarization of photon B:

$$|\Phi^+_{\mathrm{hybrid}}\rangle = \frac{1}{\sqrt{2}}(|b\rangle_{\mathrm{A}}\,|V\rangle_{\mathrm{B}} + |a\rangle_{\mathrm{A}}\,|H\rangle_{\mathrm{B}}), \tag{3.1}$$

The superposition states of the two paths of photon A are varied and analyzed by a modified Mach-Zehnder interferometer, as shown in Figure 3.2. After a phase scanner (PS) and a beam splitter (BS), the state becomes

$$|\Phi^{+\prime}_{\mathrm{hybrid}}\rangle = \frac{1}{2}[(|d\rangle_{\mathrm{A}} + \mathrm{i}\,|c\rangle_{\mathrm{A}})\,|V\rangle_{\mathrm{B}} + \exp(\mathrm{i}\alpha)(|c\rangle_{\mathrm{A}} + \mathrm{i}\,|d\rangle_{\mathrm{A}})\,|H\rangle_{\mathrm{B}}]. \tag{3.2}$$

Here, $|c\rangle_{\mathrm{A}}$ and $|d\rangle_{\mathrm{A}}$ are the spatial modes after the BS, as shown in Figure 3.1.

The hybrid entangled state can be further written in the desired polarization-

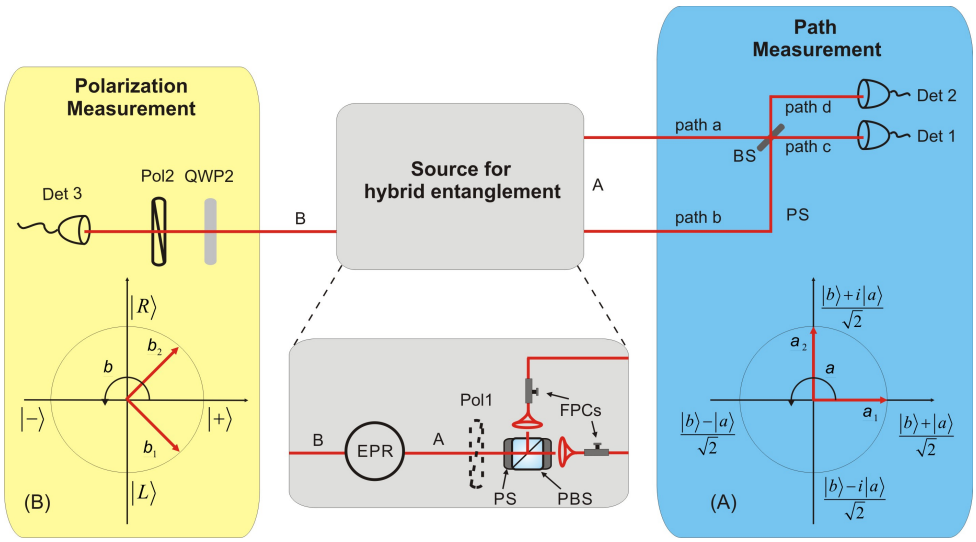

Figure 3.1.: Experimental setup used for demonstrating the hybrid entanglement. Polarization-entangled photon pairs are generated in a Bell state via spontaneous parametric down conversion. Spectral and spatial mode are overlapped by using interference filters with 1 nm bandwidth centered around 710 nm and by collecting the entangled photon pairs into single-mode fibers [KOW01] on both sides. In order to create the hybrid entangled state, as shown in Equation (3.1), the source also consists of a polarizing beam splitter (PBS), two fiber polarization controllers (FPCs) and an additional removable linear polarizer (Pol1) (see main text for details). The photon in spatial mode A is directed towards the interferometric path measurement setup. We combine both paths on a single-mode fiber beam splitter (BS). The length of the whole interferometer is about 2 m. We scan the phase by changing the position of the PBS via a phase scanner (PS). The photon in spatial mode B is directed towards the polarization measurement setup. This consists of a quarter-wave plate (QWP2) and a linear polarizer (Pol2) with the transmission axis oriented along angle ϕ. Together these allow projection of photon B into the desired polarization states. Both photon A and photon B are detected by multi-mode fiber coupled silicon avalanche photodiodes (Det 1, 2 and 3). Photon A is analyzed in the superposition of the two path states along the vectors a_1, a_2 and their orthogonal directions on its Bloch sphere, as shown in the inset (A). Photon B is projected into the polarization states along the vectors b_1, b_2 and their orthogonal directions on its Bloch sphere, as shown in the inset (B). Note that in the polarization measurements of photon B, there is only one detector Det 3. Hence, in order to measure b_1, b_2 and their orthogonal directions, four measurements corresponding to four different alignments of Pol2 are performed.

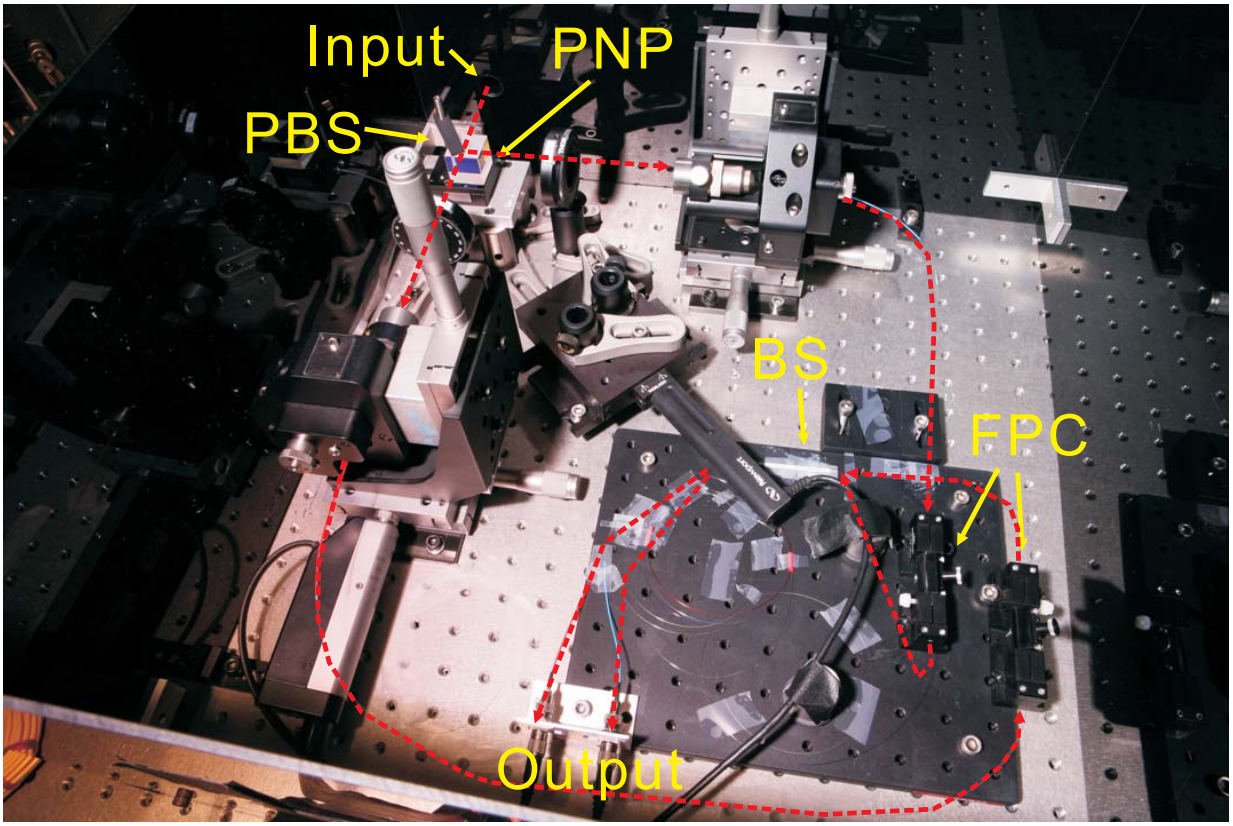

Figure 3.2.: Modified Mach-Zehnder interferometer used for analyzing the path degree of freedom of the hybrid entangled photons. The polarization state of input photon is converted to path state by a polarizing beam splitter (PBS) and then the photon is coupled into a fiber beam splitter (BS). The PBS is mounted on a piezo-nanopositioner (PNP), which scans the phase of the interferometer. Two fiber polarization controllers (FPC) are used to eliminate the polarization distinguishability. The output photon of the interferometer is detected by two multi-mode fiber coupled APDs. The beam paths are shown with red dashed lines.

state basis of photon B:

$$\begin{aligned}|\Phi^{+\prime\prime}_{\text{hybrid}}\rangle \quad = \quad & \frac{1}{2}(\mathrm{e}^{\mathrm{i}\kappa_1}\sqrt{1+\sin(\alpha+\beta)}\,|c\rangle_{\mathrm{A}}\,|\beta\rangle_{\mathrm{B}}) \\ & + \mathrm{e}^{\mathrm{i}\kappa_2}\sqrt{1-\sin(\alpha+\beta)}\,|d\rangle_{\mathrm{A}}\,|\beta\rangle_{\mathrm{B}} \\ & + \mathrm{e}^{\mathrm{i}\kappa_3}\sqrt{1-\sin(\alpha+\beta)}\,|c\rangle_{\mathrm{A}}\,|\beta^{\perp}\rangle_{\mathrm{B}} \\ & + \mathrm{e}^{\mathrm{i}\kappa_4}\sqrt{1+\sin(\alpha+\beta)}\,|d\rangle_{\mathrm{A}}\,|\beta^{\perp}\rangle_{\mathrm{B}}). \end{aligned} \tag{3.3}$$

Here, $|\beta\rangle_{\mathrm{B}} = \frac{1}{\sqrt{2}}(|H\rangle_{\mathrm{B}} + \exp(\mathrm{i}\beta)\,|V\rangle_{\mathrm{B}})$ and $|\beta^{\perp}\rangle_{\mathrm{B}} = \frac{1}{\sqrt{2}}(|H\rangle_{\mathrm{B}} - \exp(\mathrm{i}\beta)\,|V\rangle_{\mathrm{B}})$ respectively, and κ_1, κ_2, κ_3 and κ_4 are the phases of the four different coincidence terms which are not important in the present experiment.

On photon A's side, we tune the local phase difference between the two path quantum states ($|a\rangle_{\mathrm{A}}$ and $|b\rangle_{\mathrm{A}}$), which corresponds to the phase α of the interferometer in Equation 3.3. Scanning this phase α with PS to ($\alpha_1 \equiv 0°$, $\alpha_2 \equiv 90°$, $\alpha_1^{\perp} \equiv 180°$, $\alpha_2^{\perp} \equiv -90°$) and detecting the photon with Det 1 and Det 2 is like projecting the path states of photon A into the states

$$\begin{aligned} |\alpha_1\rangle \quad &\equiv \quad \frac{1}{\sqrt{2}}(|b\rangle + |a\rangle), \\ |\alpha_2\rangle \quad &\equiv \quad \frac{1}{\sqrt{2}}(|b\rangle + \mathrm{i}\,|a\rangle), \\ |\alpha_1\rangle^{\perp} \quad &\equiv \quad \frac{1}{\sqrt{2}}(|b\rangle - |a\rangle), \\ |\alpha_2\rangle^{\perp} \quad &\equiv \quad \frac{1}{\sqrt{2}}(|b\rangle - \mathrm{i}\,|a\rangle). \end{aligned} \tag{3.4}$$

The relation between the position x of the PBS and the phase of the interferometer α is $x = \frac{\alpha\lambda}{2\pi}$.

On photon B's side, we can tune the phase between the two polarization quantum states ($|H\rangle_{\mathrm{B}}$ and $|V\rangle_{\mathrm{B}}$), corresponding to phase β in Equation (3.3). In order to project the polarization states of photon B into the desired states

(shown in the inset (B) of Figure 3.1)

$$
\begin{aligned}
|\beta_1\rangle &= \frac{1}{\sqrt{2}}(|H\rangle_{\mathrm{B}} + \frac{1}{\sqrt{2}}(1-\mathrm{i})\,|V\rangle_{\mathrm{B}}),\\
|\beta_2\rangle &= \frac{1}{\sqrt{2}}(|H\rangle_{\mathrm{B}} + \frac{1}{\sqrt{2}}(1+\mathrm{i})\,|V\rangle_{\mathrm{B}}),\\
|\beta_1\rangle^{\perp} &= \frac{1}{\sqrt{2}}(|H\rangle_{\mathrm{B}} + \frac{1}{\sqrt{2}}(-1+\mathrm{i})\,|V\rangle_{\mathrm{B}}),\\
|\beta_2\rangle^{\perp} &= \frac{1}{\sqrt{2}}(|H\rangle_{\mathrm{B}} + \frac{1}{\sqrt{2}}(-1-\mathrm{i})\,|V\rangle_{\mathrm{B}}),
\end{aligned}
\tag{3.5}
$$

we set QWP2 at -45° and rotate Pol2 such that β is equal to ($\beta_1 \equiv -45^\circ$, $\beta_2 \equiv 45^\circ$, $\beta_1^{\perp} \equiv 135^\circ$, $\beta_2^{\perp} \equiv -135^\circ$), respectively. The relation between the orientation angle of Pol2 and β is $\phi = -\frac{\beta}{2}$.

Experimentally, we measure the correlation between photons A and B in three steps.

Step (I): We inserted Pol1 oriented at 45° into the setup. Then the entanglement is destroyed and photon A is in a coherent superposition of taking path a ($|a\rangle_{\mathrm{A}}$) or path b ($|b\rangle_{\mathrm{A}}$). In Figure 3.3A, we show the single counts of Det 1 (red square dots) and Det 2 (black circular dots). Two oppositely-modulated data curves, as a function of the relative phase change of the two paths, enable us to find the value of the local phase of the interferometer, α. We define $\alpha \equiv 2n\pi$ (n is an integer) when Det 2 has maximum counts.

In Figure 3.3B, The coincidence counts of Det 1 with Det 3 (green square dots) and Det 2 with Det 3 (blue circular dots) oscillate together with the corresponding single counts. This is because the modulations of the single counts detected by Det 1 and Det 2 respectively give rise to the modulations of the coincidence counts between Det 1 and Det 3 and Det 2 and Det 3, given that the single counts detected by Det 3 is constant.

Step (II): We remove Pol1 and measure the coincidence counts of Det 1 with Det 3 and Det 2 with Det 3. From these coincidence counts we construct the correlation coefficients to violate of Bell's inequality. When we take out Pol1,

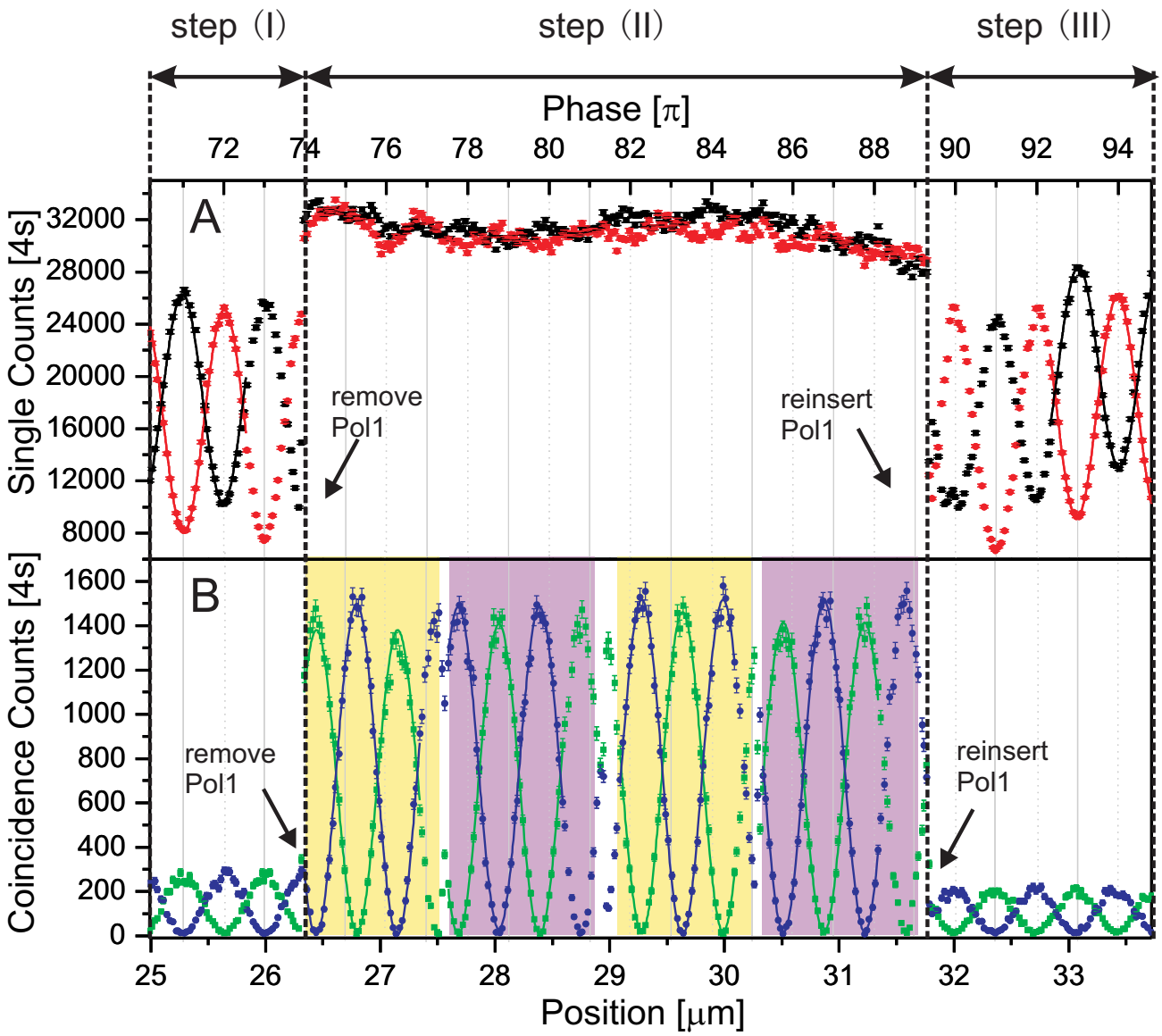

Figure 3.3.: Experimental results for the hybrid entanglement. **A**. The single counts of Det 1 (red square dots) and Det 2 (black circular dots) are fitted with sinusoidal curves (red dash and black solid lines for Det 1 and Det 2 respectively) at the beginning and the end in order to calibrate the local phase of the Mach-Zehnder interferometer. **B**. The coincidence counts between Det 1 and Det 3 (green square dots) and Det 2 with Det 3 (blue circular dots) and the corresponding sinusoidal fits (green dash and blue solid lines respectively). They are used to construct the correlation coefficients in order to violate Bell's inequality. Alternating color shadings are designating the different settings of Pol2. Three experimental steps discussed in the text are illustrated and the actions of removing and reinserting Pol1 are identified with arrows. The error bars represent statistical errors, which are ±1 standard deviations.

there are two important features in the data shown in Figure 3.3.

First, the oscillations of single counts ceased, which can be explained by Equation (3.3). For instance, one can calculate the probability amplitude for $|c\rangle_{\mathrm{A}}$, which is a sum of two oppositely-modulated sinusoidal functions. Thus, the single counts of Det 1 are insensitive to the phase change both "locally" (α) and "nonlocally" (β). The same reasoning applies to the single counts of Det 2 as well.

Second, the coincidence counts behave differently relative to the single counts. The coincidence counts oscillate as we are scanning the local phase (α) and the oscillating amplitude increases. This is because we removed Pol1. More importantly, there is a phase jump between the oscillating curves of the coincidence counts of the two cases with or without Pol1. For example, the coincidence counts between Det 1 and Det 3 are proportional to the joint probability for detecting photon A in path c ($|c\rangle_{\mathrm{A}}$) and detecting the polarization of photon B along β, which is proportional to $1+\sin\alpha$ with Pol1 and proportional to $1+\sin(\alpha+\beta)$ without Pol1. Experimentally, as stated above, we first align Pol2 at -22.5° and Pol1 at -45°, which corresponds to a phase difference of 135°. The measured value is 130°. Then we scan the local phase continuously and sequentially set the orientation angle of Pol2 to the following settings:

$$\begin{aligned} \beta_2 &= -22.5^\circ \\ \beta_1 &= 22.5^\circ \\ \beta_2^\perp &= 67.5^\circ \\ \beta_1^\perp &= 112.5^\circ. \end{aligned} \tag{3.6}$$

These four different settings are designated by four alternated color shaded regions in Figure 3.3B. Due to the reasons stated above, there are phase jumps of the coincidence counts between the different settings of Pol2. The phase jumps between the neighboring regions are expected to be 90°, while 89.2°, 92.4° and 86.8° were the measured values. These four regions of the data are

sufficient to construct the correlation coefficients and to violate Bell's inequality.

Note that this is an analogue of the elegant gedankenexperiment presented in [Zei99] and its realization [Dop98]. The detection of photon B in the equatorial plane of the Bloch sphere (shown in Figure 1.1) will completely erase the which-path information of photon A carried by photon B. Therefore, conditional on the specific polarization measurement of photon B, we obtain interference fringes when we scan the phase of photon A.

Step (III): After we get the coincidence data, we reinsert Pol1 to determine the phase drift during the whole measurement cycle. We measure a 2.0° phase difference on average. Without subtracting accidental coincidence counts, the interference visibilities of the coincidence counts are above 96% for all four settings. The wavelength of all the fits (including single counts and coincidence counts) is fixed to 708.6 nm. The reason of observing the modulations of the single counts of photon A as well as the coincidence counts is the same as stated in step (I).

In Figure 3.3, we show the experimental data of the violation of Bell's inequality between two different degrees of freedom. Given a setting pair (α_i, β_j), which are the orientations of the vectors of the analyzers on the Bloch spheres of photon A and B respectively, the correlation coefficients are defined as:

$$E(\alpha_i, \beta_j) = \frac{C(\alpha_i, \beta_j) + C(\alpha_i^\perp, \beta_j^\perp) - C(\alpha_i^\perp, \beta_j) - C(\alpha_i, \beta_j^\perp)}{C(\alpha_i, \beta_j) + C(\alpha_i^\perp, \beta_j^\perp) + C(\alpha_i^\perp, \beta_j) + C(\alpha_i, \beta_j^\perp)}, \tag{3.7}$$

where $C(\alpha_i, \beta_j)$ and $C(\alpha_i^\perp, \beta_j)$ ($C(\alpha_i^\perp, \beta_j^\perp)$ and $C(\alpha_i, \beta_j^\perp)$) are the coincidence counts of Det 1 with Det 3 and Det 2 with Det 3 respectively, given the local phase of interferometer on photon A's side is α_i ($\alpha_i^\perp$) and the orientation of polarizer on photon B's side is such that $\beta = \beta_j$ ($\beta_j^\perp$) with $i, j = 1, 2$. From the state (3.3), it follows that $E(\alpha_i, \beta_j) = \sin(\alpha_i + \beta_j)$. If local realism is valid, such correlation coefficients must satisfy the CHSH inequality:

$$S = -E(\alpha_1, \beta_1) + E(\alpha_1, \beta_2) + E(\alpha_2, \beta_1) + E(\alpha_2, \beta_2) \leq 2 \tag{3.8}$$

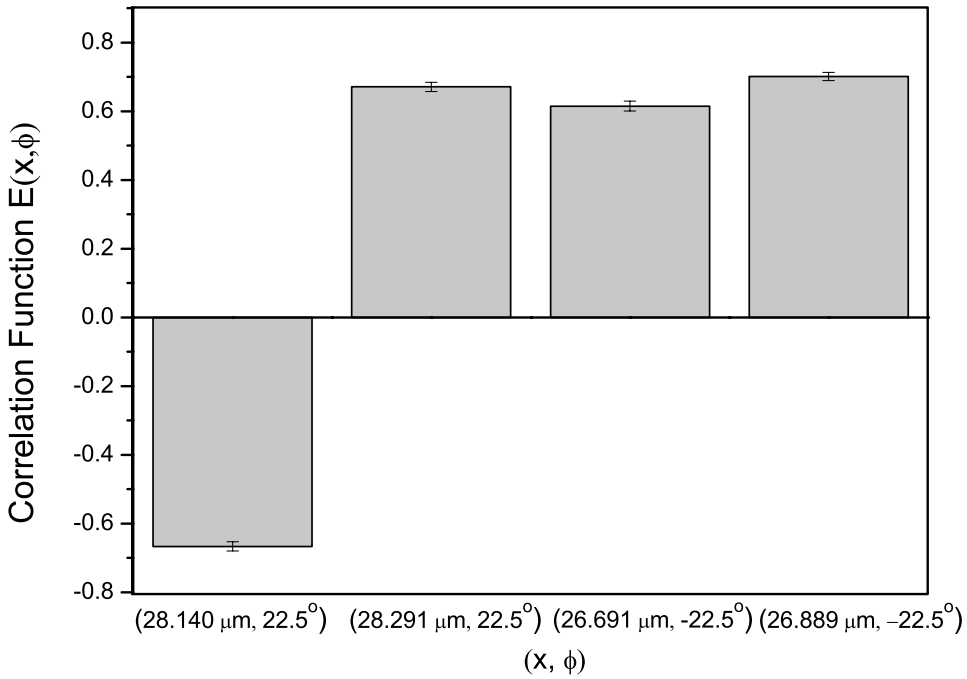

Figure 3.4.: Four correlation functions of the CHSH inequality for the four different settings. Operationally, the setting on Photon A side is given by the position of the phase scanner x and on Photon B side it is the orientation of the polarizer ϕ. This shows the hybrid nature of the entangled photon pair.

Quantum mechanics allows values up to $2\sqrt{2}$.

The correlation coefficients are calculated from the data from Figure 3.3, which are

$$\begin{aligned} E(28.140\,\mu\text{m}, 22.5^\circ) &= -0.666 \pm 0.014, \\ E(28.291\,\mu\text{m}, 22.5^\circ) &= 0.671 \pm 0.014, \\ E(26.691\,\mu\text{m}, -22.5^\circ) &= 0.615 \pm 0.014, \\ E(26.889\,\mu\text{m}, -22.5^\circ) &= 0.701 \pm 0.012. \end{aligned} \tag{3.9}$$

These results are shown in Figure 3.4. The S-parameter calculated from those four correlation coefficients is $S = 2.653 \pm 0.027$, which violates the classical bound ($|S| = 2$) by more than 24 standard deviations.

Hybrid entanglement is not only of fundamental interest. It also could be useful in quantum information processing, e.g. in a quantum repeater [DLCZ01]. It

is not limited to the case of path (linear momentum) and polarization, as shown here, but also should be possible for other degrees of freedom, e.g. frequency, orbital angular momentum etc. of photons. Additionally, the hybrid entanglement between polarization and path are of crucial importance for the non-local quantum eraser experiment, which is presented in the following chapter.

3.2. The non-local quantum eraser

We perform two experiments to demonstrate the non-local quantum eraser with two different length scales. In the first experiment (in Vienna), the system and environment photons are separated by 50 m and connected via an optical fibre between two laboratories. In the second experiment (on the Canary Islands), they are separated by 144 km and connected via a free-space link.

3.2.1. Vienna experiment

The concept of our experiment is the following: We produce hybrid entangled photon pairs, with entanglement between the path of one photon, denoted as the system photon, and the polarization of the other photon, denoted as the environment photon [MQK+09]. The system photon is sent to an interferometer, and the environment photon is sent to a polarization measurement setup. Due to the entanglement of the two photons, the environment photon's polarization carries which-path information of the system photon. A specific polarization measurement performed on the environment photon decides whether we acquire which-path information of the system photon and observe no interference or erase which-path information and observe interference. The scheme of the Vienna experiment is shown in Figure 3.5.

First, we prepare a polarization-entangled state [KMW+95]:

$$|\Phi\rangle^+ = \frac{1}{\sqrt{2}}(|H\rangle_s|V\rangle_e + |V\rangle_s|H\rangle_e), \tag{3.10}$$

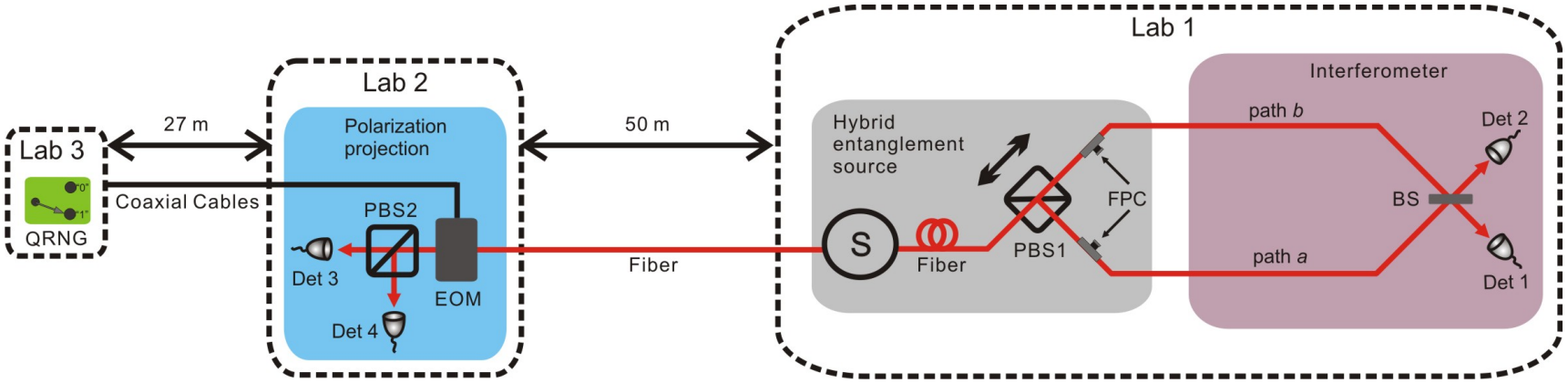

Figure 3.5.: Scheme of the Vienna experiment on the non-local quantum eraser: In Lab 1, the source (S) emits polarization-entangled photon pairs via type-II spontaneous parametric down-conversion, where good spectral and spatial mode overlapping is achieved by using interference filters with 1 nm bandwidth and by collecting the entangled photon pairs into single-mode fibres on both sides [KOW01]. They are subsequently converted into a hybrid entangled state with a polarizing beam splitter (PBS1) and two fibre polarization controllers (FPC), which eliminate the polarization distinguishability of the system photon. The system photon is delayed by 28 m single-mode fiber in order to fulfill the space-like separation condition. The interferometric measurement of the system photon is performed with a single-mode fibre beam splitter (BS) with the path lengths of 2 m, where the relative phase between path a and path b is adjusted by moving PBS1's position with a piezo-nanopositioner (not shown). We put the polarization projection setup of the environment photon in Lab 2, Which is about 50 m away from Lab 1. The polarization projection setup consists of one electro-optical modulator (EOM) and another polarizing beam splitter (PBS2). Both photons are detected by silicon avalanche photodiodes (Det 1-4). In Lab 3, a quantum random number generator (QRNG) decides the polarization measurement basis of the environment photon. See text for details.

where s and e index the system and environment photons, respectively. The orthogonal polarization states of the system photon are coherently converted into two different interferometer path states $|a\rangle_s$ and $|b\rangle_s$ via a polarizing beam splitter and two fiber polarization controllers, as introduced in Section 3.1.2. This generates the hybrid entangled state [MQK+09]:

$$|\Phi_{hybrid}\rangle_{se} = \frac{1}{\sqrt{2}}(|b\rangle_s|V\rangle_e + |a\rangle_s|H\rangle_e). \tag{3.11}$$

From the state given in the Equation (3.11), one can see that the polarization of the environment photon carries the path information of the system photon because of this hybrid entanglement. Hence, we are able to perform two complementary polarization measurements on the environment photon and acquire or erase which-path information of the system photon, respectively:

(i) We project the environment photon into the $|H\rangle/|V\rangle$ basis. If the environment photon is detected in $|H\rangle$, we know for certain that the corresponding system photon takes path a ($|a\rangle_s$). And if the environment photon is detected in $|V\rangle$, we know for certain that the corresponding system photon takes path $b(|b\rangle_s)$. In both cases, which-path information of the system photon is revealed and no interference shows up.

(ii) As an alternative measurement, we can project the environment photon into the $|L\rangle/|R\rangle$ basis, where $|L\rangle$ and $|R\rangle$ denote the left-handed or right-handed circular polarization states. It is convenient to write state (3.11) in the $|L\rangle/|R\rangle$ basis as:

$$|\Phi_{hybrid}\rangle_{se} = \frac{1}{2}((|a\rangle_s + \mathrm{i}|b\rangle_s)|L\rangle_e + (|a\rangle_s - \mathrm{i}|b\rangle_s)|R\rangle_e). \tag{3.12}$$

Due to the hybrid entanglement, if the environment photon is detected in $|L\rangle$, the corresponding system photon is in the state of $\frac{(|a\rangle_s+\mathrm{i}|b\rangle_s)}{\sqrt{2}}$. The system photon has a equal probability of taking path a or b and thus no which-path information of the system photon can be obtained, therefore, interference appears. The same reasoning applies to the case when the environment photon is detected in $|R\rangle$,

where the system photon is in the state of $\frac{(|a\rangle_s - \mathrm{i}|b\rangle_s)}{\sqrt{2}}$. Note that there is a π phase difference between $|a\rangle_s$ and $|b\rangle_s$ in these two cases, which corresponds to a π phase shift in the interference patterns.

In order to fulfill the Einstein locality conditions for a conclusive test, the relevant events must be identified: (E) the emission of the photon pair from the source, (C) the choice of the polarization measurement basis of the environment photon, (P) the polarization projection of the environment photon, and (I) all events related to the system photon inside the interferometer including: the entry of the system photon into the interferometer, the propagation of it in the interferometer and the exit of it from the interferometer. Locality can be enforced by space-like separations of (I) and (P), (I) and (C), as well as (E) and (C), as shown in Figure 3.6.

The space-like separation between (I) and (P) is achieved by sending the environment photon via a 55 m (275 ns) single-mode fibre to the polarization measurement setup in Lab2 located 50 m away from Lab1 (straight spatial distance), as shown in Figure 3.5. The system photon is delayed with a 28 m (140 ns) single-mode fibre in Lab1 and then sent into a 2 m (10 ns) fibre based interferometer. In Lab2, the above mentioned polarization measurements (i) and (ii) are implemented by a fast electro-optical modulator (EOM) followed by a polarizing beam splitter. In measurement (i) the EOM is switched off, and in measurement (ii) the EOM is switched on by applying a quarter-wave voltage. The repetition rate of the EOM is about 2 MHz and the on-time of EOM is about 20 ns, which results in a switching duty cycle of approximately $20\text{ns} \times 2\text{MHz} = 4.0\%$.

To fulfil the space-like separation between (C) and (I) as well as (C) and (E), the type of measurement is randomly determined by a quantum random number generator (QRNG) located in Lab3 with a 27 m straight spatial distance to Lab2 and a 77 m distance to Lab1. The random bits are transmitted via a 35 m (175 ns) coaxial cable to the EOM.

The QRNG developed for this experiment is based on a previous work of

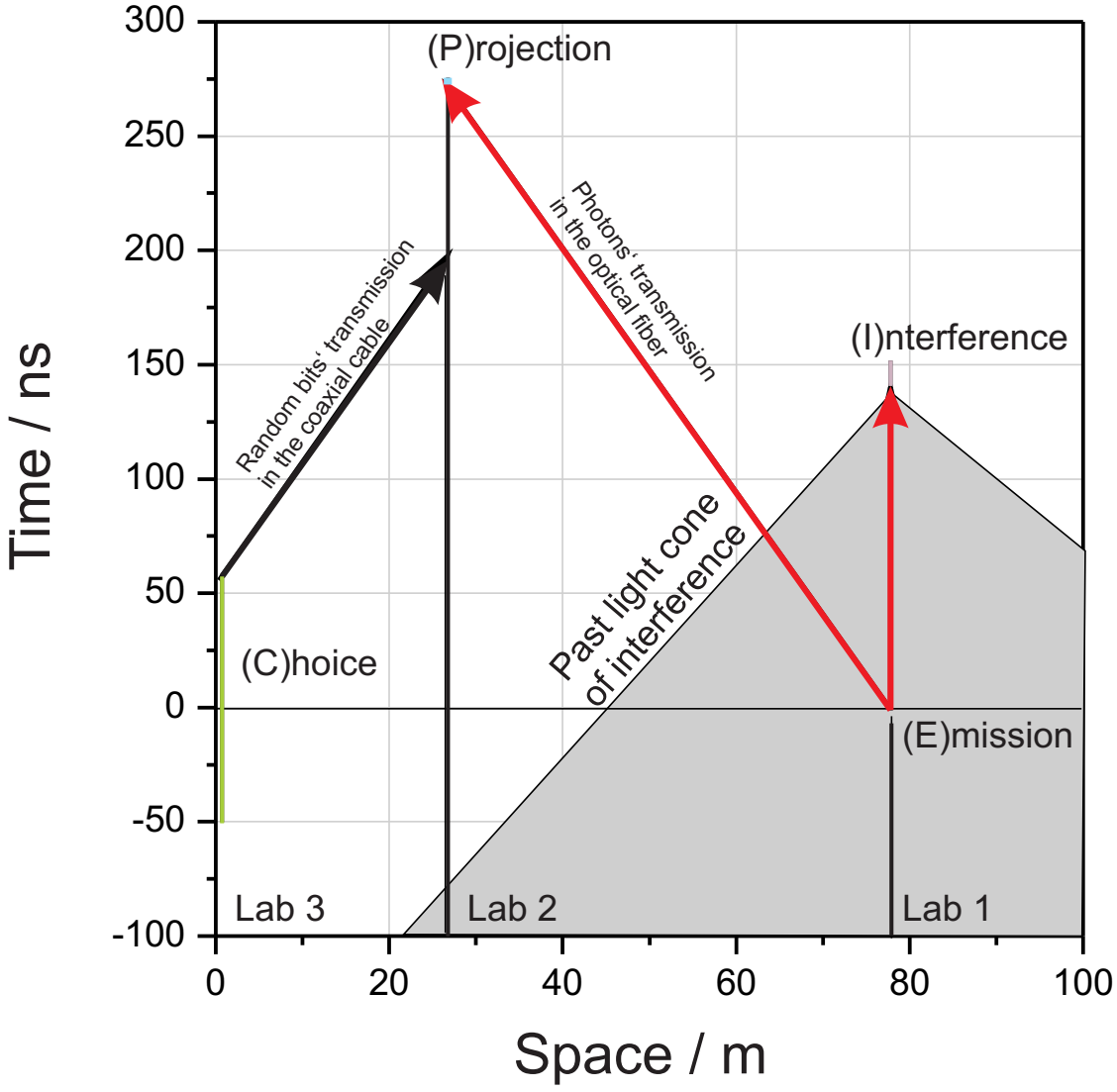

Figure 3.6.: Space-time diagram of the non-local quantum eraser experiment performed in Vienna. The choice-related events (C) and the polarization projection of the environment photon (P) are space-like separated from all events of the interferometric measurement of the system photon (I). Additionally, events (C) are also space-like separated from the emission of the entangled photon pair from the source (E). The red arrows indicate the photons transmission in the optical fibers. The black arrow indicates the random bits' transmission in the coaxial cable. The shaded area is the past light cone of event (I). With this configuration, Einstein locality conditions are fulfilled.

Thomas Jennewein [JAW+00]. The QRNG employs the splitting single photons at a 50:50 beam splitter as physical source of randomness. Each individual photon propagating through the beam splitter, has equal probability to be either transmitted or reflected [Wei99, Sch09]. Quantum physics predicts that the each individual decision is genuinely random. The total amount of the delays occurring in the electronics and optics of our QRNG was measured to be 75 ns. Allowing for another 33 ns (3 times of the autocorrelation time of QRNG), to be sure that the autocorrelation of the QRNG output signal is sufficiently low, it was safe to assume that the specific choice of a measurement would not be influenced by any event happening more than 108 ns earlier. This is why the choice event (C) consists of a series of events in Figure 3.6 instead of being a single well-defined event.

In total, we excluded any influences between the measurements of the two photons as well as between the choice event and the system photon, at a speed equal to or less than speed of light. It is worthy to note that, since (C) is space-like separated from (E), we also excluded any causal influence between the QRNG and the photon source [Bel64]. In [KYK+00], however, the choice was made by the environment photon itself and was situated in the future light cone of both the emission of the photon pair and the measurement event of the system photon. Therefore, in that experiment it is in principle conceivable that the emission event and system photon measurement event could have influenced the choice, which then only appears to be free or random.

In Figure 3.7, we present the experimental results for measurements of the system photon conditioned on the detection of the environment photon with Det 4. In Figure 3.7**A**, the probabilities that the system photon either took path a or b are shown when measurement (i) is performed. When the environment photon is subjected to measurement (i) and detected in the state $|V\rangle_e$, the probability that the system photon propagated through path a is $P(a||V\rangle_e) = 0.023 \pm 0.005$, and the one for propagation through path b is $P(b||V\rangle_e) = 0.978 \pm 0.005$. These are obtained by blocking two arms alternatively and by measuring

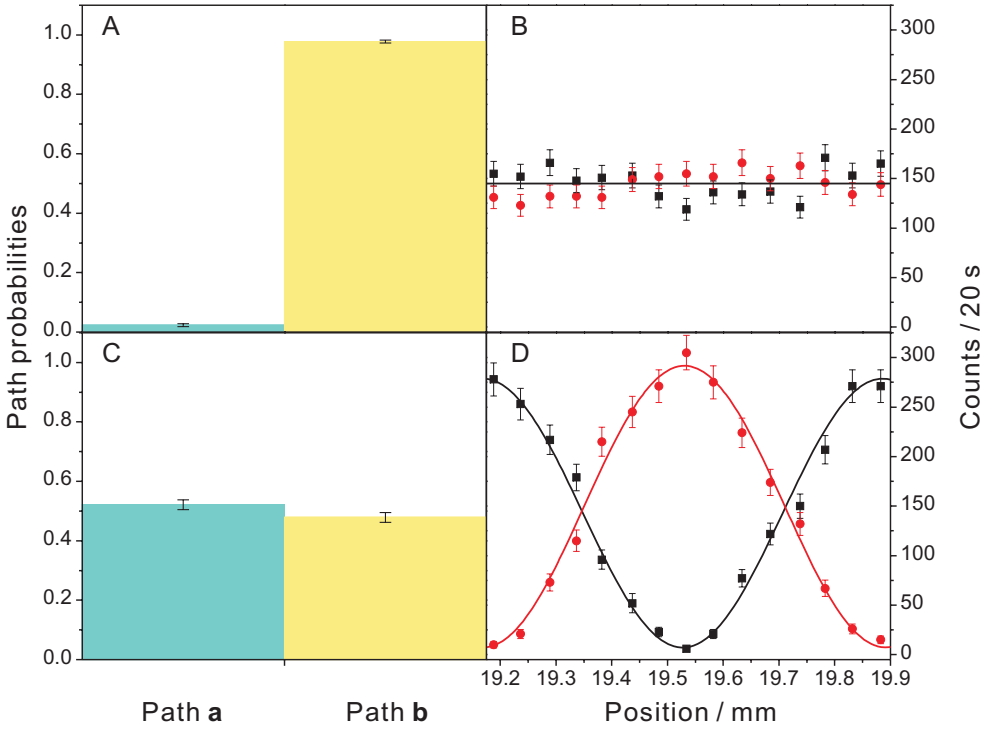

Figure 3.7.: Results of the non-local quantum eraser obtained in the Vienna experiment. The counts of Det 1 and Det 2 conditional on the detection of the environment photon in Det4 under Einstein locality conditions are shown in: **A**. When measurement (i) is performed (EOM was off), the detection of the environment photon in the state $|V\rangle_e$ revealed the which-path information of the system photon. This is confirmed by the fact that the system photon propagates through path a and b with probabilities 0.023 ± 0.005 (green) and 0.978 ± 0.005 (yellow), respectively. **B**. Consequently, phase insensitive counts are obtained, where the residual oscillations' amplitudes are smaller than the statistical error of the mean value of the counts, which is indicated with a black line. **C**. When measurement (ii) is performed (EOM is on), detection of the environment photon in $|R\rangle_e$ erases which-path information of the system photon. The probabilities of the system photon propagating through path a and b are 0.521 ± 0.016 (green) and 0.478 ± 0.016 (yellow), respectively. **D**. The coincidence counts of Det 1 and Det 4 (black squares), and Det 2 and Det 4 (red disks) are shown as a function of the position change of PBS1 and fitted by two oppositely-modulated sinusoidal curves. The average visibility is $95.1\% \pm 1.8\%$. The error bars are calculated from the Poisson statistics.

the sum of the coincidence counts between Det 1 and Det 4, as well as Det 2 and Det 4.

To quantify the amount of the which-path information acquired upon measurement (i) or (ii), we used the so-called which-path information parameter [GY88, Eng96]:

$$I_i = |P(a||V\rangle_e) - P(b||V\rangle_e)|, I_{ii} = |P(a||R\rangle_e) - P(b||R\rangle_e)|, \tag{3.13}$$

where I_i and I_{ii} stand for that the which-path information parameters for measurement (i) and (ii) respectively. The measured value of information parameter I_i of 0.955 ± 0.007 reveals almost full which-path information of the system photon. As a consequence, when the relative phase between path a and b is scanned, no interference pattern is observed, as shown in Figure 3.7B.

On the other hand, when the environment photon is subjected to measurement (ii) and detected in the state of $|R\rangle_e$, we obtain the probabilities of the system photon propagating through path a, $P(a||R\rangle_e) = 0.539 \pm 0.016$, and through path b, $P(b||R\rangle_e) = 0.461 \pm 0.016$ (Figure 3.7C). In this case, the which-path information is erased, as confirmed by I_{ii} having the small value 0.077 ± 0.022. Accordingly, interference shows up with the visibility of $V_{ii} = 95.1 \pm 1.8\%$ as shown in Figure 3.7D. This visibility is defined as $V = (C_{max} - C_{min})/(C_{max} + C_{min})$, where C_{max} and C_{min} are the maximum and minimum counts of the system photon conditioned on the detection of environment photon with Det 4, respectively. These results conclusively confirm the nonlocal nature of the quantum eraser.

We want to emphasize that the results shown in Figure 3.7 have been acquired with two independent time-tagging units. For each environment photon, we record the time stamp of the detection event and the random bit from QRNG. For system photon, we recorded the position of the piezo-nanopositioner and the time stamp of the detection event. These data are then compared and sorted to reconstruct the coincidence counts, long after the experiment has

been finished [WJS+98].

We realize five additional different space-time scenarios, whose space-time diagrams are illustrated in Figure 3.8. Experimentally we use optical fibres and coaxial cables to delay and distribute the optical and electrical signals in order to fulfil the requirements of each scenario. For instance, in order to achieve scenario V we arrange the location of each apparatus in the following way. The environment photon is delayed locally (close to the source and interferometer) with a 630 m single-mode fibre and there is no delay on the system photon side. The direct spatial distance between the QRNG and interferometer is about 101 m. The random bits used to control the EOM are transmitted with a 630 m coaxial cable. In scenario V, the choice of the measurement basis of the environment photon is space-like separated from the interference events of the system photon. Therefore, based on special relativity, no subluminal or luminal physical signal can travel between these two events and causally influence each other. But from our experimental results, whether interference can be observed or not strongly depends on the choice.

The other scenarios are realized in similar ways by changing the length of the fibres and coaxial cables. The experimental arrangement and results of all six different space-time scenarios are summarized in Figure 3.9. There similar results, within the statistical error, are obtained. We therefore conclude that, in agreement with quantum mechanics, there are no observable differences in the experimental results in all six different space-time scenarios.

In order to quantitatively demonstrate the quantum eraser and the complementarity principle under Einstein locality conditions, we employ a bipartite complementarity inequality [GY88, Eng96], namely,

$$I^2 + V^2 \leq 1. \tag{3.14}$$

Instead of investigating the properties of single particles (realized in [JWG+08]), here I and V are the parameters for two particles, as defined above. When an

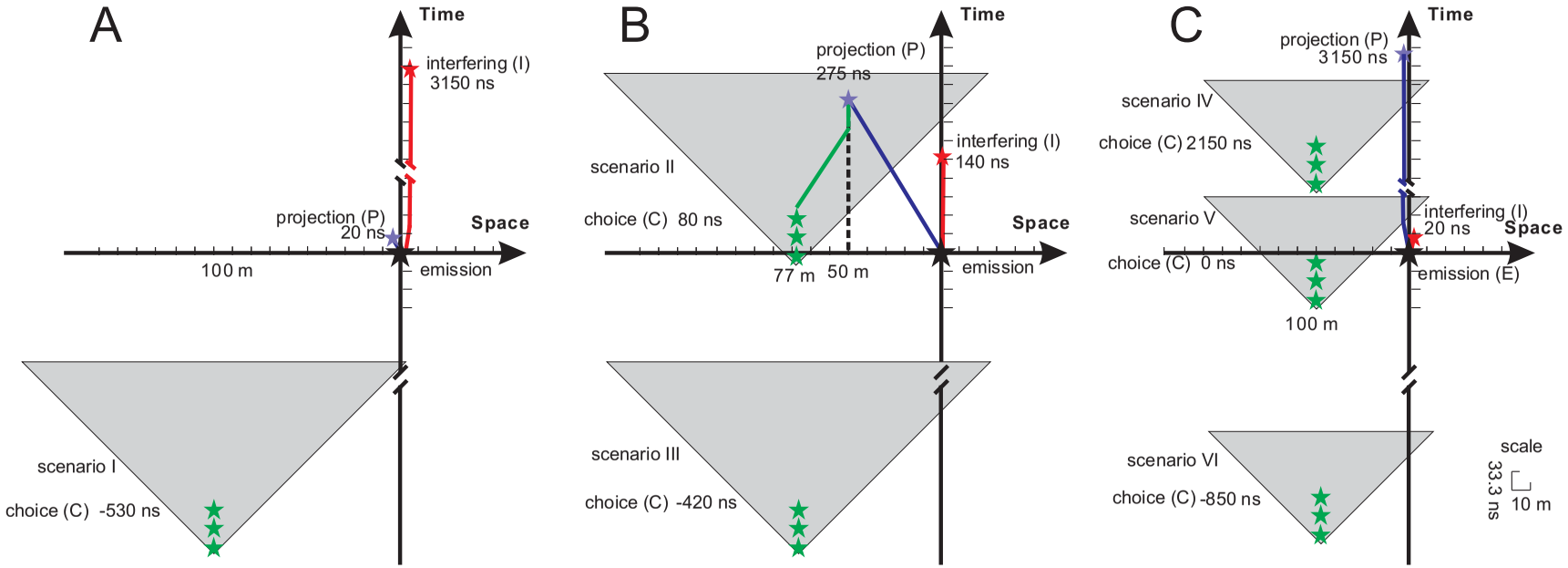

Figure 3.8.: Six space-time scenarios arranged in Vienna experiment are illustrated with space-time diagrams in **A**, **B** and **C**. The green stars stand for the choice-related events (C) and the grey light cone represents for the future light cone of the choice. The polarization projection (P) of the environment photon according to the choice is represented by blue star, the interfering event of the system photon (I) by the red star and the emission event of the photon pairs (E) by the black star. Each unit of the space-axis and the time-axis stands for 10 m and 33.3 ns respectively. Scenarios I, III to VI are not scaled because of the large amount of delay on either the system or the environment photon side.

Scenarios	Relations between events									Results	
	(P) before (I)	(P) s.l. sep. (I)	(P) after (I)	(I) before (C)	(I) s.l. sep. (C)	(I) after (C)	(E) before (C)	(E) s.l. sep. (C)	(E) after (C)	Path information of measurement (i)	Visibility of measurement (ii)
I	X					X			X	95.6% ±1.6%	95.0% ± 2.0%
II		X			X			X		95.5% ± 1.6%	95.1% ± 1.8%
III		X				X			X	95.3% ± 1.5%	95.2% ± 1.8%
IV			X	X			X			95.7% ± 1.6%	94.6% ± 2.1%
V			X		X			X		95.7% ± 1.6%	94.3% ± 2.1%
VI			X			X			X	95.4% ± 1.6%	95.0% ± 1.9%

Figure 3.9.: Summary of the space-time relations and experimental results for the six scenarios performed in the Vienna experiment. There are three different relations possible relations for two events. For the events (P) and (I), e.g., there are the relations: (P) before (I), (P) s.l. sep. (I), and (P) after (I), which mean that in all reference frames including the lab frame event (P) happens time-like before, in a space-like separated region with respect to, and time-like after event (I), respectively. There is an 'X' when the relation is fulfilled in the corresponding scenario. Scenario II is the scenario discussed in the text and shown in Figure 3.7. When the measurement (i) was performed, there is no interference as a consequence of almost full which-path information of the system photon was acquired via the polarization projection of the environment photon. When measurement (ii) was performed, high visibility interference fringes showed up indicating that nearly all of the which-path information was erased.

ideal experimental arrangement is realized, equality in Inequity (3.14) holds. Under locality, we measure I and V separately as a function of the applied voltage of the EOM, which changes the polarization projection basis of the environment photon. Hence, it allows us to obtain a continuous transition between measurement (i) and (ii). For each measurement, according to the QRNG output, the voltage of the EOM is randomly and rapidly switched between 0 and a definite value. The results are shown in Figure 3.10. The dashed line is the ideal curve, where $I^2 + V^2 = 1$. The solid line is computed using actual non-ideal experimental parameters, which were measured independently. There is an excellent agreement between the calculation and the experimental data.

The imperfections include: The measurement of the which-path information is limited by the correlation in the $|H\rangle/|V\rangle$ basis (98.0%) and the imperfection of the PBS (extinction ratio is about 180:1). These are taken into account by a correction factor η_I of about 0.97. On the other hand, the visibility V, is limited by the correlation in the $|L\rangle/|R\rangle$ base (96.9%), the imperfection of the PBS, the imperfection of polarization rotation of the Pockels cell (extinction ratio is about 250:1). This is taken into account by a correction factor η_V of about 0.95. So the inequality (3.14) becomes: $\frac{I^2}{\eta_I^2} + \frac{V^2}{\eta_V^2} \leq 1$, which can be rewritten as:

$$V \leq \eta_V \sqrt{(1 - \frac{I^2}{\eta_I^2})}. \tag{3.15}$$

When all the other imperfections are excluded, the upper limit should be reached. The experimental data agrees well with $\eta_I = 0.97$ and $\eta_V = 0.95$.

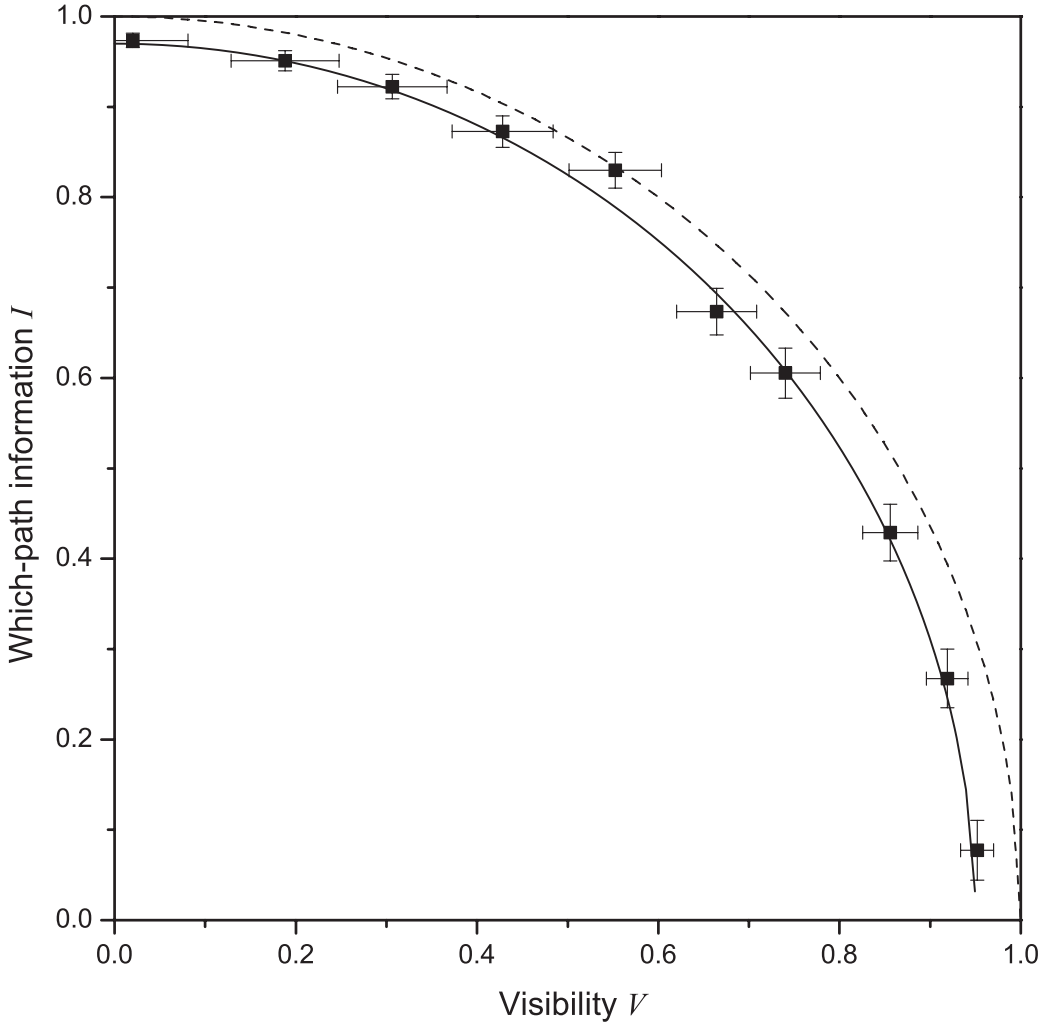

Figure 3.10.: Experimental test of the complementarity inequality under Einstein locality conditions manifested by a trade-off of the which-path information parameter, I, and visibility, V. The dashed line is the ideal curve given in Equation (3.14). The solid line is the estimation taking actual experimental imperfections into account, which are measured independently. It is $I = 0.97\sqrt{1 - (\frac{V}{0.95})^2}$.

3.2.2. Canary Islands experiment

In a dramatically expanded experiment, we utilize significantly larger spatial and temporal separations and build the nonlocal eraser setup with a 144 km free-space link between the interferometer and the polarization projection setup, as shown in Figure 3.11. Two labs are located on two of the Canary Islands, La Palma and Tenerife.

There are three main differences between the Canary Islands's experiment and Vienna experiment. First, the brightness of the photon pair source is enhanced in order to obtain a reasonable signal-to-noise ratio after signal attenuation over the 144 km free-space link. The polarization-entangled photon pairs are generated by type-II SPDC in a 10 mm ppKTP crystal which is placed inside a polarization Sagnac interferometer [FHP+07]. Using a 405 nm laser diode with a maximum output power of 50 mW, we generate 810 nm degenerate entangled photon pairs in the $|\Psi^-\rangle$ Bell state with a production rate of 3.5×10^7 Hz. This number is inferred from locally detected 250000 photon pairs/s at a pump power of 5 mW and a coupling-detecting efficiency of 27% (calculated from the ratio between the coincidence and singles counts). Furthermore, operation at 5 mW pump power yields a locally measured visibility of the generated entangled state in the $|H\rangle/|V\rangle$ ($|+\rangle/|-\rangle$) basis of about 99% (98%) (accidental coincidence counts subtracted).

Secondly, the duty cycle of the EOM is increased to about 97%, which allows us to obtain more signals than in the Vienna experiment. In this experiment, the EOM serves as a switchable half-wave plate (HWP) for polarization rotations of 0° and 45°. We align the optical axes of the Rubidium-Titanyl-Phosphate (RTP) crystals, used in the EOM, to 22.5°. Additionally, we place a quarter-wave plate (QWP) with its optical axis oriented parallel to the axis of the RTP crystals in front of the EOM. Applying a positive quarter-wave voltage (+QV) causes the EOM to act as an additional QWP, such that the overall effect is the one of a HWP at 22.5°, rotating the polarization by 45°. By applying a negative quarter-wave voltage (-QV), the EOM compensates the action of the QWP, such that

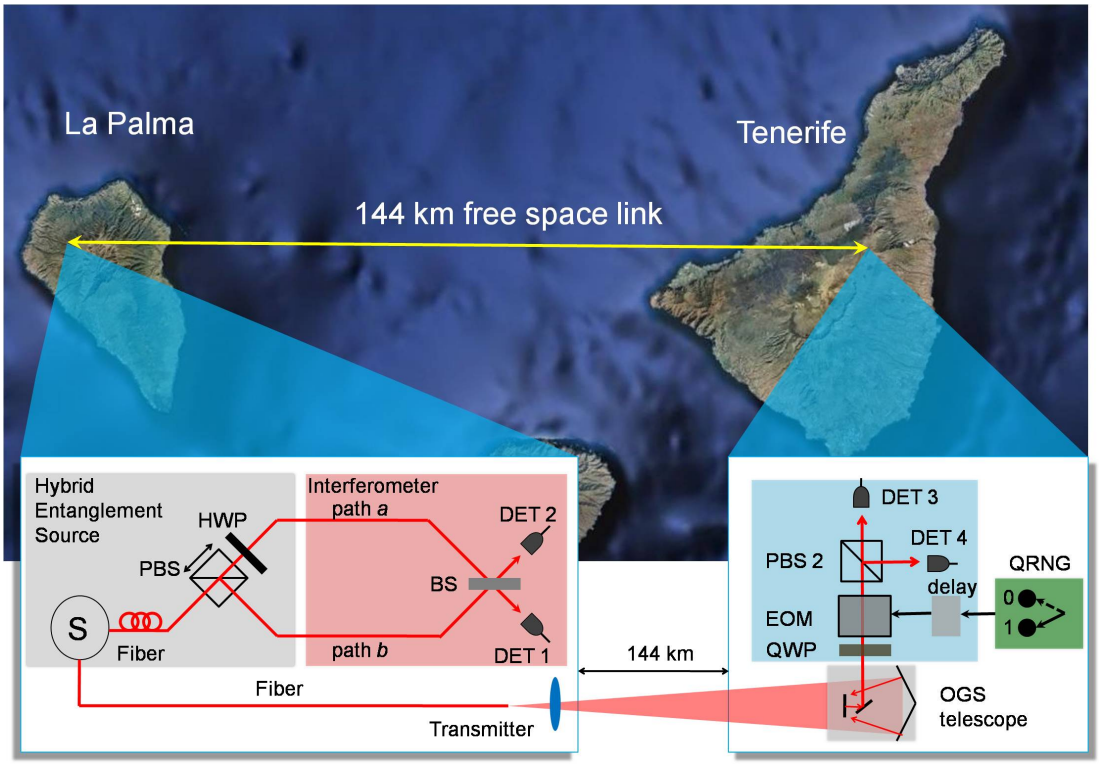

Figure 3.11.: The layout of the Canary Islands' experimental setup. The two parts of the setups are distributed in two labs on the Canary Islands of La Palma and Tenerife respectively, which are spatially separated by 144 km. In La Palma, the source (S) emits polarization-entangled photon pairs. The interferometer setup consists of a polarizing beam splitter (PBS), which is used to convert the orthogonal polarizations of the system photon into two different optical paths a and b, a half-wave plate oriented at 45° to eliminate the polarization distinguishability of the two paths, and a 50:50 beam splitter (BS) to analyze the superposition of the two path states. The length of the whole interferometer is about 0.5 m. The PBS is equipped with a piezo-nanopositioner which allows scanning of the relative phase between paths a and b via changing its position. In Tenerife, the polarization projection setup consists of a quarter-wave plate (QWP), an electro optical modulator (EOM) and a polarizing beam splitter (PBS2), which together project the environment photon into either the $|H\rangle/|V\rangle$ or the $|+\rangle/|-\rangle$. A quantum random number generator (QRNG) defines the choice for the experimental configuration fast and randomly. A delay card, which stores the random bits generated from the QRNG, is used to adjust the relative time delay between the event of the choice and the other events. Both the system photon and the environment photon are detected by silicon avalanche photodiodes (Det 1-4). Independent data registrations are performed by individual time tagging units on both the system and the environment photons' sides. The time bases on both sides are established using the Global Positioning System (GPS).

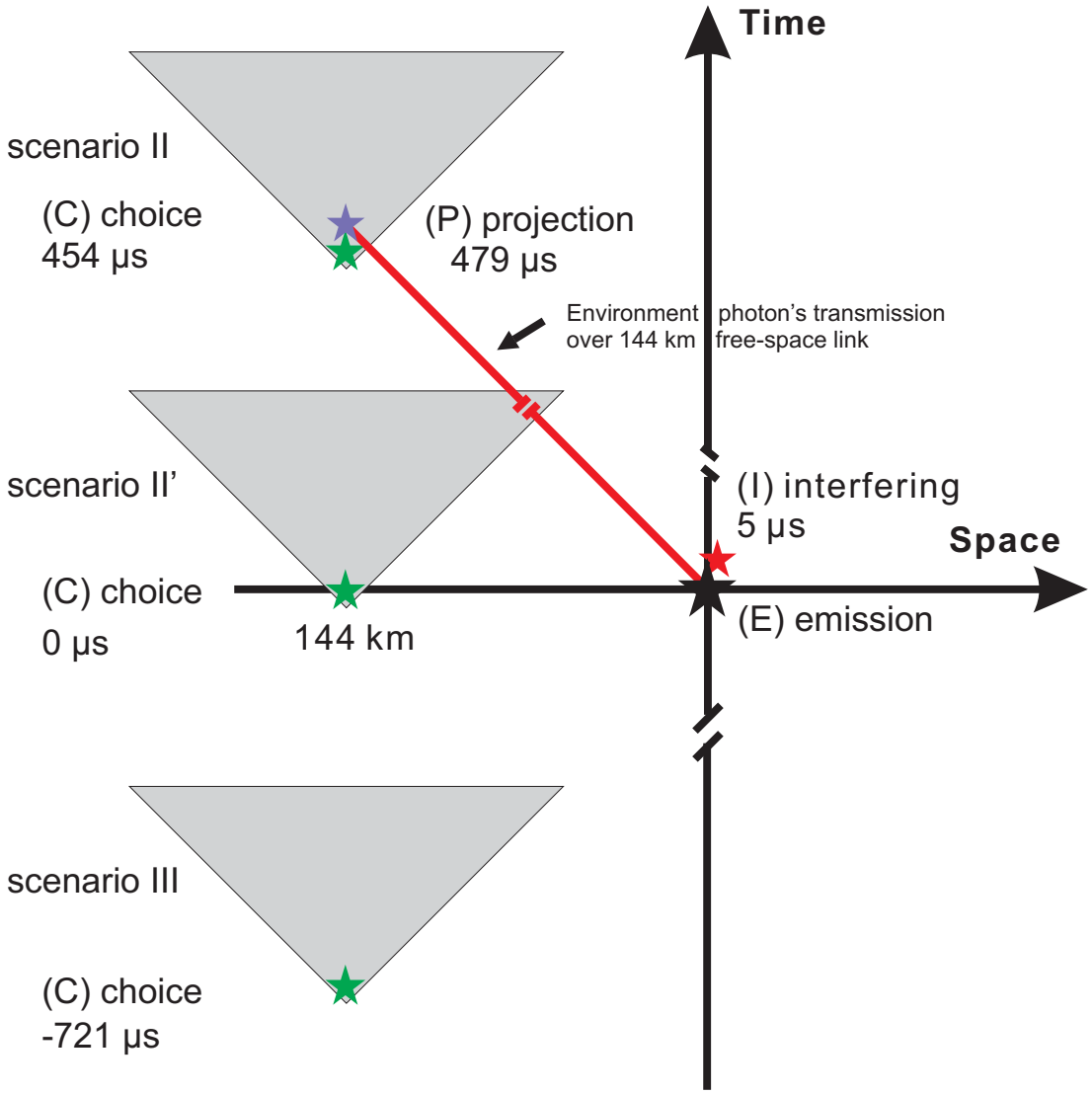

Figure 3.12.: The space-time diagrams of three experiments, performed between the Canary Islands, correspond to two different scenarios. The green stars stands for the choice (C) of the polarization projection basis of the environment photon (made by the QRNG) and the grey triangles for the future light cones of the choice for three different space-time scenarios respectively. The polarization projection of the environment photon (P) according to the choice, all events related to the system photon inside the interferometer (I) and the emission of the photon pairs (E) are blue, red and black stars respectively. Scenario II, II' and III are the arrangements where the event (C) is later, at the same time and earlier than the event (E) respectively in the lab reference frame.

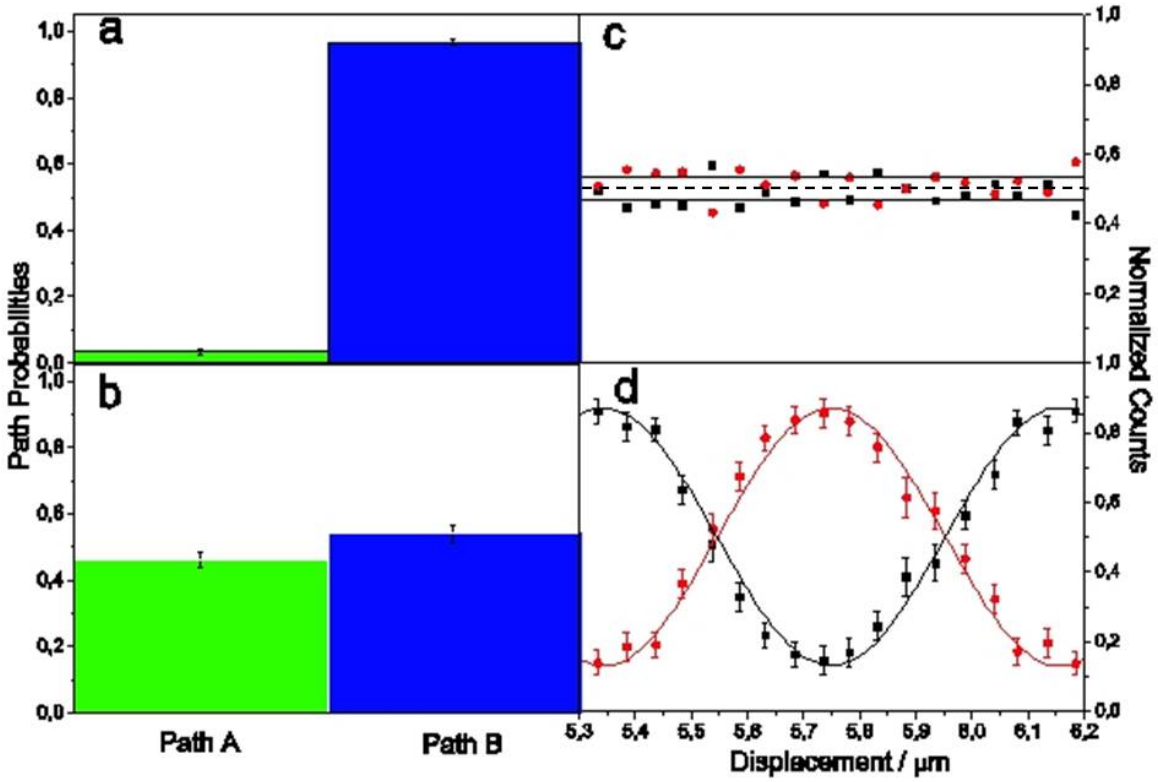

Figure 3.13.: Results of the Canary Island experiment. We show the counts of Det 1 and Det 2 conditional on the detection of the environment photon in Det 4 for the space-time scenario II. **a**. When measurement (i) is performed, the probabilities of the system photon propagating through path a and b are 0.034 ± 0.008 and 0.966 ± 0.008 respectively. This reveals almost complete which-path information and hence no interference is obtained, as shown in **c**. **b**. When measurement (ii) is performed, the probabilities of the system photon propagating through path a and b are 0.461 ± 0.025 and 0.539 ± 0.025 respectively. This reveals almost no which-path information and hence interference is obtained, as shown in **d**. In **c**, a dashed line indicates the mean value of the normalized counts (equal to 0.5). Plus and minus one standard deviation from the mean value is indicated with two black lines. In **d**, two oppositely-modulated sinusoidal fringes with average visibility 0.75 ± 0.016 can be seen. This is the raw visibility. The visibility after subtracting the accidental coincidence counts is 95.0%. The error bars are calculated using Poisson statistics.

the overall polarization rotation is 0°. As in the Vienna experiment, a QRNG determines which voltage will be applied. A random bit "0" ("1") requires a polarization rotation of 0° (45°) and -QV (+QV) is applied to the EOM. A certain setting is not changed until the occurrence of an opposite trigger signal. However, since our QRNG is balanced, within statistical uncertainties, +QV and -QV are applied equally often. For optimal operation of the EOM a toggle frequency of 1 MHz is chosen. The rise time of the EOM is measured to be < 15 ns. Thus to be sure that the switching process has been finished, we discard all photons which are detected less than 35 ns after a trigger signal. The on-time of the EOM is $\frac{1}{1\text{MHz}} - 35\ ns = 965$ ns. Therefore, this kind of operation results in a switching duty cycle of 96.5%.

Thirdly, a 1 km long fibre (5 μs) is used to delay the system photon, which allows an unambiguous space-like separation between the events (P) and (I), as shown in Figure 3.12.

Two different space-time arrangements are realized. Note that the labels of the space-time scenarios are the same as in Figure 3.9. Scenario II and II' are the same in terms of space-time relations, but the amount of the delay of choice event (C) with respect to the events related to the interferometer (I) is different in the lab reference frame. Within scenario II', the speed of a hypothetical superluminal signal from the event (C) to the events (I) is about 96 times the speed of light. Within scenario II, the choice event (C) happens approximately 449 μs after the events (I) in the reference frame of the source, which adds to the record for the amount of delay by more than 5 orders of magnitude than the earlier realization in [KYK+00].

The results are shown in Figure 3.13. When we perform measurement (i), the information parameter, defined in Equation 3.13, is $I_i = 0.932 \pm 0.016$ and no interference is obtained. When we performed measurement (ii), the average visibility is 0.756 ± 0.016. The reduced visibility is mainly coming from the reduced signal-to-noise ratio due to the attenuation of the free-space link (35 dB). The average visibility becomes as high as 95.0% after subtracting the

accidental coincidence counts. The space-time relations of relevant events and the results of three experimental configurations are summarized in Figure 3.14.

In conclusion, we have realized a nonlocal quantum eraser using hybrid entangled states with spatial separations of 77 m (Vienna) and 144 km (Canaries), respectively. The latter case represents the largest spatial and temporal separation in quantum eraser experiments. Our observations show that, in agreement with quantum mechanics, the complementarity principle is independent of the spatial and temporal arrangement of the choice and measurements. Consequently, our results rule out for the first time all theories in which the system photon either behaves definitely as a wave or as a particle and causal influences establish the observed correlations.

	Relations between events					Results	
	B s.l. sep. C	C s.l. sep. A	C after A	D s.l. sep. A	D after A	Path information of measurement (i)	Visibility of measurement (ii)
II	X	X		X		93.2%±1.6%	75.6%±1.6%
II'	X	X		X		93.0%±1.6%	77.6%±1.7%
III	X		X		X	92.8%±1.4%	75.1%±1.3%

Figure 3.14.: Summary of the space-time relations between events and the results for three scenarios of the Canary Islands' experiments. The conventions of the relationship between different events are the same as that in Figure 3.9. The results of Scenario II are also shown in Figure 3.13. When the measurement (i) is performed, there is no interference as a consequence of almost full which-path information of the system photon is acquired via the polarization projection of the environment photon. When measurement (ii) is performed, interference fringes show up because of the erasure of the which-path information.

4. Delayed choice entanglement swapping

In this chapter, I will present an experimental realization of delayed-choice entanglement swapping, as described in Section 2.5. First, I will introduce a high-speed tunable beam splitter, which will be used as a switchable bipartite-state analyzer in the delayed-choice entanglement-swapping experiment. The performance of this high-speed tunable beam splitter is tested with heralded single photons from SPDC. Second, we use this high-speed tunable beam splitter to perform two-photon interference under Einstein's locality condition, which extends Wheeler's delayed-choice gedankenexperiment from single-photon interference to two-photon interference. Finally, I will describe the realization of the delayed-choice entanglement-swapping experiment.

4.1. A high-speed tunable beam splitter

There are two motivations for building a high-speed tunable beam splitter (TBS): First, it is an essential component of some experiments to test the foundations of quantum physics, importantly the delayed-choice entanglement swapping [Per00, JABZ05] and complementarity of two bipartite entangled systems [BAZ05]. Second, it is also a crucial building block of modern quantum information processing. This device can be used as a high-speed single-photon router and integrated into an array of SPDC photon pair sources. Assisted by classical feed-forward, one can build a nearly on-demand single-photon source from these probabilistic SPDC photon pairs sources [MBC02, SW07]. One can also utilize it for quantum teleportation [BBC+93, BPM+97], entangle-

ment swapping [ZZHE93, PBWZ98, JWPZ02], quantum telecloning [ZZZ+05] with active switching and one-way quantum computation with feed-forward [PWT+07].

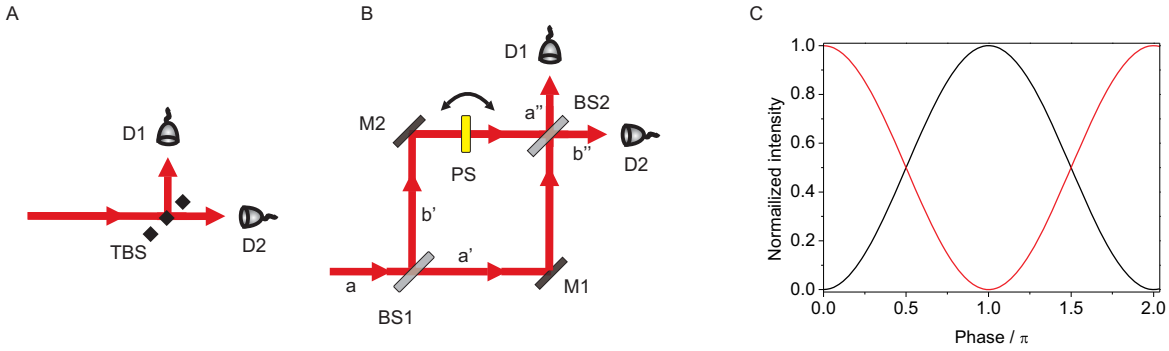

Figure 4.1.: The concept of a tunable beam splitter. **A**. The splitter ratio of a tunable beam splitter (TBS) can be adjusted and hence the counts from detector 1 (D1) and 2 (D2) vary according to the splitting ratio of this TBS. **B**. The realization of a TBS with a Mach-Zehnder interferometer, which consists of two beam splitters (BS1 and BS2), two mirrors (M1 and M2) and a phase shifter (PS). The splitting ratio can be tuned by adjusting PS. **C**. The normalized intensities of D1 (red line) and D2 (black line) are plotted as a function of the phase. For instance, if phase is 0 there is no beam splitting and if the phase is $\frac{\pi}{2}$ the splitting ratio is 1.

In order to build a tunable beam splitter (Figure 4.1A), one would need a knob to adjust the splitting ratio of the TBS. One of the possibilities is to vary the phase of a Mach-Zehnder interferometer, as shown in Figure 4.1B. The splitting ratio can be tuned by adjusting the phase of the Mach-Zehnder Interferometer (MZI). It is represented as the intensity modulations detected by D1 and D2. The normalized intensities of D1 (red line) and D2 (black line) are plotted as a function of the phase in Figure 4.1C. For instance, if phase is 0 there is no beam splitting and if the phase is $\frac{\pi}{2}$ the splitting ratio is 1.

As shown in Figure 4.2, we employ a MZI to realize the high-speed TBS. It consists of two 50:50 beam splitters, mirrors and most importantly two electro-optic modulators (EOM), with one in each arm of the MZI. Here we use Rubidium-Titanyl-Phosphate (RTP) crystal as the electro-optic material

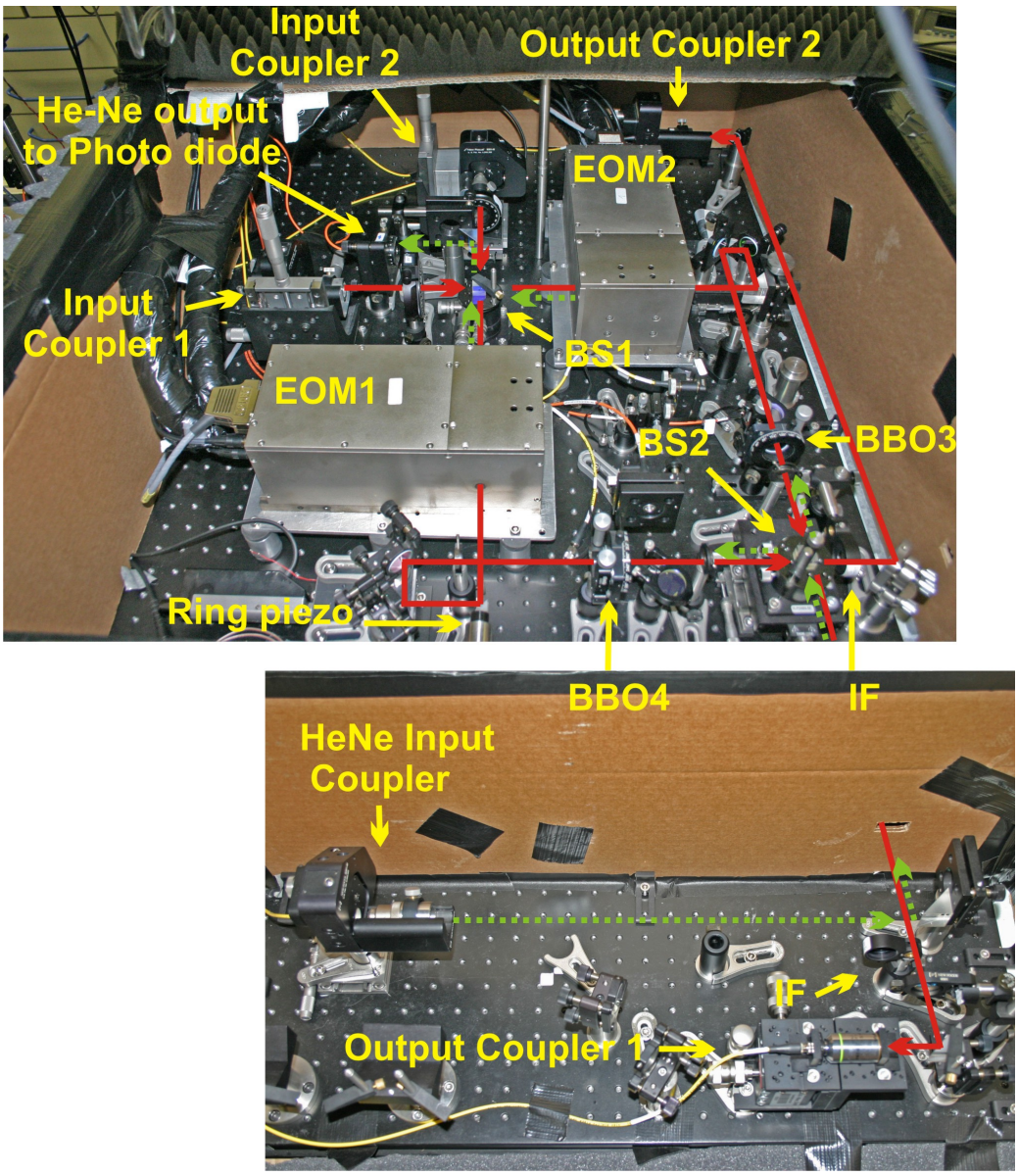

Figure 4.2.: Pictures of the high-speed tunable beam splitter. On the input and output couplers we use single-mode fibers for spatial filtering. The 3 nm bandpass interference filters (IF) guarantee good spectral filtering. To actively stabilize the interferometer we use a He-Ne laser counter propagating through the setup (dashed green line) and its intensity is detected by a photo diode. This reference signal is sent to a proportional-integral-derivative (PID) control circuit which controls a ring piezo-transducer inside the interferometer. Additionally, we enclose the setup in a box with acoustical isolation material (see text for details).

for our EOMs. The RTP crystal completely lacks piezo-electric resonances up to 200 kHz and shows very rare resonances up to 2.5 MHz. These features enable us to drive the EOMs with a high operating frequency. The electronics we use to drive these EOMs are double-push-pull switches (custom-built by Bergmann Messgeräte). The individual push-pull switch has some restrictions due to their electrical circuits: the time between an on and off event (i.e. the effective on-time) for an individual push-pull switch must not be shorter than 50 ns in order to not damage the device. This limits the minimum on-time window duration. A double-push-pull switch is made by two single push-pull switches and the above-mentioned restriction no longer applies as both single switches only have to switch once each to get an effective on-off cycle [BPJ+07]. Therefore, by using double-push-pull switches one can operate the EOM with a short on-time (about 20 ns) and a high repetition rate (up to 5 MHz). A pulse generator produces the pulse sequence for the double-push-pull switches driver from a trigger signal. See appendix for the details of the EOM and its controlling devices.

The interferometer is built in an enclosed box made from acoustic isolation materials in order to stabilize the phase passively. Additionally, an active phase stabilization system is implemented by using an auxiliary beam from a power-stabilized He-Ne laser counter-propagating through the whole MZI. This beam has a little transversal displacement from the signal beam, thus it picks up the phase fluctuations in the interferometer. The corresponding intensity variation of the output He-Ne laser beam is measured with a silicon photon detector (PD) and the signal is fed into an analogue proportional-integral-derivative (PID) control circuit. A ring-piezo transducer attached to one of the mirrors in the MZI is controlled by this PID and compensates the phase fluctuation actively.

The active optical axes of both EOMs are oriented along 45° and the voltages applied to them are always of the same amplitudes but with opposite signs. Varying the voltage applied to the EOMs, we are able to the tune the phase of the MZI. Hence the whole MZI acts as a high-speed TBS and the splitting ratio

is controlled by the applied voltage of the EOMs. We define the phase of the MZI to be 0 when all the photons that enter from input a exited into f. This also corresponds to the phase locking point of the MZI.

The functionality of the TBS is best seen by describing how the quantum state of polarization and path of the input photon evolves in the MZI. Since the optical axes of the EOMs are along 45°, without loss of the generality, it is convenient to decompose the input polarization into $|+\rangle$ and $|-\rangle$ basis. The arbitrarily polarized input photon's quantum state in spatial mode a is $|\Psi\rangle = (\alpha|+\rangle + \beta|-\rangle)|a\rangle$, where $|\alpha|^2 + |\beta|^2 = 1$. It evolves as:

$$\begin{aligned}
|\Psi\rangle \quad \xrightarrow{\text{BS1}} \quad & \frac{1}{\sqrt{2}}(\alpha|+\rangle + \beta|-\rangle)(|c\rangle + \mathrm{i}|d\rangle) \\
\xrightarrow{\text{EOMs}} \quad & \frac{1}{2}(\alpha e^{\mathrm{i}\phi(U)}|+c\rangle + \mathrm{i}\alpha|+d\rangle + \beta|-c\rangle + \mathrm{i}\beta e^{\mathrm{i}\phi(U)}|-d\rangle) \\
\xrightarrow{\text{BS2}} \quad & \sin\frac{\phi(U)}{2} e^{\mathrm{i}(\frac{3\pi}{2} - \frac{\phi(U)}{2})}(\alpha|+\rangle - \beta|-\rangle)|e\rangle \\
& + \cos\frac{\phi(U)}{2} e^{\mathrm{i}(\frac{\pi}{2} + \frac{\phi(U)}{2})}(\alpha|+\rangle + \beta|-\rangle)|f\rangle,
\end{aligned} \tag{4.1}$$

where $\phi(U)$ is the voltage dependent phase given by the EOMs. From Equation 4.1, it is straightforward to see that one can tune the splitting ratio of outputs of spatial mode e and f by varying $\phi(U)$. The transmittivity (T) and reflectivity (R) of the TBS are:

$$\begin{aligned}
T &= \sin^2\frac{\phi(U)}{2}, \\
R &= \cos^2\frac{\phi(U)}{2}.
\end{aligned} \tag{4.2}$$

Additionally, the input polarization will be rotated from $(\alpha|+\rangle + \beta|-\rangle)$ to $(\alpha|+\rangle - \beta|-\rangle)$ in the spatial mode e. This polarization rotation can be dynamically compensated with an additional EOM on path e applied with half-wave voltage to flip the polarization.

We test the performance of this TBS with the setup as in Figure 4.3. By using

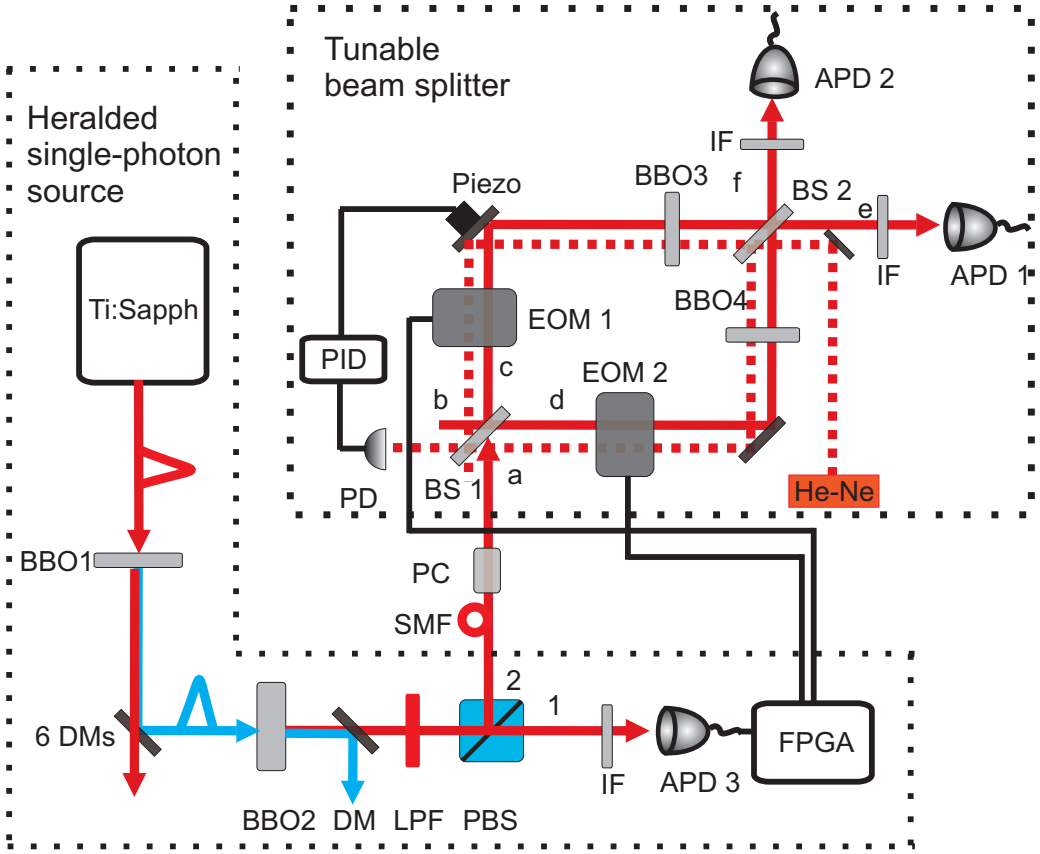

Figure 4.3.: Experimental setup of testing the high-speed tunable beam splitter with heralded single photons. Femtosecond laser pulses from a Ti:Sapphire oscillator (λ= 808 nm) are up-converted with a BBO crystal (BBO1) cut for type-I phase-matching. This produces vertically polarized second harmonic pulses center at 404 nm. The correlated photon pair is generated from the crystal BBO2, which is cut for type-II collinear phase-matching. Since the photon pair is generated in the same time, by detecting photon 1 in the transmitting arm of the polarizing beam splitter (PBS) with avalanche photon detector (APD 3), we can herald the presence of photon 2 in the reflecting arm of PBS. Photon 2 is delayed with optical fiber (about 100 m in length) and the polarization rotation of the fiber is compensated by a polarization controller (PC). Then it is sent to the high-speed tunable beam splitter. The output TTL pulse of the detection of photon 1 is used to trigger two EOMs, which are placed in both arms of the interferometer, respectively. The scheme of using two EOMs is crucial, because the tunability of this high-speed tunable beam splitter relies on the first-order interference. By employing two EOMs with one on each arm, we can maintain photon 1's polarization states through paths c and that through path d to be indistinguishable and hence allow the first-order interference. See text and Equation 4.1 for details. The time delay between trigger pulse and the arrival of the photon 2 at EOMs is adjusted via the field-programmable gate array (FPGA) logic.

the correlation of the emission time of the photon pair generated via SPDC, we herald the presence of one photon with the detection of its twin, the trigger photon. The detection signal of the trigger photon is used to control the EOMs in the TBS, which operate on the heralded single photon.

Femtosecond laser pulses from a Ti:Sapphire oscillator (4 W average power, 80 MHz repetition rate, 140 fs pulse duration, λ= 808 nm) are up-converted with a 0.7 mm BBO crystal (BBO1) cut for type-I phase-matching at 808 nm. This produces vertically polarized second harmonic pulses center at 404 nm with an average power of around 250 mW. In this experiment, we deliberately attenuate the UV power in order to reduce the higher order emissions from the SPDC which would otherwise compromise the result. In SPDC process, in addition to the probability of generating a pair of photons there is also a finite probability for generating more than one pair, which decreases the quality of the heralded single photon source. This latter generation probability increases nonlinearly with interaction strength of the pump and nonlinear crystal.

The up-converted pulses and the remaining fundamental pulses are separated with a combination of six dichroic mirrors (6 DMs), which are all highly reflective at 404 nm and highly transmissive at 808 nm. The collinear photon pairs are generated via SPDC from a 2 mm BBO crystal (BBO2) cut for collinear type-II phase-matching at 808 nm. See Appendix for the details of SPDC. The UV pulses are removed from the down converted photons with a dichroic mirror (DM) and long pass filter (LPF). The photon pair is separated by a polarizing beam splitter (PBS) and each photon is coupled into a single-mode fiber (SMF). The transmitted photon (photon 1) is detected by APD 3 directly and the output TTL pulse is used to control the EOMs, while the reflected photon (photon 2) is guided into the single-mode fiber with the length of 100 m and then to the TBS. The short on-time of the EOMs we set, 20 ns, requires fine time delay adjustment of the TTL pulse used to trigger the EOMs. We achieve this with a field-programmable gate array (FPGA) electronics. Because of the short coherence time of the photon 1, which is defined by the transmission bandwidth

of the interference filter (IF, 3 nm), one has to match path lengths of the two arms of the MZI accurately. We minimize the path length difference by maximizing the interference visibility. Inside the TBS, two pairs of crossed oriented BBO crystals (BBO3 and BBO4) are placed in each arm of the MZI in order to compensate the unwanted birefringence induced by optical elements.

One important feature of our TBS is polarization independence, i.e. it works for any polarized photons. Experimentally this is tested by preparing the polarization state of the photon 2 with fiber polarization controller (PC). The experimental results for horizontal polarization are shown in Figure 4.4a and for $+45^\circ$ in Figure 4.4b. We fit the sinusoidal curves to the measurement results and determined that the Michelson visibilities of horizontal and $+45^\circ$ are $95.9\% \pm 0.2\%$ and $95.3\% \pm 0.3\%$, respectively. For input b, we have observed the same results, which allows us to use this device to perform a two-photon interference experiment.

Two other important features of our TBS are high-frequency operation and short rise and fall time. Note that, rise and fall time are typical parameters used to quantify the response speed of devices and are defined as the time required for a signal to change from 10% and 90% of the step height for the rise time (90% and 10% for the fall time). These are challenges for both the electro-optical active crystals and the driving electronics. As stated above, thanks to the advantages of both RTP crystals, and the custom-made electronics, we are able to drive the EOMs with frequencies up to 2.5 MHz. We measure the rise/fall time of the TBS with a continuous wave laser with a Si photon detector and an oscilloscope. As shown in Figure 4.5, the π-phase modulated optical signal shows a rise time to be 5.6 ns. The insertion loss of the TBS is about 70%, which is mainly due to single-mode fiber coupling and the Fresnel loss at optical surfaces. With current technology, it is in principle possible to improve the transmission of a TBS to be about 95%, including Fresnel loss on each optical surface (0.5% per surface) and a finite fiber coupling efficiency of 98%.

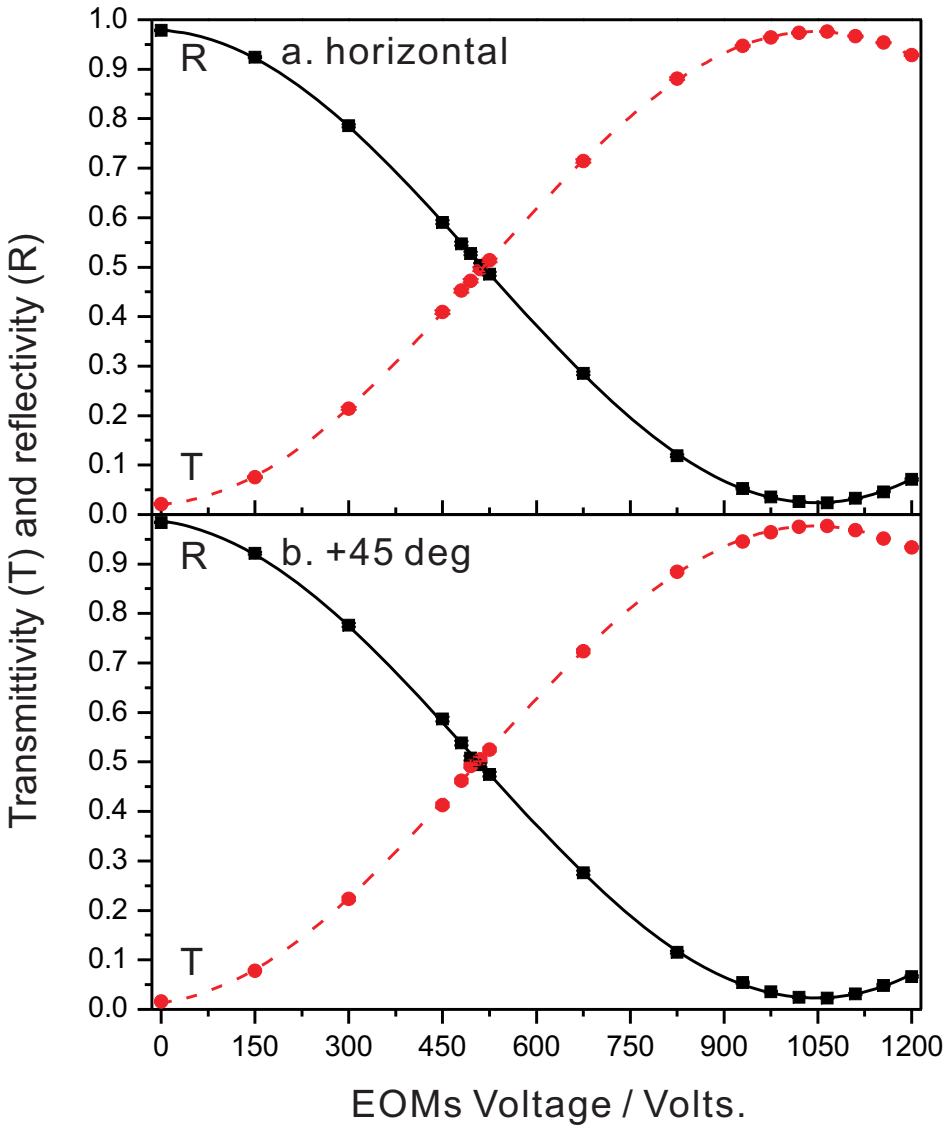

Figure 4.4.: Demonstration of the polarization independence of the TBS. Experimental results for **a** the horizontally and **b** +45° polarized single photons. The black squares (red circles) are the values of the reflectivity (transmittivity) of the ultrafast tunable beam splitter, which are calculated from the coincidence counts between APD 2 and APD 3 (APD 1 and APD 3) and fitted with black solid (red dash) sinusoidal curve. Error bars represent statistical errors of ±1 standard deviation.

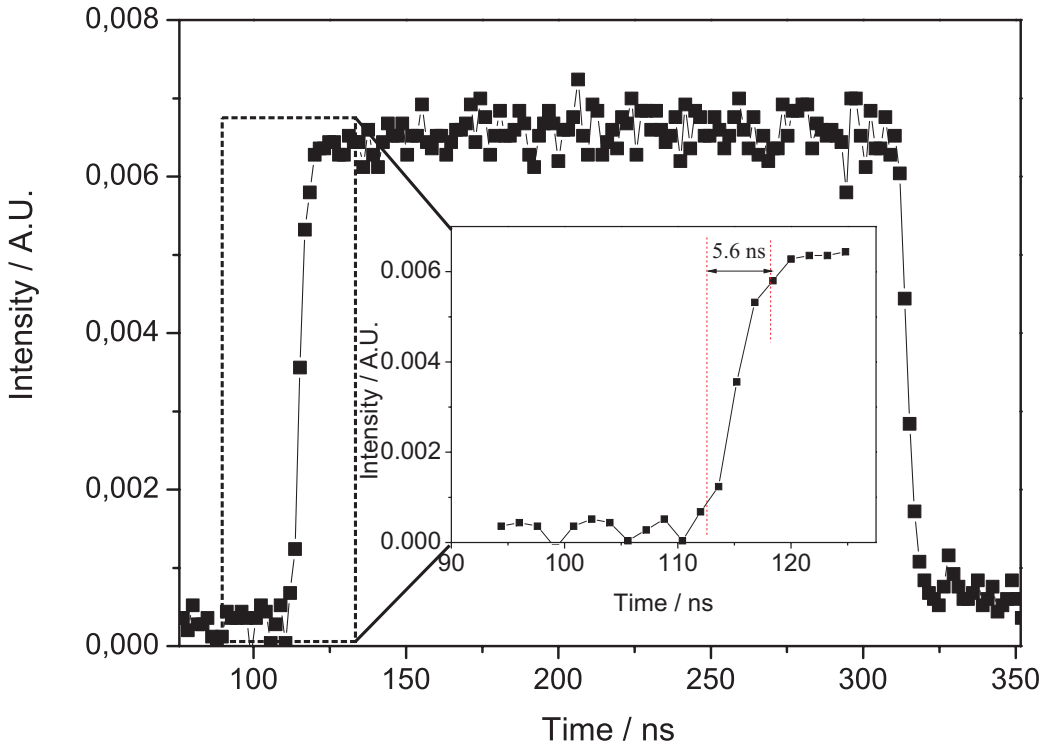

Figure 4.5.: Experimental result for a π-phase modulated optical signal. These are measured with a continuous wave laser and a Si photon detector. A rise time, which refers to the time required for a signal to change from 10% and 90% of the step height, of 5.6 ns is obtained.

4.2. Two-photon interference under Einstein's locality condition

As reviewed in the Chapter 2, Wheeler strikingly illustrated the complementarity principle with single-photon interference in the delayed-choice gedankenexperiment. The experimental scheme is shown in Figure 4.6A, where one decides to observe the wave property or the particle property after the photon's entry into MZI. Two recent experiments [JWG+07, JWG+08], which were carried out with a single photon as input, showed the validity of the complementarity principle even if the choice and the entry of the photon into the interferometer were space-like separated, as discussed in Chapter 2.

However the complementarity principle should not be restricted to single-

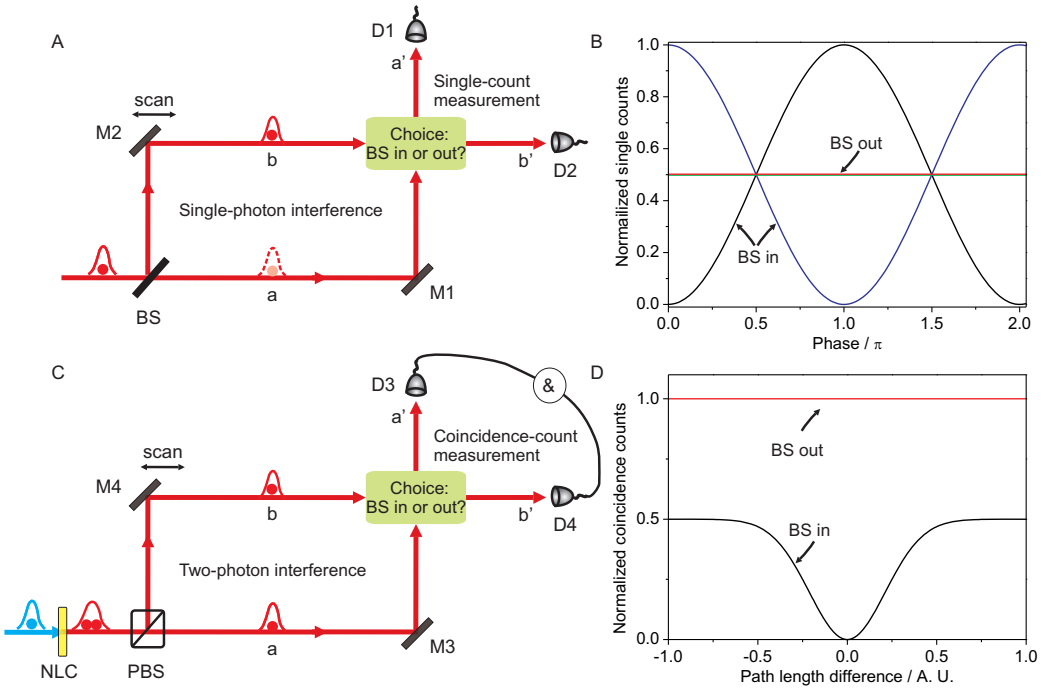

Figure 4.6.: Comparison of Wheeler's delayed-choice experiment (single-photon interference) and delayed-choice two-photon interference experiment. **A**. The scheme of Wheeler's delayed-choice experiment. In this experiment, one and only one photon is present in the Mach-Zehnder interferometer (MZI), and this single photon interferes with itself. One can choose whether to put in the output beam splitter (BS) or take it out after the photon's entry into MZI. **B**. The predicted results of Wheeler's delayed-choice experiment can be obtained via the detection of the single counts with D1 and D2 as a function of relative phase between two paths, realized by scanning a mirror (M2). If the BS is put in, interference patterns show up (black and blue curves). If the BS is taken out, there are no interference patterns (overlapped red and green curves). **C**. The scheme of delayed-choice two-photon interference experiment. In this experiment, the pump photon (blue) decays into a pair of down-converted photons (red) via type-II SPDC in the nonlinear crystal (NLC). A polarizing beam splitter (PBS) separates them into path a and b of the Hong-Ou-Mandel (HOM) interferometer. A half-wave plate (HWP) on path b oriented at 45° erases the polarization distinguishability and hence allows for the fourth-order interference. One can choose whether to put in the BS or take it out after the photon's entry into HOM interferometer. **D**. The predicted results of delayed-choice two-photon interference experiment can be obtained via the detection of the coincidence counts between D3 and D4 in **C** as a function of length differences between two paths, realized by scanning a mirror (M4). If the BS is put in, destructive interference pattern, HOM dip, shows up (black curve). If the BS is taken out, there is no interference pattern (red curve).

photon interference (second-order interference). It should apply to more phenomena, for instance the so-called Hong-Ou-Mandel (HOM) two-photon interference (fourth-order interference) as we will present next [HOM87]. This type of interference is different from the above mentioned second-order interference. It originates from the statistics of bosons and the unitary transformation of a beam splitter. For a comprehensive review on HOM two-photon interference, see Ref. [Kal08]. The experimental scheme of two-photon interference under Einstein's locality condition is shown in Figure 4.6B, where one allows the two photons generated from nonlinear crystal (NLC) to interfere or not, after the photons' entry into the HOM interferometer.

The crucial part of this experiment is the implementation of fast and random complementary measurements, which allow the two photons to interfere or not. We realize this with the above mentioned high-speed tunable beam splitter controlled by a quantum random number generator (QRNG). This demonstration significantly extends the delayed-choice gedankenexperiment proposed by Wheeler in two aspects: Firstly, complementarity is not only valid in the single-photon experiment, but also in the HOM two-photon experiment; Secondly, independent of the space-time arrangement between the photon's entry of the interferometer and the setting the choice of the setting of last beam splitter, complementarity is valid.

The experimental setup of the up conversion and down conversion is the same as used in the last experiment (see section 4.1) and the two photons are again separated with a polarizing beam splitter (PBS). Then they are coupled into two single-mode fibers (SMF) each with the length of 104 m and guided to the high-speed tunable beam splitter (TBS). The polarization rotations of the photons in the SMFs are compensated with fiber polarization controllers (PC).

In this experiment, we first adjust the phase of the MZI to be zero, defined by maximizing the photon counts of APD 1 (avalanche photodiode) and minimizing that of APD 2 when input a of the TBS is blocked. Then two fast complementary measurements are realized in the following ways: Measurement

(I) corresponds to switching the EOMs off. In this case, the phase of the MZI stays zero and the reflectivity of the TBS equals to 1 and the transmittivity of it equals to 0. Therefore, the two photons will not interfere. Measurement (II) corresponds to switching the EOMs on with the opposite quarter-wave (QW) phase modulating voltage, i.e. we apply the positive QW voltage to EOM1 and negative QW voltage to EOM2. In this case, the phase of the MZI is $\pi/2$ and both the transmissivity and the reflectivity of the TBS equal to 1/2, which allows the two photons to interfere.

Next we will describe how the polarization and path quantum states of the two photons evolve in the TBS. We align the optical axes of the EOMs along 45°. The input two photons are polarized along horizontal and vertical directions. In conjunction with the spatial mode of them, the initial quantum state can be written as: $|\Phi\rangle = |H\rangle|a\rangle \otimes |V\rangle|b\rangle = \frac{1}{2}(|+\rangle + |-\rangle)|a\rangle \otimes (|+\rangle - |-\rangle)|b\rangle$. The two-photons state evolution is described as following:

$$
\begin{aligned}
|\Phi\rangle \quad \xrightarrow{\text{BS1}} \quad & \frac{1}{4}(|+\rangle + |-\rangle)(|c\rangle + i|d\rangle) \otimes (|+\rangle - |-\rangle)(|d\rangle + i|c\rangle) \\
\xrightarrow{\text{EOMs}} \quad & \frac{1}{4}(i(e^{i2\phi_v}|++\rangle - |--\rangle)|cc\rangle + (|++\rangle - e^{i2\phi_v}|--\rangle)|dd\rangle) \\
& +(2 - 2e^{i2\phi_v})|+-\rangle|cd\rangle)) \\
\xrightarrow{\text{BS2}} \quad & \frac{1}{8}[-2\sin\phi_v(e^{i\phi_v}(|++\rangle - |--\rangle) - 2e^{i(\phi_v - \frac{\pi}{2})}|+-\rangle)|ee\rangle \\
& +2\sin\phi_v(e^{i\phi_v}(|++\rangle - |--\rangle) + 2e^{i(\phi_v - \frac{\pi}{2})}|+-\rangle)|ff\rangle \\
& -4\cos\phi_v e^{i\phi_v}(|++\rangle - |--\rangle)|ef\rangle] \qquad (4.3)
\end{aligned}
$$

In the above equation, we denote ϕ_v as the voltage dependent phase shift induced by both EOMs. It is clear to see from the equation above that the photons will bunch when $\phi_v = \frac{\pi}{2}$, because only $|ee\rangle$ and $|ff\rangle$ terms survive, and will not bunch when $\phi_v = 0$ because only $|ef\rangle$ survives. Moreover, from Eq. 4.3, in the case of $\phi_v = 0$, the coincidence count rate is twice as much as the rate at the plateau of the HOM interference fringe. Intuitively, one can understand this in

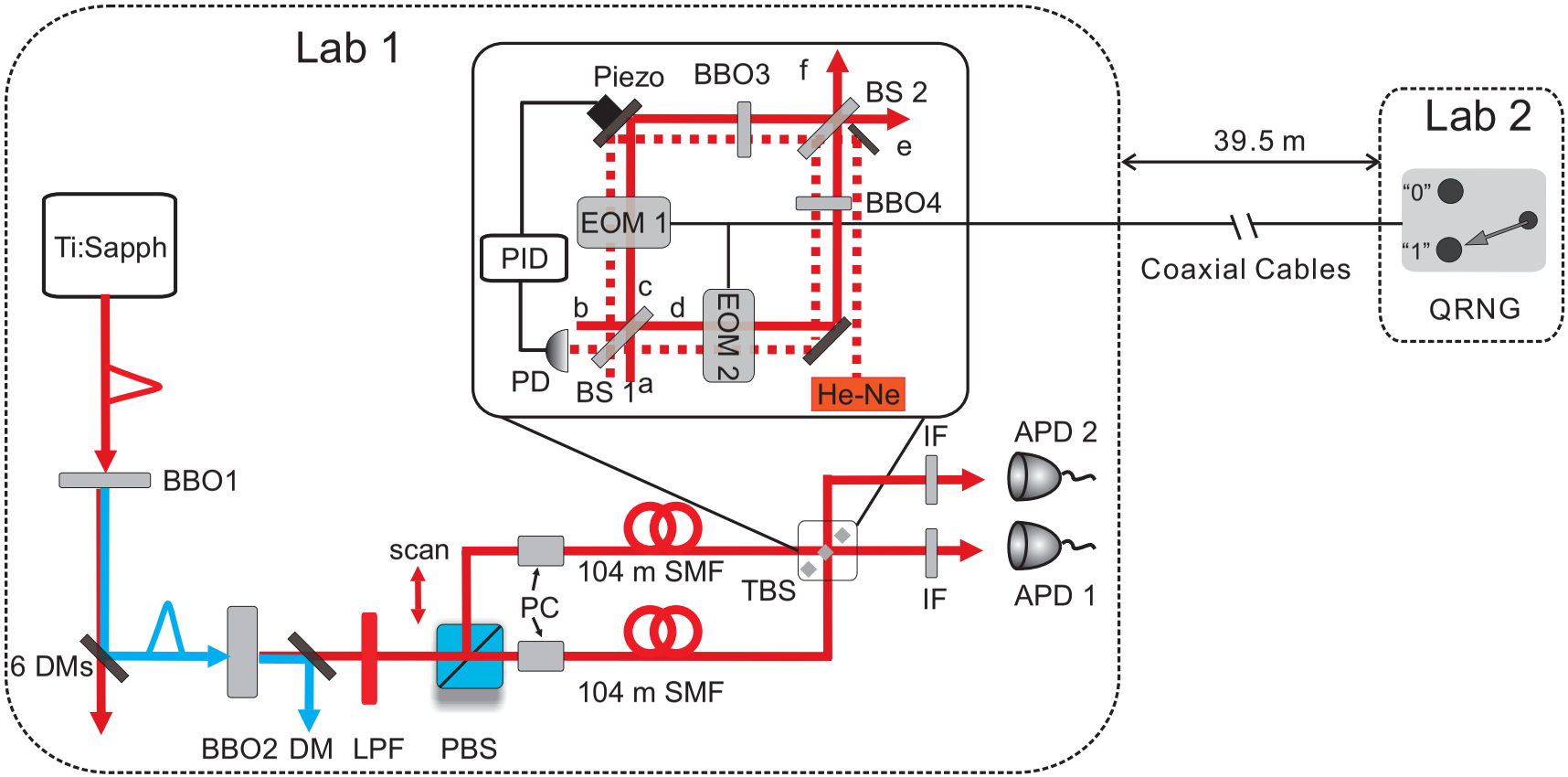

Figure 4.7.: Experimental Setup of the two-photon Hong-Ou-Mandel (HOM) interference under Einstein's locality condition. The correlated photon pair is generated from BBO2 cut for type-II collinear phase matching via SPDC (see text). Both photons are sent into the HOM interferometer, whose length is 104 m. A quantum random number generator (QRNG), which is 39.5 m away from the interferometer, decides the settings of the TBS. For the detailed description of the setup, refer to the text.

the following way: When $\phi_v = 0$, the whole TBS's reflectivity is 0. Therefore, all the photons come from mode a will exit from mode f and all the photons from mode b will exit from mode e. When $\phi_v = \pi/2$, the whole TBS's reflectivity is 0.5. In this case, when we measure the coincidence counts at the plateau of the HOM interference fringe, we will obtain the coincidence count rate to be half of the case with $\phi_v = 0$. This is because at the plateau of the HOM interference fringe, the two photons are not temporally overlapped with each other and then become distinguishable in time. Therefore, the photons come from mode a will exit either from mode e or f, and the photons from mode b will also exit either from mode e or f. These four possibilities are equal. Only when two photons exit from different modes, we will obtain a coincidence count. Hence, the coincidence count rate at the plateau in the case of $\phi_v = \pi/2$ is half of that in the case of $\phi_v = 0$. When the two photons overlap perfectly in time and are indistinguishable in all degrees of freedom, we see the HOM interference and thus the coincidence count rate is zero.

The choice of which measurement to perform is determined by a quantum random number generator (QRNG), which defines the settings for the experimental configuration both quickly and randomly. In addition, a pulse generator samples the random signal with 2.5 MHz sampling rate to match the repetition rate of the EOMs. See Chapter 3 for the details of the QRNG.

To demonstrate the complementarity under Einstein locality conditions of our HOM two-photon interference experiment, we carefully arrange the experimental setup. The QRNG is located 39.5 m away from the interferometer. The length of the coaxial cable transmitting the random bit signal is 81 m (corresponding to 405 ns time delay). There is an additional 45 ns time delay in the high voltage driver of the EOMs. Both photons are sent into the HOM interferometer, whose length is 104 m (corresponding to 520 ns time delay).

To be conservative, we include the following events as the choice-related events: a) all the choices made in a time interval of three times of the autocorrelation time ($\tau_{ac} = 11$ ns) of the QRNG, which is about 33 ns, b) the

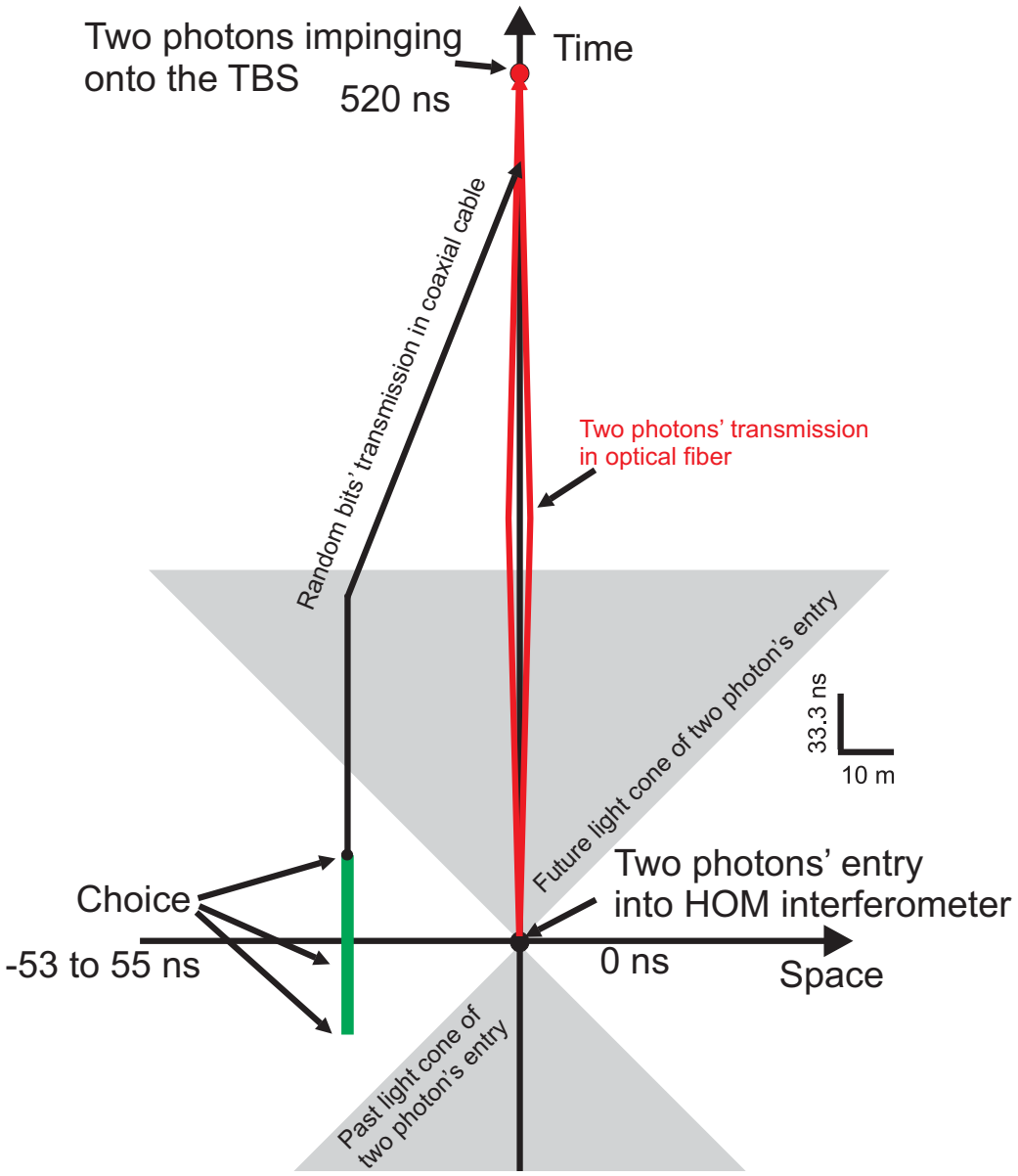

Figure 4.8.: Space-time diagram for the HOM two-photon interference under Einstein's locality condition experiment. The black, red dots, and green bar correspond to the events of the generation of the photon pairs (i.e. the entry of the two photons into the HOM interferometer), two photons impinging onto the TBS and the choice, respectively. The grey triangles represent the past and future light cones of the two photons' entry into the HOM interferometer. The propagating trajectories of random bits in the coaxial cable (black lines) and that of photons in the optical fibers (red lines) are indicated. The scales of the space-axis and the time-axis are indicated in the inset respectively.

internal delay of the QRNG (75 ns). These two times cover all the significant events related to the choice and have a total duration of about 108 ns. Therefore, the choice in the space-time diagram (Figure 4.8) consists of a series of events instead of a single well-defined event. Operationally this ensures the space-like separation between the choice and the two photons' entry into the HOM interferometer in the relativistic sense, as shown in Figure 4.8. Under space-like separation (Einstein locality conditions), luminal or subluminal communication is impossible in any and all reference frames.

The experimental results are shown in Figure 4.9. When the EOMs are on (black dots) a HOM interference pattern with a visibility $86.5\% \pm 2.4\%$ is clearly seen. This is fitted with a Gaussian function (black curve). When the EOMs are off, no HOM interference shows up, and a constant count rate, insensitive to the path length variations, is observed. The count rate in this case is twice as much as the plateau of the HOM interference, as shown in Equation (4.3). The mean value of the counts is indicated with a red line.

We realize an experiment testing the complementarity principle with the two-photon interference based on a 208 m glass fiber Hong-Ou-Mandel interferometer. The key element of the interferometer is a high-speed tunable beam splitter controlled by a quantum random number generator. Together with appropriate space-time arrangements, Einstein locality conditions are satisfied in this experiment.

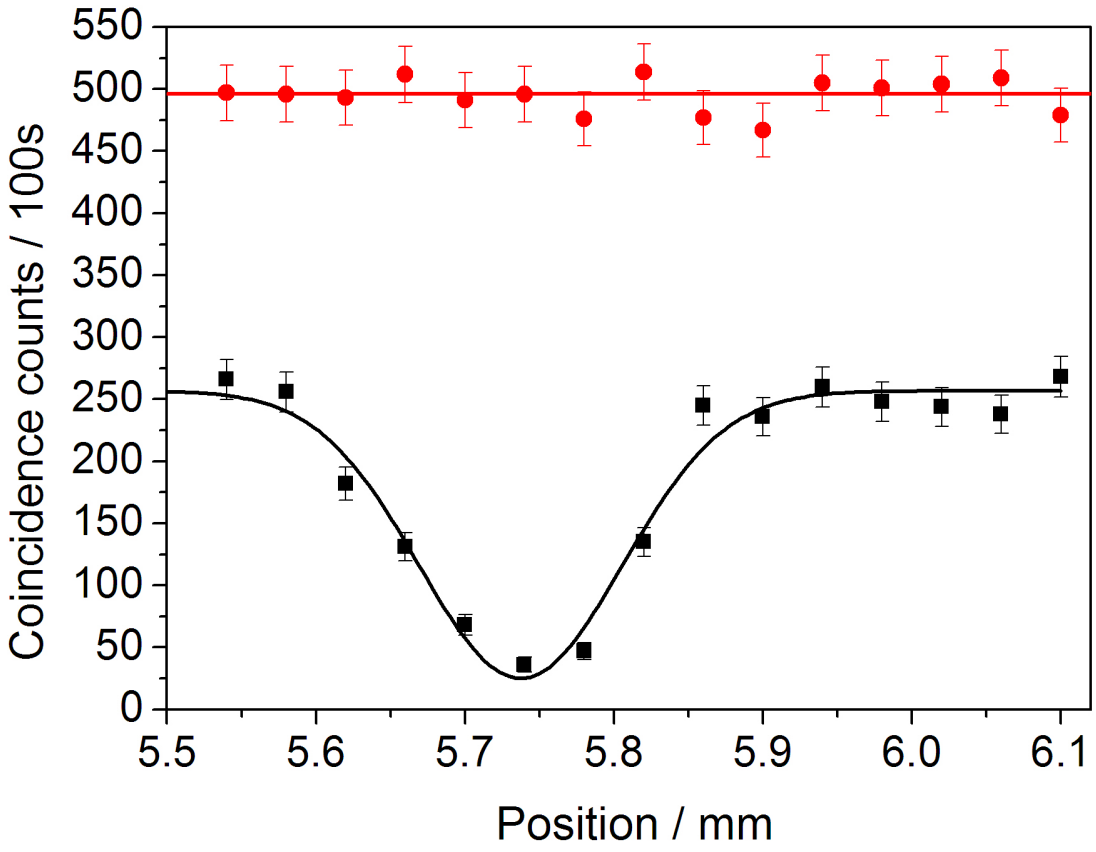

Figure 4.9.: Experimental results for the two-photon interference experiment under Einstein locality conditions. When the electro-optic modulators (EOM) are on (black square dots), HOM interference with visibility $86.5\% \pm 2.4\%$ is observed. When the EOMs are off (red circle dots), path length difference insensitive counts are obtained, where the count rate is twice as much as the plateau of the HOM interference, as shown in Equation (4.3) and explained in the text. The mean value of the counts is indicated with one red line. The error bars are calculated from Poissonian statistics.

4.3. Experimental realization of the delayed-choice entanglement swapping

Two particles in a quantum system can be in an entangled state, where the correlations of the overall system are well defined but not the properties of the individual particles, regardless of their spatial separation [UTSM+07] and life time [FUH+09]. Peres raised the question whether it is possible to entangle two particles even after they do not exist anymore [Per00]. Surprisingly, quantum mechanics allows this via entanglement swapping [ZZHE93], which is a quantum communication protocol we introduced in Section 1.3.2. This protocol has been experimentally demonstrated with various physical systems [PBWZ98, JWPZ02, HBG+07, KPAZ09, RHR+04, BCS+04, MMM+08, YCZ+08]. Entanglement swapping is one of the important ingredients for the quantum repeaters [BDCZ98, DLCZ01] and may play an important role in a loop-hole free Bell test [SI03], which are at the heart of both quantum information technology and foundations of quantum physics.

Peres combined entanglement swapping with the delayed-choice paradigm proposed by Wheeler [Whe84]. He illustrated this with two pairs of entangled photons, namely photons 1&2 and photons 3&4. He proposed that photons 1 and 4 can be entangled even after they have been detected via a later projection of photons 2 and 3 into an entangled state [Per00]. This leads to a seemingly paradoxical situation, that "entanglement is produced *a posteriori*, after the entangled particles have been measured and may even no longer exist" [Per00]. Let's imagine a setup as in Figure 4.10A and identify the relevant space-time events of this experiment: Two polarization-entangled photon pairs (1&2 and 3&4) are generated from Einstein-Podolsky-Rosen (EPR) Sources I and II. We denote these two generation events to G_I and G_{II}. The polarization states of photon 1 and photon 4 are measured by Alice (event A) and Bob (event B) right after their generation. The other two photons (photons 2 and 3) are delayed and then sent to Victor. He may entangle photons 2 and 3 by projecting them into

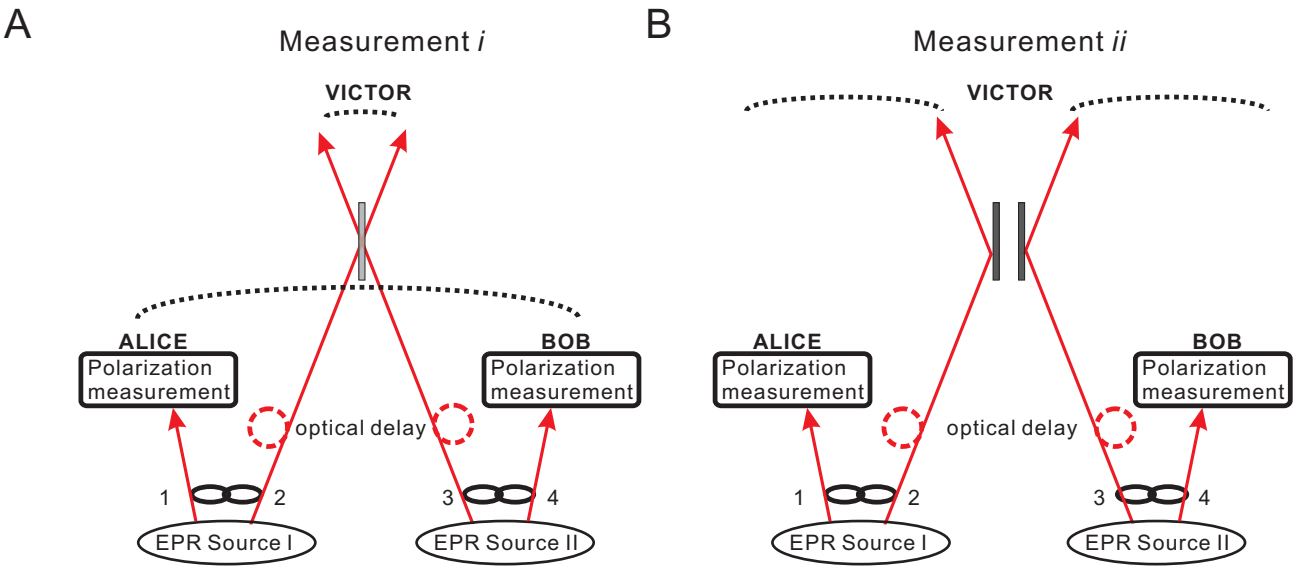

Figure 4.10.: Idea of entanglement swapping with delayed-choice. In both cases, photons 1 and 2 are generated from EPR source I in an entangled state; photons 3 and 4 are generated from EPR source II in the same entangled state. Photons 1 and 4 are sent to Alice and Bob, who perform polarization measurements. Photons 2 and 3 are delayed with respect to photons 1 and 4 and then sent to Victor. **A**. Victor chooses to swap the entanglement. Consequently, photons 2 and 3 are entangled, and hence photons 1 and 4 are also entangled. **B**. Victor chooses not to swap the entanglement. Consequently, photons 1 and 2, and photons 3 and 4 remain entangled as generated from the sources. See text for further details.

a Bell state (event V), thus also projecting photons 1 and 4 into a polarization-entangled state. This is done after Alice's and Bob's measurements. Note that after the entanglement swapping, particles 1&2 and 3&4 are no longer entangled, which manifests the monogamy of entanglement [CKW00].

Furthermore, Victor is even free to choose the type of measurement he wants to perform on photons 2 and 3. We assign this choice to be event C_V. Instead of a Bell-state measurement (measurement i), he could also project photons 2 and 3 into a separable state (measurement ii), as shown in Figure 4.10. Whether Alice's and Bob's earlier measurement outcomes indicate entanglement of photons 1 and 4 therefore depends on which of these two complementary bipartite-state projections of photons 2 and 3 is later performed by Victor. In the case of

measurement *ii*, photons 1&2 and 3&4 are entangled just as generated from the sources. Remarkably, the choice of Victor can be delayed even until after photons 1 and 4 have been measured and no longer exist, indicating that, in this experiment the temporal order of Victor's choice and measurement with respect to Alice's and Bob's measurements is not relevant. There are two experimental temporal configurations:

1. Victor makes the choice and performs either the Bell-state measurement or the separable-state measurement on photons 2 and 3 first. Then Alice and Bob measure the polarization states of photons 1 and 4;

2. Alice and Bob measure the polarization states of photons 1 and 4 first. Then Victor makes the choice and performs either the Bell-state measurement or the separable-state measurement on photons 2 and 3.

The experimental results should be the same. Note that if we analyze the correlation between photons 1 and 4 independent of the results of photons 2 and 3, we will obtain a completely uncorrelated results. This is because either the Bell-state measurement or the separable-state measurement performed on photons 2 and 3 will consequently project photons 1 and 4 into a Bell state or a separable state. If no measurement has been performed on photons 2 and 3 or the result of the measurement has been ignored, photons 1 and 4 will be completely uncorrelated.

Here we follow this above-mentioned idea and demonstrate an entanglement-swapping experiment in which the measurement on photons 2 and 3 is delayed and the type of measurement that Victor performs is actively and independently defined by a quantum random number generator (QRNG). The QRNG provides a truly random sequence of Victor's choices and an ideal delayed-choice configuration. See Chapter 3 for the details of the QRNG.

The detailed setup of this experiment is shown in Figure 4.11. A high intensity pulsed ultraviolet laser beam (UV) with a central wavelength of 404 nm, a pulse duration of 180 fs, and a repetition rate of 80 MHz successively passes through

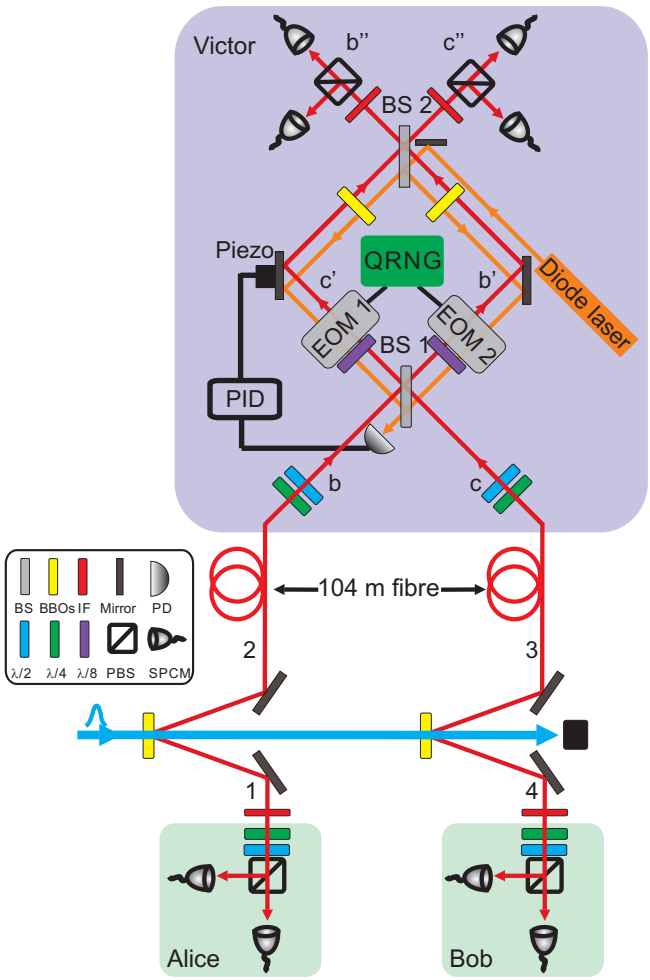

Figure 4.11.: Experimental setup used for entanglement swapping with a delayed-choice configuration. Photons 1 and 4 are directly subject to the polarization measurements performed by Alice and Bob (green blocks). Photons 2 and 3 are each delayed with 104 m single-mode fiber and then were coherently overlapped on the bipartite-state analyzer (BiSA) (blue block). The single-mode fiber coupler of photon 2 is mounted on a step motor and used to scan the four-photon interference pattern. An active phase stabilization system is employed in order to compensate the phase noise, which is composed with an auxiliary power-stabilized diode laser counter-propagating through the whole MZI, a photon detector (PD) monitoring the intensity fluctuation, and a ring piezo-transducer controlled by an analogue proportional-integral-derivative (PID) regulator. Two pairs of cross oriented BBO crystals (BBOs3 and BBOs4) are placed in each arm of the MZI in order to compensate the unwanted birefringence.

two BBO crystals to generate two polarization-entangled photon pairs (photons 1&2 and photons 3&4) via non-collinear type-II spontaneous parametric down conversion (SPDC) [KMW+95]. Photons 1 and 4 are spectrally filtered with two interference filters (IF) of 3 nm FWHM bandwidth, and photons 2 and 3 are filtered with 1 nm IFs. All four photons are coupled into single-mode fibers. Therefore, good spectrum and spatial mode overlapping is achieved. With the pump power of 700 mW, the 2-fold count rate is directly measured and found to be 20 kHz, and the 4-fold count rate is 5 Hz. There are two reasons for the relative low count rates in our experiment. First, in order to avoid the higher order emissions from SPDC to decrease the fidelities of states, we can't increase the pump power too much. Thus, in this experiment, we only use 700 mW, half of the maximum power we have (1.5 W). The second reason is the loss of various optical components and the duty cycle of the EOMs. We lose 79% of the photons on each individual input of the bipartite-state analyzer (BiSA). The probabilistic nature of the Bell-state projection with linear optics decreases the success probability to 1/4. The random choices to either perform measurement *i* or *ii* determined by the QRNG give an additional factor of 1/2 reduction. The duty cycle of the EOMs is 60%. Combining all these losses, we are only left with a fraction of $(1-0.79)^2 * 1/4 * 1/2 * 0.6 = 0.0033$ of all generated four-photon coincidence events being recorded. Therefore the detected four-fold rate is about $0.0033 * 5\text{Hz} = 0.016\text{Hz}$.

In order to satisfy the delayed-choice condition, the lengths of the fibers guiding each photon are chosen suitably. Photons 1 and 4 are sent to Alice and Bob each with a 7 m fiber (35 ns), where their polarization states are measured. Photons 2 and 3 are each delayed with a 104 m fiber (520 ns) and sent to Victor, who projects photons 2 and 3 either into an entangled state or a separable state according to the choice determined by the QRNG. See Chapter 3 for the details of the QRNG. One crucial component of our setup is the high-speed bipartite-state analyzer (BiSA) used for photons 2 and 3, which is modified from the TBS introduced in the last two sections and shown in blue box in Figure 4.11. Com-

paring to the TBS we used previously we place two eighth-wave plates (EWP) with their optical axes oriented parallel (in front of the EOM1) and orthogonal (in front of the EOM2) to the axes of the Rubidium-Titanyl-Phosphate (RTP) crystals, respectively. For EOM1 and EWP1, applying positive eighth-wave voltage (+EV) makes the EOM1 act as an additional eighth-wave plate. Given that the optical axis of EWP1 is oriented parallel to that of RTP crystals, the overall effect is the one of a quarter-wave plate (QWP) at 45°. On the contrary, applying negative eighth-wave voltage (-EV) makes EOM1 compensate the action of EWP1, such that there is no overall effect. For EOM2 and EWP2, because the optical axis of EWP2 is oriented orthogonal to that of RTP crystals, the overall effect is the one of a QWP at $-45°$ by applying -EV and identity by applying +EV.

We realize a $\pi/2$ phase change of the Mach-Zehnder Interferometer (corresponding to measurement i) by applying +EV to EOM1 and -EV to EOM2, and no phase change (corresponding to measurement ii) when -EV is applied to EOM1 and +EV to EOM2. We define the phase of the MZI to be zero when all the photons that enter from input b exited into b", which we also set to be the phase locking point. The advantage of using the combination of EWP and EOM is that this allows a continuous operation of the EOM without damaging the crystals. This is because the application of DC voltage with long time duration will induce the ion wandering effect and hence damage the crystals. By using this bipolar operation mode, the mean fields in the crystals are on average zero. Therefore, this configuration allows us to operate the EOMs with a high duty cycle and a high repetition rate. (See Appendix for details.)

The choice-dependent bipartite-state measurement on photons 2 and 3 is represented as:

$$\hat{M}_c = c \cdot \hat{M}_i + (1 - c) \cdot \hat{M}_{ii}, \tag{4.4}$$

where c (0 or 1) is the value of the random bit from the QRNG, $\hat{M}_i = |\Phi^-\rangle_{23}\langle\Phi^-|$ is the operator for measurement i and $\hat{M}_{ii} = |HH\rangle_{23}\langle HH| - |VV\rangle_{23}\langle VV|$ for measurement ii.

When we perform measurement i, we can project photons 2 and 3 into either $|\Phi^-\rangle_{23}$ or $|\Phi^+\rangle_{23}$. The state evolution in the BiSA can be seen as the following:

$$\begin{aligned} |\Phi^-\rangle_{23} \quad & \xrightarrow{\text{BS1}} \quad \frac{i}{2\sqrt{2}}(|HH\rangle_{b'b'} + |VV\rangle_{b'b'} + |HH\rangle_{c'c'} + |VV\rangle_{c'c'}) \\ & \xrightarrow{\text{EWPs and EOMs}} \quad \frac{1}{2\sqrt{2}}(|RR\rangle_{b'b'} + |LL\rangle_{b'b'} + |LL\rangle_{c'c'} + |RR\rangle_{c'c'}) \\ & \xrightarrow{\text{BS2}} \quad \frac{i}{\sqrt{2}}(|HH\rangle_{b''c''} - |VV\rangle_{b''c''}) \end{aligned} \tag{4.5}$$

and

$$\begin{aligned} |\Phi^+\rangle_{23} \quad & \xrightarrow{\text{BS1}} \quad \frac{i}{2\sqrt{2}}(|HH\rangle_{b'b'} - |VV\rangle_{b'b'} + |HH\rangle_{c'c'} - |VV\rangle_{c'c'}) \\ & \xrightarrow{\text{EWPs and EOMs}} \quad \frac{1}{2\sqrt{2}}(|RR\rangle_{b'b'} - |LL\rangle_{b'b'} + |LL\rangle_{c'c'} - |RR\rangle_{c'c'}) \\ & \xrightarrow{\text{BS2}} \quad \frac{i}{\sqrt{2}}(|HV\rangle_{b''b''} - |HV\rangle_{c''c''}). \end{aligned} \tag{4.6}$$

So if we detect a coincidence count of different spatial modes and same polarization (either $|HH\rangle_{b''c''}$ or $|VV\rangle_{b''c''}$), we project photons 2 and 3 into $|\Phi^-\rangle_{23}$. If we detect a coincidence count of the same spatial mode and different polarizations (either $|HV\rangle_{b''b''}$ or $|HV\rangle_{c''c''}$), we project photons 2 and 3 into $|\Phi^+\rangle_{23}$.

The time diagram of the relevant events is shown in Figure 4.12. We assign that G_I happened at 0 ns, as the origin of the diagram. G_{II} happens 1.6 ns later. At 35 ns, events A and B occur. Victor's choice is made by the QRNG in the time interval ranging from 49 ns to 348 ns (event C_V) and sent to the BiSA. Due to the fibre delay of photons 2 and 3, at 520 ns Victor performs

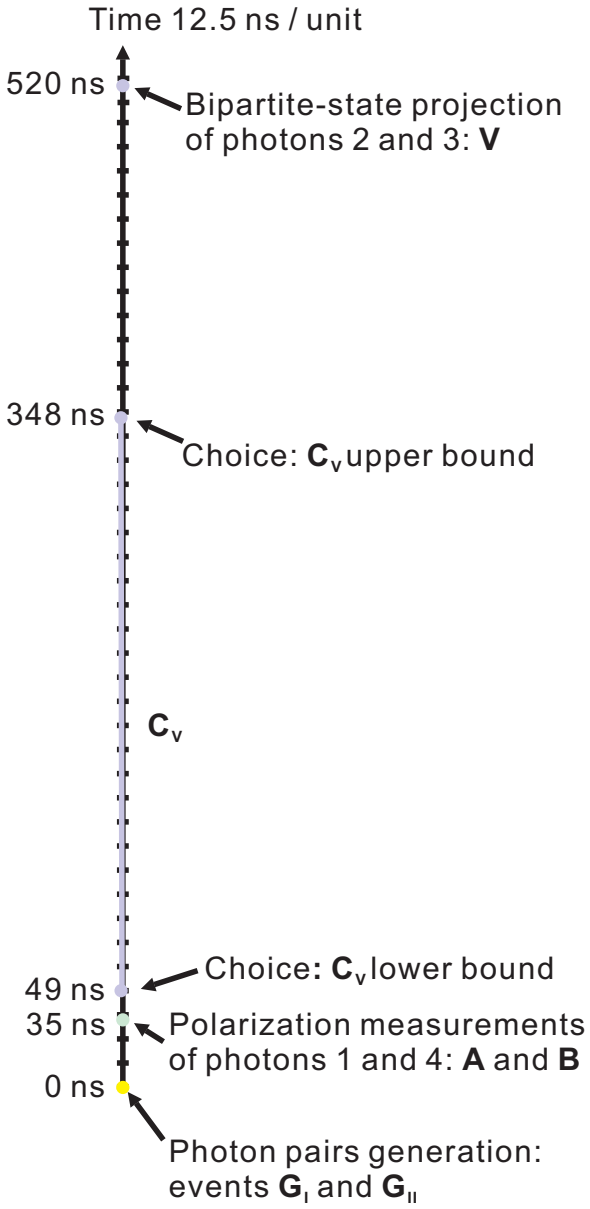

Figure 4.12.: Time diagram of the delayed-choice entanglement swapping. Two polarization-entangled photon pairs (1&2 and 3&4) are generated from Einstein-Podolsky-Rosen (EPR) sources I and II (events G_I and G_{II}). The polarizations of photon 1 and photon 4 are measured by Alice (event A) and Bob (event B) directly. The other two photons (photons 2 and 3) are delayed and then sent to Victor. He can entangle photons 2 and 3 by projecting them into a Bell state (event V), thus also projecting photons 1 and 4 into a polarization-entangled state. This is done 485 ns after Alice's and Bob's measurements. Furthermore, Victor is even free to choose (event C_V) the type of measurement to perform on photons 2 and 3. Instead of a Bell-state measurement, he can also project photons 2 and 3 into a separable state. The choice between creating entanglement or not is made by a quantum random number generator, and is delayed at least 14 ns after the measurements. See text for details.

the bipartite-state projection (event V) according to the bit value of his choice. Note that our definition of the choice event is very conservative. Because in addition to the fixed amount of the delay in the electronics of the EOM driver (45 ns), QRNG (75 ns) and connecting cables (20 ns), we also include 3 times the QRNG autocorrelation time (32 ns) and the on-time of the EOMs (299 ns). This on-time of the EOMs gives the time of C_V a lower bound of 49 ns and an upper bound of 348 ns. As shown in Figure 4.12, it is clear to see for each run (a 4-fold coincidence count) that not only V happened 485 ns later than A and B, but also C_V happened 14 ns to 313 ns later than A and B even in this conservative consideration. Therefore, in this configuration we unambiguously satisfied the delayed-choice condition for entanglement swapping.

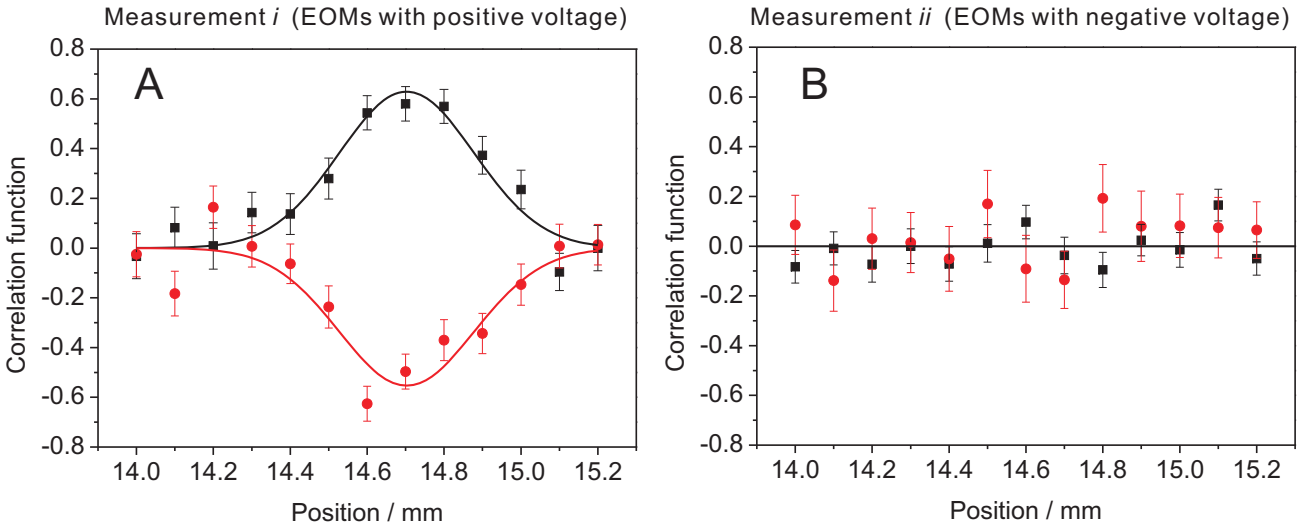

Figure 4.13.: Results of the correlation functions for photons 1 and 4 in the $|L\rangle/|R\rangle$ basis. **A**. The correlation functions depend on the relative delay of photons 2 and 3 interfering on the BiSA when measurement i is performed. The maximal correlation occurs for the optimal temporal overlap of photons 2 and 3. Two correlations are obtained in the same measurement by sorting the detection events corresponding to the two outcomes of the Bell-state measurement, red circular dots for $|\Phi^-\rangle_{23}$ and black square dots for $|\Phi^+\rangle_{23}$. **B**. On the contrary, the correlation functions for photons 1 and 4 in the $|L\rangle/|R\rangle$ basis *does not* depend on the relative delay of photons 2 and 3, when measurement ii is performed.

In order to interfere photons 2 and 3 on the BiSA, we use the fiber polariza-

tion controller to eliminate the polarization distinguishability and single-mode fiber to eliminate the spatial mode distinguishability. In order to temporally overlap photons 2 and 3 on the BiSA, we scan the delay between them with a motorized translation stage mounted on the single-mode fiber coupler of photon 2. Figure 4.13 presents a characteristic set of results for the correlation functions for photons 1 and 4 in the $|L\rangle/|R\rangle$ basis. They are calculated from the coincidence counts of photons 1 and 4 conditional on projecting photons 2 and 3 into $|\Phi^-\rangle_{23}$ (red circular dots) or $|\Phi^+\rangle_{23}$ (black square dots) when measurement *i* is performed, and to $|HH\rangle_{23}$ or $|VV\rangle_{23}$ when measurement *ii* is performed. The modulation of the correlation function in the $|L\rangle/|R\rangle$ basis for measurement *i* stems from the two-photon interference effect and indicates that photons 1 and 4 are in an entangled state. While for measurement *ii*, there is no modulation, which indicates photons 1 and 4 are in a separable state. In additional to the $|L\rangle/|R\rangle$ basis, we have also measured the correlation functions in the $|H\rangle/|V\rangle$ and the $|+\rangle/|-\rangle$ bases. The results are shown in Figure 4.14.

We quantify the quality of the output state via the fidelity defined as:

$$F(\hat{\rho}, |out\rangle) = Tr(\hat{\rho}|out\rangle\langle out|). \tag{4.7}$$

This is the overlap of the density matrix of the experimentally measured output state $\hat{\rho}$ with the theoretically expected output state $|out\rangle$. An entanglement witness is also employed to characterize whether entanglement exists between the photons [GHB+02]. It is defined as:

$$\hat{W}(|out\rangle) = \frac{1}{2}\hat{I} - |out\rangle\langle out|, \tag{4.8}$$

where $\hat{I}$ is the identity operator. A negative expectation value of this entanglement witness operator is a sufficient condition to show the presence of entanglement.

Figure 4.14A shows the results when Victor performs measurement *i*. The correlation of photons 1 and 4 exists in all three bases with the values of $0.511 \pm$

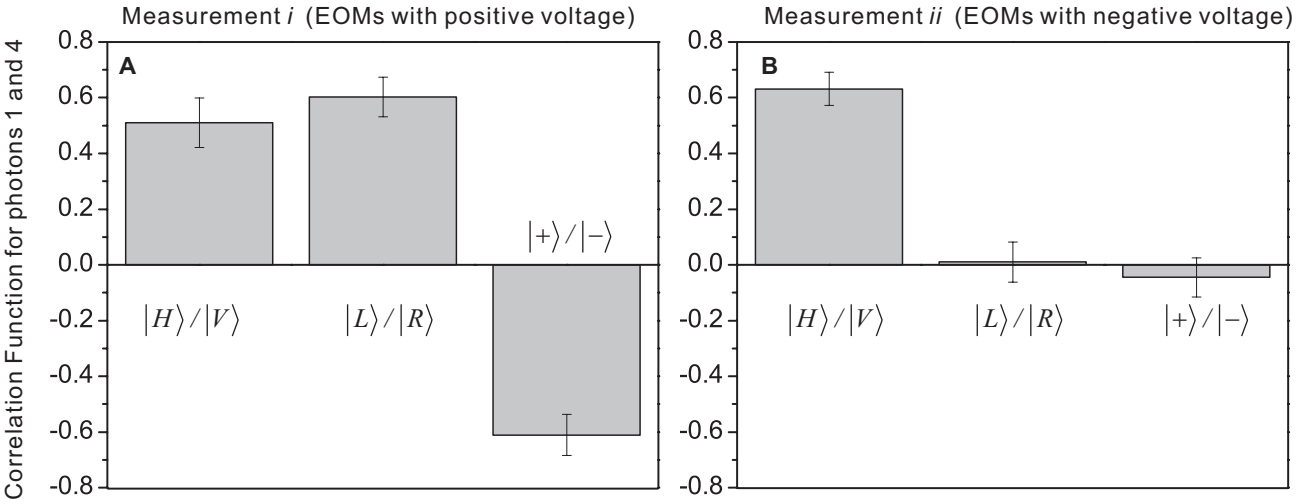

Figure 4.14.: Experimental results of the correlation functions of photons 1 and 4 in three mutually unbiased polarization bases, conditionally on coincidence counts of different spatial modes and same polarization produced by photons 2 and 3 in the $|H\rangle/|V\rangle$ basis. **A**. When Victor performs measurement i, entanglement is swapped to photons 1 and 4 ($|\Phi^-\rangle_{14}$). The values of the correlation functions of photons 1 and 4 in the $|H\rangle/|V\rangle$, the $|L\rangle/|R\rangle$ and the $|+\rangle/|-\rangle$ bases are 0.511 ± 0.089, 0.603 ± 0.071, -0.611 ± 0.074, respectively. **B**. When Victor performs measurement ii, entanglement is not swapped. The values of the correlation functions of photons 1 and 4 in the $|H\rangle/|V\rangle$, the $|L\rangle/|R\rangle$ and the $|+\rangle/|-\rangle$ bases are 0.632 ± 0.059, 0.01 ± 0.072 and -0.045 ± 0.070, respectively.

0.089 ($|H\rangle/|V\rangle$ basis), 0.603 ± 0.071 ($|L\rangle/|R\rangle$ basis) and -0.611 ± 0.074 ($|+\rangle/|-\rangle$ basis). The state fidelity $F(|\Phi_{14}^-\rangle_i)$ is 0.681 ± 0.034 and the expectation value of the entanglement witness $Tr(\hat{W}(|\Phi_{14}^-\rangle_i)\hat{\rho})$ is -0.181 ± 0.034. This negative value confirms entanglement between photons 1 and 4 by more than 5 standard deviations. The imperfections of the results stem from the following reasons: Firstly, the limited state fidelities are mainly due to the higher order emissions from SPDC, although we have deliberately decreased the UV pump power. We have also developed a numeric model to calculate the expected results. This model is based on the interaction Hamiltonian of SPDC. Given an interaction strength (or squeezing parameter) of the pump and nonlinear crystal, which can be measured experimentally, one can expand the Hamiltonian into a Taylor series. From this expansion, we can estimate the noise from the higher order

Photon pairs	Measurement i		Measurement ii	
	Fidelities	Witness	Fidelities	Witness
Photons 2 and 3	0.645 ± 0.031	-0.145 ± 0.031	0.379 ± 0.026	0.120 ± 0.026
Photons 1 and 4	0.681 ± 0.034	-0.181 ± 0.034	0.421 ± 0.029	0.078 ± 0.029
Photons 1 and 2	0.301 ± 0.039	0.199 ± 0.039	0.908 ± 0.016	-0.408 ± 0.016
Photons 3 and 4	0.274 ± 0.039	0.226 ± 0.039	0.864 ± 0.019	-0.346 ± 0.019

Table 4.1.: Results of the state fidelities and the expectation values of the entanglement witness operator for different pairs of photons with delayed-choice condition. When measurement i is performed, photons 2&3 and 1&4 are in the entangled states $|\Phi^-\rangle_{23}$ and $|\Phi^-\rangle_{14}$, i.e. the entanglement is swapped. When measurement ii is performed, photons 1&2 and 3&4 remain in the entangled states $|\Psi^-\rangle_{12}$ and $|\Psi^-\rangle_{34}$, i.e. the entanglement is not swapped.

emission. We utilize the quantum optics toolbox in Matlab [Tan99] which is based on a matrix representation of quantum states with up to three photons per mode. With this model, it is straightforward to reproduce the count rates and visibilities of our system. In the model the detection efficiency is determined by the specifications of the single-photon detectors and coupling efficiency is measured and derived from the ratio of the 2-fold coincidence counts and single counts. From this calculation, the expected correlation function of photons 1 and 4 is about 0.674. Secondly, the state fidelities are reduced due to the group velocity mismatch of pump photons and the down converted photons in the type-II phase matching of BBO crystal [MLS+08]. A rigorous model for calculating that can be found in [JUAZ09, Kal08]. The expected correlation function of photons 1 and 4 decreases by 0.964. At last, we are also limited by experimental imperfections. For instance, the degradation due to the limited performance of the BiSA, which is limited by the visibility of the MZI (0.95) and the switching fidelity (0.99), is about 0.94. The polarization alignment in the fibers, which quantifies the transmission fidelity of the photon in the fibers, is about 0.99. The overall expected correlation function of photons 1 and 4 is the product of all above listed values and equals to 0.605, which is in good agreement with our measured value.

When Victor performed measurement *ii*, the correlation only exists in the $|H\rangle/|V\rangle$ basis (0.632 ± 0.059) and vanishes in the $|L\rangle/|R\rangle$ (0.01 ± 0.072) and the $|+\rangle/|-\rangle$ (-0.045 ± 0.070) bases, as shown in Figure 4.14B. This is a clear signature that photons 1 and 4 are not entangled but in a separable state. The state fidelity $F(|\Phi_{14}^{-}\rangle_{ii})$ is 0.421 ± 0.029 and the expectation value of the entanglement witness $Tr(\hat{W}(|\Phi_{14}^{-}\rangle_{ii})\hat{\rho})$ is 0.078 ± 0.029 which is consistent with a separable state. Similar choice dependent results are obtained for photons 2 and 3, as summarized in Table 4.1.

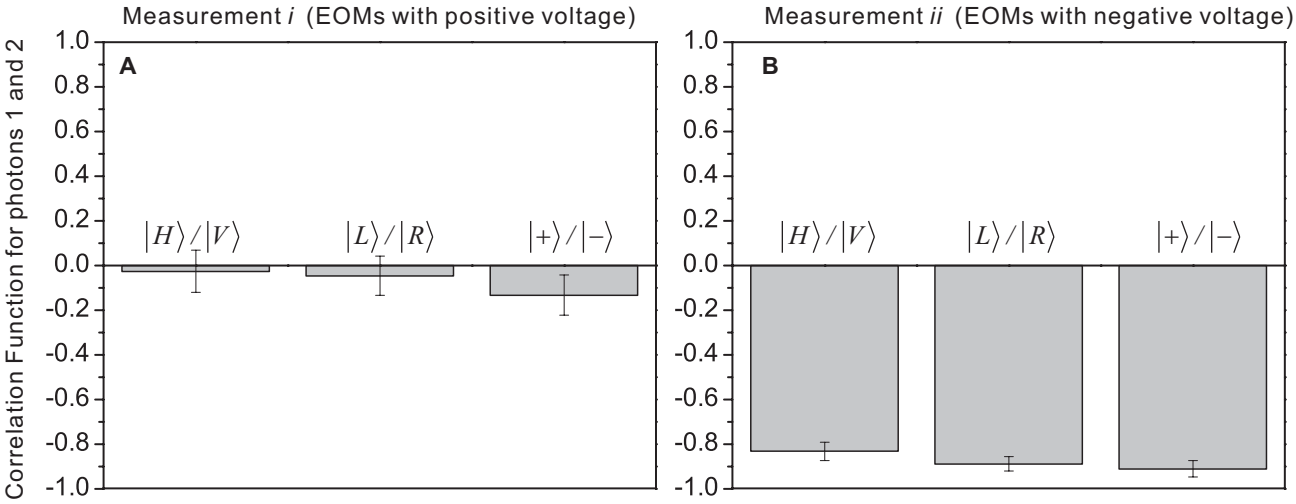

Figure 4.15.: Experimental results of the correlation functions of photons 1 and 2 in three mutually unbiased polarization bases. **A**. When Victor performs measurement *i*, photons 1 and 2 are not entangled. The values of the correlation functions of photons 1 and 2 in the $|H\rangle/|V\rangle$, the $|L\rangle/|R\rangle$ and the $|+\rangle/|-\rangle$ bases are 0.026 ± 0.094, 0.046 ± 0.088 and 0.133 ± 0.09 respectively. **B**. When Victor performs measurement *ii*, entanglement is not swapped. The values of the correlation functions of photons 1 and 2 in the $|H\rangle/|V\rangle$, the $|L\rangle/|R\rangle$ and the $|+\rangle/|-\rangle$ bases are -0.832 ± 0.041, -0.888 ± 0.033 and -0.91 ± 0.036 respectively.

As we stated above, when Victor performs measurement *ii*, entanglement remains between photons 1 & 2 (and photons 3 & 4) and vanishes when Victor performs measurement *i*. Figure 4.14 gives the correlation functions of photons 1 and 2. When measurement *i* is performed, we obtain the correlation functions of photons 1 and 2 in the $|H\rangle/|V\rangle$, the $|L\rangle/|R\rangle$ and the $|+\rangle/|-\rangle$ bases with the values of 0.026 ± 0.094, 0.046 ± 0.088 and 0.133 ± 0.09. On the contrary, when

measurement ii is performed, we obtain the correlation functions of photons 1 and 2 in the $|H\rangle/|V\rangle$, the $|L\rangle/|R\rangle$ and the $|+\rangle/|-\rangle$ bases with the values of -0.832 ± 0.041, -0.888 ± 0.033 and -0.91 ± 0.036. Therefore, the state fidelity $F(|\Psi_{12}^{-}\rangle_{ii})$ ($F(|\Psi_{34}^{-}\rangle_{ii})$) of photons 1 & 2 is 0.908 ± 0.016 when measurement ii is performed, and 0.301 ± 0.039 when measurement i is performed. Similar results are obtained for photons 3 and 4, as summarized in Table 4.1.

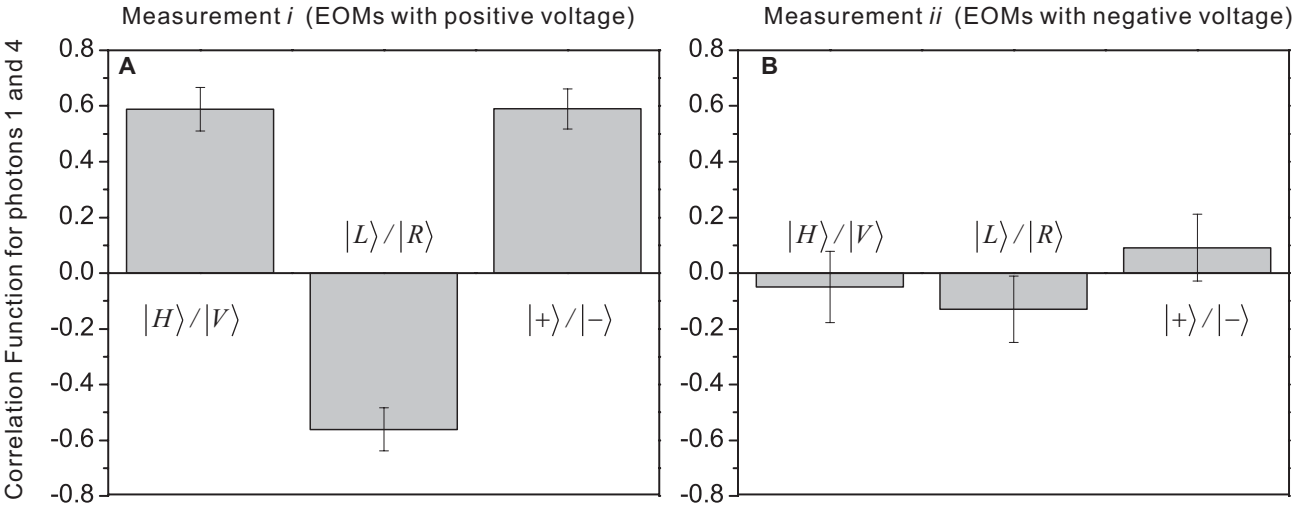

Figure 4.16.: Experimental results of the correlation functions of photons 1 and 4 in three mutually unbiased polarization bases, conditionally on coincidence counts of same spatial mode and different polarizations produced by photons 2 and 3 in the $|H\rangle/|V\rangle$ basis. **A**. When Victor performs measurement i, photons 1 and 4 are entangled. The values of the correlation functions of photons 1 and 4 in the $|H\rangle/|V\rangle$, the $|L\rangle/|R\rangle$ and the $|+\rangle/|-\rangle$ bases are 0.589 ± 0.078, -0.561 ± 0.078 and 0.59 ± 0.072, respectively. **B**. When Victor performs measurement ii, entanglement is not swapped. The values of the correlation functions of photons 1 and 4 in the $|H\rangle/|V\rangle$, the $|L\rangle/|R\rangle$ and the $|+\rangle/|-\rangle$ bases are -0.049 ± 0.128, -0.13 ± 0.119 and 0.091 ± 0.12, respectively.

Moreover, when Victor performs measurement i, he is also able to project photons 2 and 3 into $|\Phi_{23}^{+}\rangle$ with the BiSA, see Equation (4.3). As shown in Equation(1.36), then photons 1 and 4 are in the state of $|\Phi_{23}^{+}\rangle$ as well.

Figure 4.16 presents the correlation functions of photons 1 and 4 ($|\Phi^{+}\rangle_{14}$). When measurement i is performed, we obtain the correlation functions in the $|H\rangle/|V\rangle$, the $|L\rangle/|R\rangle$ and the $|+\rangle/|-\rangle$ bases with the values of 0.589 ± 0.078,

-0.561 ± 0.078 and 0.59 ± 0.072, respectively. On the contrary, when measurement *ii* is performed, we obtain the correlation functions in the $|H\rangle/|V\rangle$, the $|L\rangle/|R\rangle$ and the $|+\rangle/|-\rangle$ bases with the values of -0.049 ± 0.128, -0.13 ± 0.119 and 0.091 ± 0.12, respectively. When we perform measurement *i*, a state fidelity $F(|\Phi_{14}^{+}\rangle_i)$ of 0.685 ± 0.033 is obtained and the expectation value of entanglement witness $Tr(\hat{W}(|\Phi_{14}^{+}\rangle_{ii})\hat{\rho})$ is -0.185 ± 0.033. Therefore entanglement between photons 1 and 4 is confirmed.

According to Peres, "[t]he point is that it is meaningless to assert that two particles are entangled without specifying in which state they are entangled, just as it is meaningless to assert that a quantum system is in a pure state without specifying that state." For our experiment, this means when Victor performs measurement *i*, we are able to assert that photons 1 and 4 are entangled only by specifying whether they are entangled in the state $|\Phi_{14}^{-}\rangle$ or $|\Phi_{14}^{+}\rangle$. Otherwise, photons 1 and 4 are in a completely separable state. This is confirmed by averaging the correlation functions of $|\Phi_{14}^{-}\rangle$ and $|\Phi_{14}^{+}\rangle$ in each basis. Then there exists correlation only in the $|H\rangle/|V\rangle$ basis (0.55) and no correlations in the $|+\rangle/|-\rangle$ (0.021) and the $|L\rangle/|R\rangle$ (0.01) bases, similar to the situation when Victor performs measurement *ii* (no entanglement swapping).

With our realization of the delayed-choice entanglement-swapping gedanken-experiment, we significantly extend Wheeler's proposal from the wave-particle duality of a single particle to the entanglement of two particles. In our experiment, the measurements of Alice and Bob are the prime events. But in order to interpret the results of these events, it is necessary to obtain more information. This information depends on the later choice and performance of measurements on other particles. This leads to an allegedly paradoxical situation, in which the interpretation of already recorded data depends on future actions.

5. Conclusion and outlook

5.1. Conclusion

In the first part of the experimental work of this thesis, we demonstrated hybrid entanglement of photon pairs with two different degrees of freedom, namely the path of one photon and the polarization of the other. The correlations between these two degrees of freedom gave an S-parameter of $S = 2.653 \pm 0.027$ in a CHSH inequality and thus violated the bound set by local realism by more than 24 standard deviations.

We then used this hybrid entanglement to realize a nonlocal quantum eraser with spatial separations of 77 m (Vienna) and 144 km (Canaries). The latter case represented the largest spatial and temporal separation in all quantum erasure experiments. The decision to erase or not erase the which-path information of one photon was decided by relativistically space-like separated measurements on the distant twin. Our observations showed that, in agreement with quantum physics, the complementarity principle in a quantum eraser experiment is independent of the spatio-temporal arrangement of the choice and measurements.

In the second part of this thesis we have designed, implemented and characterized a high-speed tunable beam splitter. It was controlled by a quantum random number generator (QRNG), and used in a Hong-Ou-Mandel interferometer made from two 104 m long optical fibers. These allowed an experimental realization of two-photon interference under Einstein locality conditions.

Finally, we significantly extended Wheeler's proposal from the wave-particle duality of a single particle to the entanglement of two particles with our realiza-

tion of the delayed-choice entanglement-swapping gedankenexperiment. In this experiment, two photons were first measured, and 485 ns thereafter entanglement between them was created via entanglement swapping with a high-speed bipartite state analyzer. The choice of creating entanglement or not was made by a QRNG, and was delayed at least 14 ns after the measurements. The observed correlations, as characterized by an entanglement witness, show that the quantum predictions are fully confirmed, and therefore the temporal ordering of the choice and the measurement events in this experiment is irrelevant.

5.2. Outlook

The work presented in this thesis demonstrates the realization of three gedankenexperiments and includes the answers to fundamental questions of quantum physics. I will summarize the near term outlook for future experiments in this section, including *entanglement swapping under strict Einstein locality conditions*, *long distance quantum state teleportation* and *probabilistic instantaneous quantum computation*.

Entanglement swapping under strict Einstein locality conditions

As an extension of delayed-choice entanglement swapping, one could even impose Einstein locality conditions for an improved demonstration of delayed-choice entanglement swapping, where the polarization measurements of photons 1 and 2 are space-like separated from the choice and the bipartite state measurements of photons 3 and 4. This will exclude any causal influence between the measurements of photons 1 and 2, and the choice and the bipartite state measurements of photons 3 and 4.

On-demand single-photon generation via multiplexing with active feed-forward

An on-demand single-photon source is a fundamental building block in quantum information processing using photonic qubits, such as quantum communication

and linear optical quantum computing [KMN+07]. Schemes for creating on-demand single photons via multiplexing several heralded photons probabilistically generated from pulsed spontaneous parametric down conversions (SPDC) have been proposed in [MBC02, SW07]. By utilizing photon-pair sources, an active feed-forward technique and ultrafast single-photon routers, one can enhance the single-photon rate while the quality of the single photon is maintained. The quality of this single photon can then be confirmed by correlation measurements. By using the high-speed tunable beam splitter and four-photon source developed for the entanglement-swapping experiment, we can build a 4-SPDC multiplexed system and demonstrate the principle of single-photon multiplexing. Since the photons will be generated by the SPDC process pumped with a femtosecond pulsed laser which has been successfully used in multi-photon experiments in the past, a single-photon source based on our scheme will be suitable for high quality multi-photon interferences.

Long distance quantum state teleportation

Quantum state teleportation is of great fundamental interest and is a critical ingredient for modern quantum information processing networks. Over the last decade, several experiments were carried out [BPM+97, BBDM+98, MdRT+03, UJA+04, BCS+04, RHR+04, OMM+09, SKO+06, CCY+08]. In the near future it is planned to perform an experiment extending the distance of teleportation to about 144 km from La Palma island to Tenerife island. The quantum channel between Alice and Bob will be realized with the free-space link presented in Chapter 3.

The challenges of this long distance quantum state teleportation are: (1) count rate; (2) visibility. We need high count rate due to the high attenuation of the 144 km free-space link. The attenuation of the link is about 30 dB in good weather conditions.

Due to the Poisson statistics of pair generation probabilities of pulsed spontaneous parametric down conversion, there is a tradeoff between the pair's generation rate and quality. To surmount this problem, one needs to improve the

link efficiency and optimize the source. To improve the link efficiency, one can employ a tip-tilt adaptive optical system to reduce the beam wandering due to the turbulent atmosphere. To optimize the source of the photon pairs, one needs to increase the coupling efficiencies with better mode matching between the pump laser and the single-mode fibers used to collect the single photons.

Probabilistic instantaneous quantum computation

Instantaneous quantum computing is an interesting application where quantum state teleportation and entanglement swapping imply a gain in time over a classical procedure [BPS+03, Jen02]. This can be realized by sending one photon of a Bell state into the input of a quantum computer and perform quantum computation with it. Since this photon is a part of a Bell state, its individual property is not well defined. Therefore, the output of the quantum computation will not be defined. However, as soon as the required input is known, it can be teleported onto the state of the photon which was fed into the quantum computer. If the Bell-state measurement (BSM) gives the result of a singlet which requires no unitary transformation, then immediately the output of the quantum computer will be projected into the correct result, and hence the computation is performed instantaneously. Note that this instantaneous quantum computation is intrinsically probabilistic because we can only obtain a singlet after the BSM with 0.25 probability, as explained in Section 1.3.2.

A. Appendix

A.1. Spontaneous parametric down conversion

Spontaneous parametric down conversion (SPDC) is commonly used to generate entangled photons in which the $\chi^{(2)}$ optical nonlinearity of a birefringent crystal is used. In the photon picture, SPDC can be viewed as a decay of a pump photon into two photons: signal photon and idler photon. SPDC photons can only be emitted if the so-called phase matching conditions are fulfilled. In this conversion process, energy and momentum are conserved. Energy conservation requires that

$$h\nu_{pump} = h\nu_s + h\nu_i, \tag{A.1}$$

where ν_{pump}, ν_s and ν_i are the frequencies of the pump, signal and idler photons, respectively. And momentum conservation requires that

$$\hbar\vec{k}_{pump} \simeq \hbar\vec{k}_s + \hbar\vec{k}_i, \tag{A.2}$$

where $\vec{k}_{pump}$, $\vec{k}_s$ and $\vec{k}_i$ are the wave numbers of the pump, signal and idler photons, respectively, and $|\vec{k}| = \frac{n2\pi}{\lambda}$ (the vacuum wavelength λ and the refractive index n of the media). Given a well defined pump, these two conditions govern the wavelengths and the directions of emission of the down converted photons. Due to energy and momentum conservation the down converted photons are strongly correlated in these two degrees of freedom: frequency and direction. Note Equation A.2 would only be exact if the crystal is infinitely thick.

In a birefringent crystal, the refractive indices of the extraordinary and or-

Negative uniaxial crystal:	$n_o > n_e$
Refractive Index for $\lambda = 0.404$ μm	$n_o = 1.691935$, $n_e = 1.630319$
Refractive Index for $\lambda = 0.808$ μm	$n_o = 1.660043$, $n_e = 1.603531$
Point group:	3m
Transparency range:	0.189 - 3.5 μm

Table A.1.: Some optical properties of BBO [DGN90] crystal.

dinary polarization mode are different and given by the Sellmeier equations. When a birefringent crystal is pumped by an extraordinarily polarized beam, there are two different types phase matching of SPDC. Type I: The signal and idler photons have the same polarization and are ordinarily polarized. Type II: Signal and idler photons are orthogonally polarized, i.e. one ordinarily (o-photon), the other extraordinarily (e-photon). The experiments described in this work are based on type-II SPDC.

A.1.1. Generation of entangled photon pairs with type-II SPDC in BBO

We used β-Barium-Borate (β-BaB_2O_4, BBO) crystals to generate entangled photon pairs. We chose the wavelength of the pump and down converted photon to be 404 nm and 808 nm. Some of the optical properties of BBO crystal are shown in Table A.1.

θ and ϕ are the coordinate angles shown in Figure A.1. θ is the phase matching angle and determines the geometry of the down converted photons. ϕ is the angle determining the efficiency of SPDC.

The crystals we used are cut to $\theta = 42.7°$ and $\phi = 30°$. With these angles, the emission of the down converted photon with the degenerate wavelengths, is non-collinear, as shown in Figure A.2A. G. Weihs [Wei99] developed a Matlab program, based on the phase matching condition, the crystal parameters and conservations of energy, to determine the geometry of the emerging light of

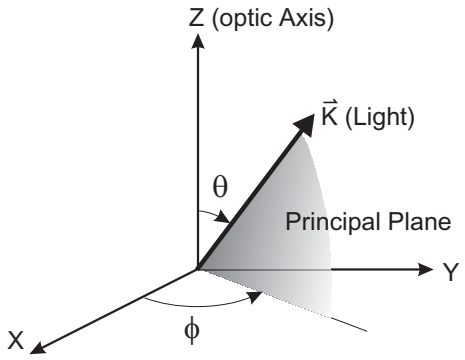

Figure A.1.: Polar coordinates for describing BBO crystal. $\vec{K}$ is the pump propagation direction, Z is the optic axis, and θ and ϕ are the coordinate angles. The principal plane is defined by the optical axis and the wave vector $\vec{K}$. Light with polarization normal to the principal plane is called the ordinary beam, and light with polarization parallel to the plane is called extraordinary beam.

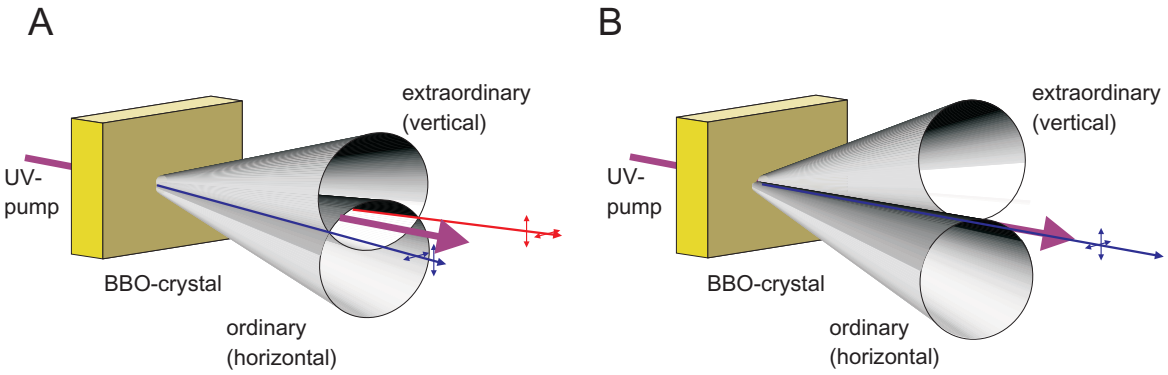

Figure A.2.: A schematic overview of type-II SPDC for the non-collinear (**A**) and collinear cases (**B**). In the non-collinear case, a pair of polarization-entangled photons are generated. In the collinear case, a pair of polarization separable photons are generated. (The figures are taken and adapted from [Wei99].)

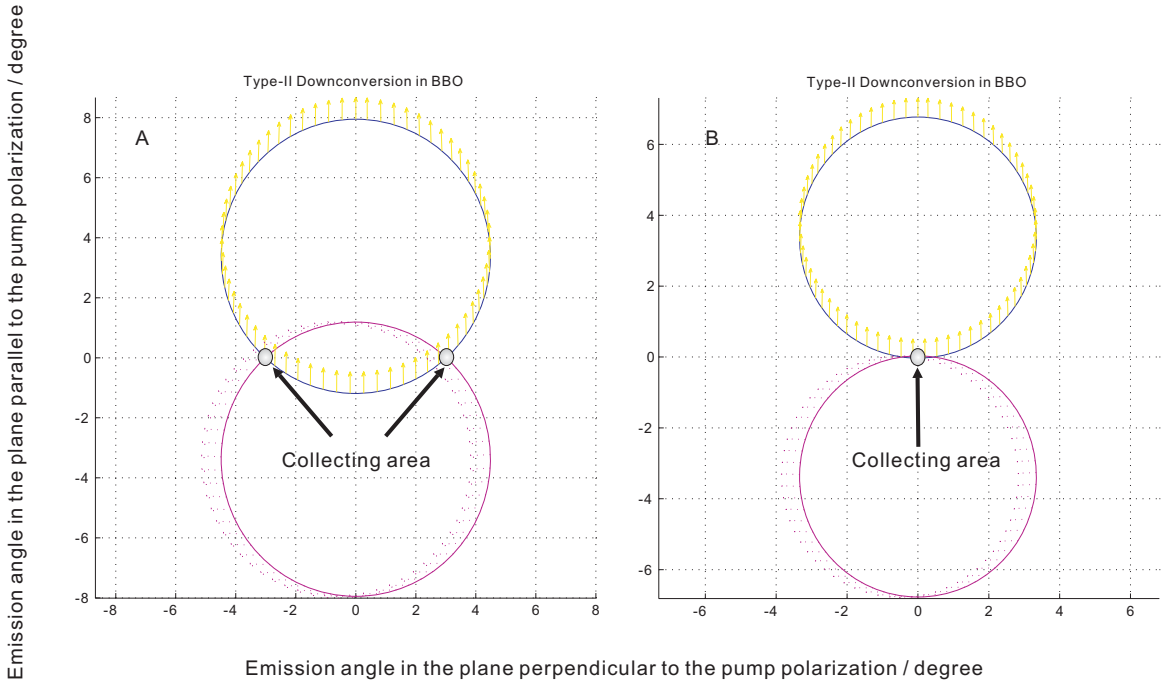

Figure A.3.: The calculation's results of type-II SPDC for the non-collinear (**A**) and collinear cases (**B**). In the non-collinear case, a pair of polarization-entangled photons emit symmetrically at 3° with respect to the pump. In the collinear case, a photon pair emits along the pump direction.

a specific angle θ. The emission angles of the down converted photons are calculated with this program. If $\theta = 42.7°$, the down converted photons are emitted symmetrically at 3° with respect to the pump, as shown in Figure A.2A. The results of the calculation are shown in Figure A.3A. One can adjust θ and control the emission directions of the down converted photons. If $\theta = 41.96°$, a collinear configuration can be realized, as schematically shown in Figure A.2B. The calculation result is shown in Figure A.3B.

In order to obtain high quality entangled photon pairs from the non-collinear configuration, it is necessary to erase timing information about the photons stemming from the walk-off effect. Because of the birefringent properties of BBO, the e-photon and the o-photon travel with different speeds. Therefore this time information is correlated with the polarization of the photon in the same spatial mode and provides distinguishability. One uses a combination of a

half-wave plate (HWP) and compensation BBO crystals (Comp BBO) in each arm to erase this information. The polarization of the down converted photon is rotated by 90° via the HWP oriented along 45°, such that the e-photon and o-photon are exchanged. The Comp BBO is oriented the same as the down conversion crystal, but is half the thickness of the down conversion crystal. This reverses the walk-off effects by half, which consequently erases the time information and reduces the effect of the transverse walk-off as well. A detailed description of this compensation scheme is given in Ref. [KMW+95, Mat97].

A.1.2. The state produced via SPDC

The ideal polarization-entangled state produced by down conversion has the form

$$|\Psi\rangle = \frac{1}{\sqrt{2}}(|H_1V_2\rangle - \mathrm{e}^{i\varphi}|V_1H_2\rangle), \tag{A.3}$$

where φ is the phase. By adjusting this phase φ, we can change the state $|\Psi\rangle$ between $|\Psi^-\rangle$ or $|\Psi^+\rangle$. Experimentally, this can be realized by tilting one of the compensation BBOs.

A.2. Electro-optical modulator

Electro-optical modulators (EOM) vary the phase of transmitted light by the application of a transverse or longitudinal electric field (with respect to the propagation direction) which induces a modification of the refractive index of a crystal. If this modification depends linearly on the applied electric field, it is called Pockels effect, discovered by Friedrich Pockels in 1893. Hence, an EOM of this kind is called Pockels cell.

In the Taylor series expansion, the refractive index can be written as [ST91]

$$n(E) = n(0) + \frac{dn}{dE}E + ... \tag{A.4}$$

Here we only consider the first two orders of expansion, which describe the Pockels effect. It is convenient to rewrite this equation in terms of $r = -\frac{2}{n^3}\frac{dn}{dE}$ which is known as the electro-optic coefficient. So the refractive index can be rewritten as:

$$n(E) = n(0) - \frac{1}{2}rn^3E - ... \tag{A.5}$$

Pockels cells as tunable wave plates

Let's assume that light propagates along the z-axis through the crystal of a Pockels cell. If an electric field is applied to the crystal, the refractive index of it in the x-axis and the y-axis changes to [ST91]:

$$n_x(E) = n_x(0) - \frac{1}{2}r_x n_x^3 E \tag{A.6}$$

$$n_y(E) = n_y(0) - \frac{1}{2}r_y n_y^3 E \tag{A.7}$$

If we decompose the polarization of the incoming light into the bases along the x-axis and the y-axis, these two polarization modes travel with different speeds. After a distance L (length of the crystal) the phase difference between the two modes becomes

$$\Phi = \frac{2\pi}{\lambda}(n_x(E) - n_y(E))L = \frac{2\pi}{\lambda}(n_x(0) - n_y(0))L - \frac{\pi}{\lambda}(r_x n_x^3 - r_y n_y^3)LE. \tag{A.8}$$

If the voltage V applied between the surfaces of the crystal is separated by the distance d, then $E = \frac{V}{d}$ and we can rewrite equation A.8 as [ST91]

$$\Phi = \Phi_0 - \pi\frac{V}{V_\pi}, \tag{A.9}$$

where

$$V_\pi = \frac{d}{L}\frac{\lambda}{r_x n_x^3 - r_y n_y^3} \tag{A.10}$$

and

$$\Phi_0 = \frac{2\pi}{\lambda}(n_x(0) - n_y(0))L \tag{A.11}$$

denote the half-wave voltage and the static phase shift (voltage independent). At voltage V_π the phase difference between the ordinary and extraordinary beam is π and therefore the Pockels Cell acts as a half-wave plate. Since Φ scales linearly with the applied voltage, one can obtain an arbitrary phase difference by adjusting the voltage. Hence Pockels cells can be used as a tunable wave plates.

As in the case of normal wave plates, if the polarization of the input light is parallel (or orthogonal) to the optics axis of the crystal in the Pockels cell, the polarization will remain unchanged but a phase shift will be introduced. If the polarization of the input light is not parallel (or orthogonal) to the optics axis of the crystal, the polarization will be rotated.

Specifications of the Pockels cells

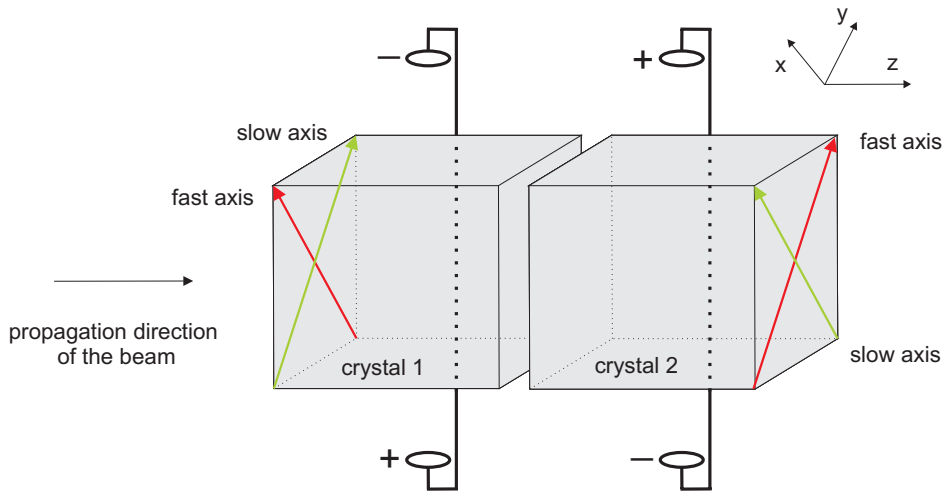

Figure A.4.: *A schematic diagram of the Pockels Cells. The voltage on the first crystal has opposite polarity to the second one. The optical axes of the two crystals are complementary to each other. This figure is adapted from [Zot09].*

The crystals we used are manufactured by the company *Leysop LTD* and are made of Rubidium-Titanyl-Phosphate (RTP) crystal. Every Pockels cell

consists of two RTP crystals mounted in series, as shown in Figure A.4. The light propagates along the z-axis and the voltage is applied along the y-axis. The optical axes of the crystals are oriented along 45°. The voltage on the first crystal has opposite polarity to the second one. Therefore the fast and slow axes of the two crystals are complementary to each other, i.e. the fast axis of crystal 1 is parallel to the slow axis of crystal 2 and the slow axis of crystal 1 is parallel to the fast axis of crystal 2. This arrangement has the advantage that both crystals are electronically switched on together, thus the required voltage is decreased to half compared to the case of single crystal.

The product specifications are given in table A.2.

Model	RTP-4-20
Aperture crystal dimensions	4mm
Total crystal length (2crystals)	20mm
Approximate half-wave voltage (1064nm)	1.3kV
Typical dynamic extinction ratio (1064nm)	$> 200 : 1$
Typical capacitance	6pF
Peak damage threshold (1064nm, 1ns pulse)	$> 1GWcm^{-2}$
Insertion loss	$< 2\%$
Physical dimensions (mm)	35x55

Table A.2.: The RTP crystal specifications.

Optical alignment of the Pockels Cells

In order to achieve the specified extinction ratio ($> 200 : 1$), one needs to: (1) align the Rubidium-Titanyl-Phosphate (RTP) crystals to be perpendicular to the incoming light; (2) ensure the optics axes of the RTP crystals are orientated along the desired direction (45° in our case). This could be done by observing isogyre patterns [Kal03], which is a signature of good alignment of the crystals, as shown in Figure A.5. The isogyre pattern can be obtained via the divergent light propagating through a birefringent crystal which is placed between two crossed polarizers.

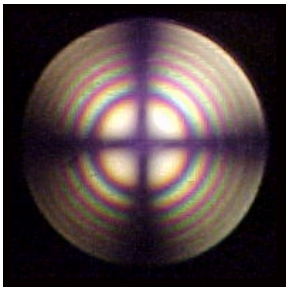

Figure A.5.: *An isogyre pattern for a uniaxial calcite crystal which is optimally aligned. In this case the input beam is parallel to the optical axis. Figure taken from http://www.uwgb.edu/dutchs/petrolgy/intfig1.html.*

The origin of isogyre patterns is as follows. The polarization of the light traveling into the crystal, parallel to the optical axis of the crystal, will remain unchanged. And since the crystal is placed between two crossed polarizers no light will be transmitted through the second polarizer. However, the polarization of the light traveling not in parallel to the optical axis of the crystal will be changed by the crystal. This change is rotationally symmetric around the optical axis. Thus in a situation where all directions are equally probable, as for the diverging light, this will lead to a isogyre pattern.

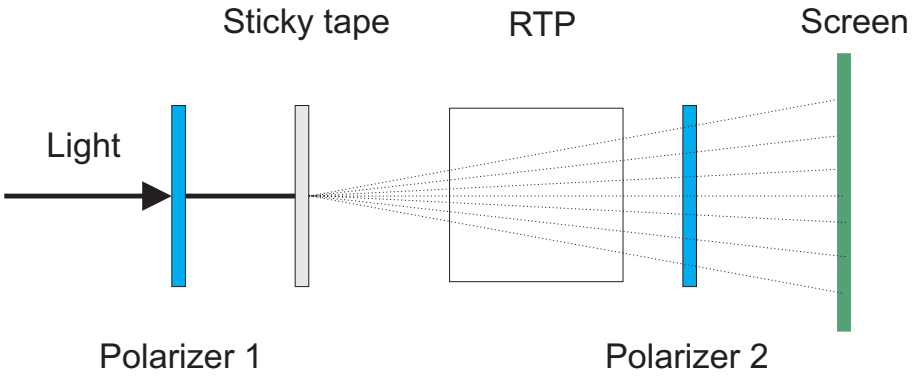

Figure A.6.: *Setup for adjusting the crystal orientation in the Pockels cells with isogyre patterns. Two polarizers are aligned orthogonal to each other. The sticky tape scatters the beam such that it diverges on its way through the Pockels cells. The interference pattern is recorded with a screen.*

The scheme of this alignment setup is shown in Figure A.6. Polarizer 1 and 2 are set along $+45°$ and $-45°$. The transparent sticky tape scatters the light

and makes it diverge. One could also use a lens with a short focal length for this purpose. Then the diverging light travels through RTP crystals. Finally the light can be obtained on a screen. One can rotate and tilt the crystal until the desired isogyre pattern is shown. This indicates that the polarization of the incident light is parallel to the optical axis.

After this alignment with the isogyre pattern, one should optimize the Pockels cell with a heralded single-photon source. In this optimization procedure, after detection of one single photon, the Pockels cell should be switched on in order to modify the polarization of its twin [BPJ+07]. Normally, one can achieve $> 150 : 1$ extinction ratio after a few iterations.

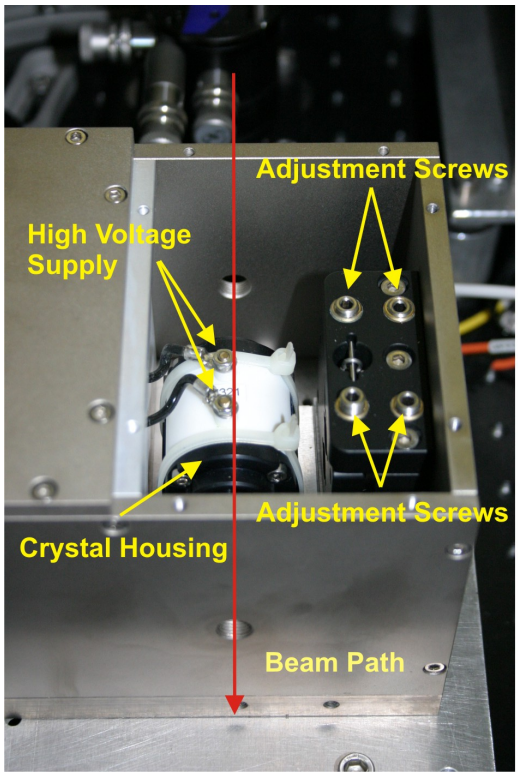

Figure A.7.: *A Pockels Cell mounted inside a driver box. The crystal can be tilted with four adjustment screws. The figure is adapted from [Zot09].*

In Figure A.7, we show a Pockels cell mounted inside a driver box.

Operation of the Pockels Cell driver

The electronics system used to drive the Pockels cell is manufactured by the company *Bergmann Messgeräte* and consists of a high voltage supply, a pulse generator (splitter box) and a driver box. The driver box is a double-push-pull switch with a maximal repetition rate of 5 MHz. This double-push-pull-switch drivers offer the advantage over single push-pull switch drivers that there is no recharge time restriction on the "on and off" states since each circuit only has to switch once in order to get an effective on-off cycle [BPJ+07], as explained in Section 4.1 of the main text. A splitter box (pulse generator) produces the pulse sequence for the double-push-pull switches driver from a trigger signal.

The splitter box (see figure A.8) uses a TTL signal as input and generates four output pulses (*A-On, B-On, A-Off, B-Off*) operating in a double push pull switch scheme.

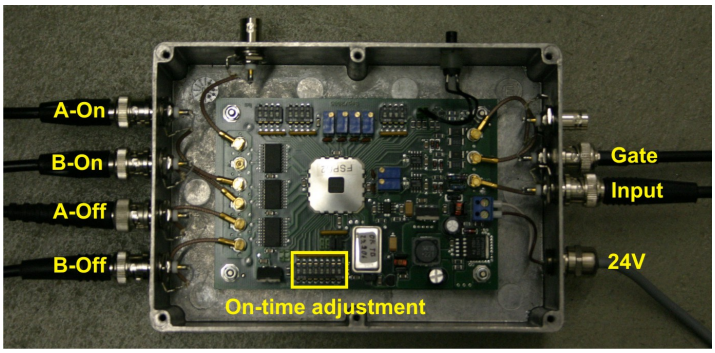

Figure A.8.: *A picture of the splitter box. The input signal is used to generate four output pulses (A-On, B-On, A-Off, B-Off). The four output connectors on the left side control the Pockels cell. The on-time of the Pockels cell can be adjusted by several switches inside the "splitter box". The figure is adapted from [Zot09].*

These four TTL signals and the high voltage supply are plugged into the driver box. The on-time of the Pockels Cell can be set inside the splitter box (see figure A.8). The rise time of our Pockels Cells was measured by observing the switching on an oscilloscope. We used the 10% and 90% levels of the rising and falling edges of the signal to calculate the rise and fall time and they are

about 5.6 ns and 5.8 ns respectively for a π phase shift.

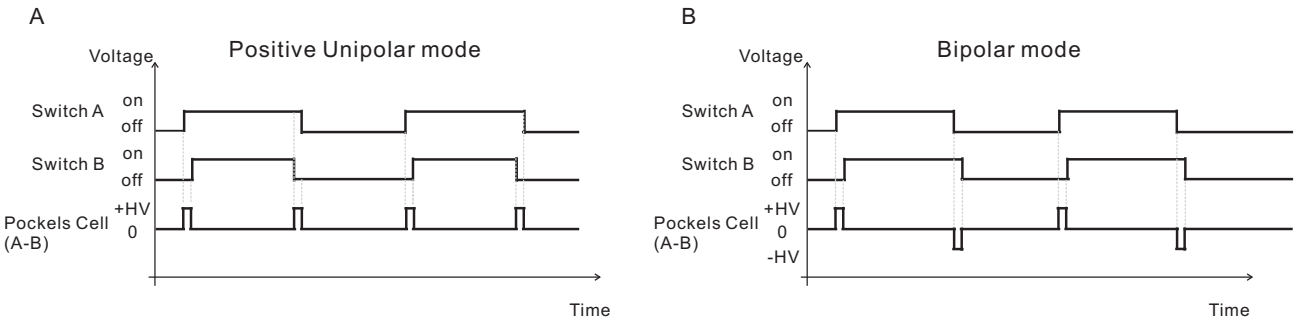

Figure A.9.: *Different operation modes of the Pockels Cells. Positive unipolar mode is shown in* ***A*** *and has been used in the experiments of the non-local quantum eraser in Vienna and two-photon interference under Einstein locality conditions. A-on and B-on signals switch on, with a positive high voltage (+HV), and off the Pockels cell. So do B-off and A-off signals. Bipolar mode is shown in* ***B*** *and has been used in the non-local quantum eraser in the Canary Islands and the delayed-choice entanglement-swapping experiments. A-on and B-on signals switch on, with a positive high voltage (+HV), and off the Pockels cell. A-off and B-off signals switch on, with a negative high voltage (-HV), and off the Pockels cell. (The figure is taken from Fast Splitter Manual BME FSP01, Bergmann Messgeraete, http://www.bme-bergmann.de)*

The different operation modes of the push pull switch can be seen in Figure A.9. The positive unipolar mode is shown in **A** and has been used in the experiments of the non-local quantum eraser in Vienna and two-photon interference under Einstein locality conditions. A-on and B-on signals switch on, with a positive high voltage (+HV), and off the Pockels cell. So do B-off and A-off signals. The bipolar mode is shown in **B** and has been used in the non-local quantum eraser in the Canary Islands and the delayed-choice entanglement-swapping experiments. In this mode, A-on and B-on signals switch on, with a positive high voltage (+HV), and off the Pockels cell. Different from the positive unipolar mode, in this bipolar mode, A-off and B-off signals switch on, with a negative high voltage (-HV), and off the Pockels cell.

Bibliography

[ADR82] Alain Aspect, Jean Dalibard, and Gérard Roger. Experimental test of bell's inequalities using time- varying analyzers. *Phys. Rev. Lett.*, 49(25):1804–1807, Dec 1982. 10

[ANVA+99] Markus Arndt, Olaf Nairz, Julian Vos-Andreae, Claudia Keller, Gerbrand van der Zouw, and Anton Zeilinger. Wave-particle duality of c60 molecules. *Nature*, 401(6754):680–682, October 1999. 8

[AZ05] Yakir Aharonov and M. Suhail Zubairy. Time and the Quantum: Erasing the Past and Impacting the Future. *Science*, 307(5711):875–879, 2005. i, 31

[BAZ05] Časlav Brukner, Markus Aspelmeyer, and Anton Zeilinger. Complementarity and information in "delayed-choice for entanglement swapping". *Foundations of Physics*, 35(11):1909–1919, 2005. 41, 77

[BBC+93] Charles H. Bennett, Gilles Brassard, Claude Crépeau, Richard Jozsa, Asher Peres, and William K. Wootters. Teleporting an unknown quantum state via dual classical and einstein-podolsky-rosen channels. *Phys. Rev. Lett.*, 70(13):1895–1899, Mar 1993. 12, 77

[BBDM+98] D. Boschi, S. Branca, F. De Martini, L. Hardy, and S. Popescu. Experimental realization of teleporting an unknown pure quan-

tum state via dual classical and einstein-podolsky-rosen channels. *Phys. Rev. Lett.*, 80(6):1121–1125, Feb 1998. 46, 113

[BCS+04] M. D. Barrett, J. Chiaverini, T. Schaetz, J. Britton, W. M. Itano, J. D. Jost, E. Knill, C. Langer, D. Leibfried, R. Ozeri, and D. J. Wineland. Deterministic quantum teleportation of atomic qubits. *Nature*, 429(6993):737–739, June 2004. 95, 113

[BDCZ98] H.-J. Briegel, W. Dür, J. I. Cirac, and P. Zoller. Quantum repeaters: The role of imperfect local operations in quantum communication. *Phys. Rev. Lett.*, 81(26):5932–5935, Dec 1998. 95

[Bel64] J. S. Bell. On the Einstein-Podolsky-Rosen paradox. *Physics*, 1:195, 1964. 8, 61

[BLPK05] Julio T. Barreiro, Nathan K. Langford, Nicholas A. Peters, and Paul G. Kwiat. Generation of hyperentangled photon pairs. *Physical Review Letters*, 95(26):260501, 2005. 45

[BMM89] J. Baldzuhn, E. Mohler, and W. Martienssen. A wave-particle delayed-choice experiment with a single-photon state. *Zeitschrift fuer Physik B Condensed Matter*, 77(2):347–352, June 1989. 24, 25, 26

[Boh28] N. Bohr. The quantum postulate and the recent development of atomic theory. *Naturwissenschaften*, 16:245, 1928. 17

[Boh35] N. Bohr. Can quantum-mechanical description of physical reality be considered complete? *Phys. Rev.*, 48(8):696–702, Oct 1935. 8

[BPJ+07] P. Böhi, R. Prevedel, T. Jennewein, A. Stefanov, F. Tiefenbacher, and A. Zeilinger. Implementation and characterization of active feed-forward for deterministic linear optics quantum computing.

Applied Physics B: Lasers and Optics, 89(4):499–505, 2007. 80, 124, 125

[BPM+97] Dik Bouwmeester, Jian-Wei Pan, Klaus Mattle, Manfred Eibl, Harald Weinfurter, and Anton Zeilinger. Experimental quantum teleportation. *Nature*, 390(6660):575–579, 1997. 77, 113

[BPS+03] Časlav Brukner, Jian-Wei Pan, Christoph Simon, Gregor Weihs, and Anton Zeilinger. Probabilistic instantaneous quantum computation. *Phys. Rev. A*, 67(3):034304, Mar 2003. 114

[BWK08] Julio T. Barreiro, Tzu-Chieh Wei, and Paul G. Kwiat. Beating the channel capacity limit for linear photonic superdense coding. *Nat Phys*, 4(4):282–286, 2008. 46

[BZKW03] C. Braig, P. Zarda, C. Kurtsiefer, and H. Weinfurter. Experimental demonstration of complementarity with single photons. *Applied Physics B: Lasers and Optics*, 76(2):113–116, 2003. 7

[CCY+08] Yu-Ao Chen, Shuai Chen, Zhen-Sheng Yuan, Bo Zhao, Chih-Sung Chuu, Jorg Schmiedmayer, and Jian-Wei Pan. Memory-built-in quantum teleportation with photonic and atomic qubits. *Nat Phys*, 4(2):103–107, February 2008. 113

[CHSH69] John F. Clauser, Michael A. Horne, Abner Shimony, and Richard A. Holt. Proposed experiment to test local hidden-variable theories. *Phys. Rev. Lett.*, 23(15):880–884, Oct 1969. 8

[CKW00] Valerie Coffman, Joydip Kundu, and William K. Wootters. Distributed entanglement. *Phys. Rev. A*, 61(5):052306, Apr 2000. 39, 96

[Cla74] John F. Clauser. Experimental distinction between the quantum and classical field-theoretic predictions for the photoelectric effect. *Phys. Rev. D*, 9(4):853–860, Feb 1974. 7

[CLZ+07] Kai Chen, Che-Ming Li, Qiang Zhang, Yu-Ao Chen, Alexander Goebel, Shuai Chen, Alois Mair, and Jian-Wei Pan. Experimental realization of one-way quantum computing with two-photon four-qubit cluster states. *Physical Review Letters*, 99(12):120503, 2007. 46

[DGN90] V.G. Dmitriev, G.G. Gurzadyan, and D.N. Nikogosyan. *Handbook of Nonlinear Optical Crystals*. Springer, 1990. 116

[DLCZ01] L. M. Duan, M. D. Lukin, J. I. Cirac, and P. Zoller. Long-distance quantum communication with atomic ensembles and linear optics. *Nature*, 414(6862):413–418, 2001. 55, 95

[Dop98] Birgit Dopfer. *Zwei Experimente zur Interferenz von Zwei-Photonen Zustaenden Ein Heisenbergmikroskop und Pendelloesung*. PhD thesis, University of Innsbruck, 1998. 29, 54

[Eng96] Berthold-Georg Englert. Fringe visibility and which-way information: An inequality. *Phys. Rev. Lett.*, 77(11):2154–2157, Sep 1996. 63, 64

[EPR35] A. Einstein, B. Podolsky, and N. Rosen. Can quantum-mechanical description of physical reality be considered complete? *Phys. Rev.*, 47(10):777–780, May 1935. 8, 39, 44

[FC72] Stuart J. Freedman and John F. Clauser. Experimental test of local hidden-variable theories. *Phys. Rev. Lett.*, 28(14):938–941, Apr 1972. 10

[FHP+07] Alessandro Fedrizzi, Thomas Herbst, Andreas Poppe, Thomas Jennewein, and Anton Zeilinger. A wavelength-tunable fiber-coupled source of narrowband entangled photons. *Optics Express*, 15(23):15377–15386, 2007. 69

[FLS63] R. P. Feynman, R. B. Leighton, and M. L. Sands. *Lectures on Physics*. Addison Wesley, 1963. i

[Fra89] J. D. Franson. Bell inequality for position and time. *Phys. Rev. Lett.*, 62(19):2205–2208, May 1989. 10

[FUH+09] Alessandro Fedrizzi, Rupert Ursin, Thomas Herbst, Matteo Nespoli, Robert Prevedel, Thomas Scheidl, Felix Tiefenbacher, Thomas Jennewein, and Anton Zeilinger. High-fidelity transmission of entanglement over a high-loss free-space channel. *Nat Phys*, 5(6):389–392, June 2009. 39, 95

[GHB+02] O. Gühne, P. Hyllus, D. Bruß, A. Ekert, M. Lewenstein, C. Macchiavello, and A. Sanpera. Detection of entanglement with few local measurements. *Phys. Rev. A*, 66(6):062305, Dec 2002. 104

[GRA86] P. Grangier, G. Roger, and A. Aspect. Experimental evidence for a photon anticorrelation effect on a beam splitter: a new light on single-photon interferences. *Europhysics Letters*, 1:173, February 1986. 7

[GRTZ02] Nicolas Gisin, Grégoire Ribordy, Wolfgang Tittel, and Hugo Zbinden. Quantum cryptography. *Rev. Mod. Phys.*, 74(1):145–195, Mar 2002. 10

[GY88] Daniel M. Greenberger and Allaine Yasin. Simultaneous wave and particle knowledge in a neutron interferometer. *Physics Letters A*, 128(8):391 – 394, 1988. 63, 64

[HBG+07] Matthaus Halder, Alexios Beveratos, Nicolas Gisin, Valerio Scarani, Christoph Simon, and Hugo Zbinden. Entangling independent photons by time measurement. *Nat Phys*, 3(10):692–695, October 2007. 95

[Hei27] W. Heisenberg. Über den anschaulichen inhalt der quantentheoretischen kinematik und mechanik. *Zeitschrift für Physik*, 43:172, 1927. 30

[HKWZ95] Thomas J. Herzog, Paul G. Kwiat, Harald Weinfurter, and Anton Zeilinger. Complementarity and the quantum eraser. *Phys. Rev. Lett.*, 75(17):3034–3037, Oct 1995. 36

[HLB+03] Yuji Hasegawa, Rudolf Loidl, Gerald Badurek, Matthias Baron, and Helmut Rauch. Violation of a bell-like inequality in single-neutron interferometry. *Nature*, 425(6953):45–48, September 2003. 46

[HOM87] C. K. Hong, Z. Y. Ou, and L. Mandel. Measurement of subpicosecond time intervals between two photons by interference. *Phys. Rev. Lett.*, 59(18):2044–2046, Nov 1987. 88

[HSZ89] Michael A. Horne, Abner Shimony, and Anton Zeilinger. Two-particle interferometry. *Phys. Rev. Lett.*, 62(19):2209–2212, May 1989. 10

[HWZS87] T. Hellmuth, H. Walther, A. Zajonc, and W. Schleich. Delayed-choice experiments in quantum interference. *Physical Review A*, 35(6):2532–2541, Mar 1987. 21, 22, 23

[HZ85] M. A. Horne and A. Zeilinger. A bell-type experiment using linear momenta. In P.Lahti Joensuu and P.Mittelstedt, editors, *Proceedings of the Symposium on the Foundations of Modern Physics*, volume 435, page 9. World Scientific Publ. (Singapore), 1985. 10

[JABZ05] T. Jennewein, M. Aspelmeyer, Č. Brukner, and A. Zeilinger. Experimental proposal of switched "delayed-choice" for entanglement swapping. *International Journal of Quantum Information*, 3:1, 2005. 77

[JAW+00] T. Jennewein, U. Achleitner, G. Weihs, H. Weinfurter, and A. Zeilinger. A fast and compact quantum random number generator. *Rev. Sci. Instrum.*, 71:1675, 2000. 61

[Jen02] Thomas Daniel Jennewein. *Quantum Communication and Teleportation Experiments using Entangled Photon Pairs*. PhD thesis, University of Vienna, 2002. 114

[JUAZ09] Thomas Jennewein, Rupert Ursin, Markus Aspelmeyer, and Anton Zeilinger. Performing high-quality multi-photon experiments with parametric down-conversion. *Journal of Physics B: Atomic, Molecular and Optical Physics*, 42(11):114008, 2009. 106

[JWG+07] Vincent Jacques, E Wu, Frederic Grosshans, Francois Treussart, Philippe Grangier, Alain Aspect, and Jean-Francois Roch. Experimental Realization of Wheeler's Delayed-Choice Gedanken Experiment. *Science*, 315(5814):966–968, 2007. 27, 28, 86

[JWG+08] Vincent Jacques, E Wu, Frédéric Grosshans, François Treussart, Philippe Grangier, Alain Aspect, and Jean-François Roch. Delayed-choice test of quantum complementarity with interfering single photons. *Physical Review Letters*, 100(22):220402, 2008. 27, 64, 86

[JWPZ02] Thomas Jennewein, Gregor Weihs, Jian-Wei Pan, and Anton Zeilinger. Experimental nonlocality proof of quantum teleportation and entanglement swapping. *Physical Review Letters*, 88(1):017903, 2002. 10, 16, 39, 41, 42, 78, 95

[Kal03] Rainer Kaltenbaek. Active switching in long distance quantum state teleportation. Master's thesis, University of Vienna, 2003. 122

[Kal08] R. Kaltenbaek. *Entanglement Swapping and Quantum Interference with Independent Sources*. PhD thesis, University of Vienna, 2008. 88, 106

[KMN+07] Pieter Kok, W. J. Munro, Kae Nemoto, T. C. Ralph, Jonathan P. Dowling, and G. J. Milburn. Linear optical quantum computing with photonic qubits. *Reviews of Modern Physics*, 79(1):135, 2007. 113

[KMW+95] Paul G. Kwiat, Klaus Mattle, Harald Weinfurter, Anton Zeilinger, Alexander V. Sergienko, and Yanhua Shih. New high-intensity source of polarization-entangled photon pairs. *Phys. Rev. Lett.*, 75(24):4337–4341, Dec 1995. 46, 47, 56, 99, 119

[KOW01] Christian Kurtsiefer, Markus Oberparleiter, and Harald Weinfurter. High-efficiency entangled photon pair collection in type-ii parametric fluorescence. *Phys. Rev. A*, 64(2):023802, Jul 2001. 48, 57

[KPAZ09] Rainer Kaltenbaek, Robert Prevedel, Markus Aspelmeyer, and Anton Zeilinger. High-fidelity entanglement swapping with fully independent sources. *Physical Review A (Atomic, Molecular, and Optical Physics)*, 79(4):040302, 2009. 95

[KYK+00] Yoon-Ho Kim, Rong Yu, Sergei P. Kulik, Yanhua Shih, and Marlan O. Scully. Delayed choice quantum eraser. *Phys. Rev. Lett.*, 84(1):1–5, Jan 2000. 36, 37, 38, 61, 73

[Man83] L. Mandel. Photon interference and correlation effects produced

by independent quantum sources. *Phys. Rev. A*, 28:929–943, 1983. ii

[Man99] L. Mandel. Quantum effects in one-photon and two-photon interference. *Rev. Mod. Phys.*, 71(2):S274–S282, Mar 1999. ii

[Mat97] Klaus Mattle. *Nichtklassische Lichtzustaende Zur Optischen Nachrichten uebertragung.* PhD thesis, Universitaet Innsbruck, 1997. 119

[MBC02] A. L. Migdall, D. Branning, and S. Castelletto. Tailoring single-photon and multiphoton probabilities of a single-photon on-demand source. *Phys. Rev. A*, 66(5):053805, Nov 2002. 77, 113

[MdRT+03] I. Marcikic, H. de Riedmatten, W. Tittel, H. Zbinden, and N. Gisin. Long-distance teleportation of qubits at telecommunication wavelengths. *Nature*, 421(6922):509–513, January 2003. 113

[MLS+08] Peter J. Mosley, Jeff S. Lundeen, Brian J. Smith, Piotr Wasylczyk, Alfred B. U'Ren, Christine Silberhorn, and Ian A. Walmsley. Heralded generation of ultrafast single photons in pure quantum states. *Physical Review Letters*, 100(13):133601, 2008. 106

[MMM+08] D. N. Matsukevich, P. Maunz, D. L. Moehring, S. Olmschenk, and C. Monroe. Bell inequality violation with two remote atomic qubits. *Physical Review Letters*, 100(15):150404, 2008. 95

[MQK+09] Xiaosong Ma, Angie Qarry, Johannes Kofler, Thomas Jennewein, and Anton Zeilinger. Experimental violation of a bell inequality with two different degrees of freedom of entangled particle pairs. *Physical Review A (Atomic, Molecular, and Optical Physics)*, 79(4):042101, 2009. 56, 58

[MWidZ00] Markus Michler, Harald Weinfurter, and Marek Żukowski. Experiments towards falsification of noncontextual hidden variable theories. *Phys. Rev. Lett.*, 84(24):5457–5461, Jun 2000. 46

[NC00] M. A. Nielsen and I. L. Chuang. *Quantum Computation and Quantum Information*. Cambridge University Press, Cambridge, 2000. 1

[OMM+09] S. Olmschenk, D. N. Matsukevich, P. Maunz, D. Hayes, L.-M. Duan, and C. Monroe. Quantum teleportation between distant matter qubits. *Science*, 323(5913):486–489, 2009. 113

[PBWZ98] Jian-Wei Pan, Dik Bouwmeester, Harald Weinfurter, and Anton Zeilinger. Experimental entanglement swapping: Entangling photons that never interacted. *Phys. Rev. Lett.*, 80(18):3891–3894, May 1998. 78, 95

[Per00] Asher Peres. Delayed choice for entanglement swapping. *Journal of Modern Optics*, 47(2):139–143, 2000. i, ii, 17, 39, 77, 95

[PWT+07] Robert Prevedel, Philip Walther, Felix Tiefenbacher, Pascal Bohi, Rainer Kaltenbaek, Thomas Jennewein, and Anton Zeilinger. High-speed linear optics quantum computing using active feed-forward. *Nature*, 445(7123):65–69, 2007. 78

[RBH01] J. M. Raimond, M. Brune, and S. Haroche. Manipulating quantum entanglement with atoms and photons in a cavity. *Rev. Mod. Phys.*, 73(3):565–582, Aug 2001. 46

[RHR+04] M. Riebe, H. Haffner, C. F. Roos, W. Hansel, J. Benhelm, G. P. T. Lancaster, T. W. Korber, C. Becher, F. Schmidt-Kaler, D. F. V. James, and R. Blatt. Deterministic quantum teleportation with atoms. *Nature*, 429(6993):734–737, June 2004. 95, 113

[RT90] J. G. Rarity and P. R. Tapster. Experimental violation of bell's inequality based on phase and momentum. *Phys. Rev. Lett.*, 64(21):2495–2498, May 1990. 10

[Sch35] E. Schroedinger. Die gegenwärtige situation in der quantenmechanik. *Naturwissenschaften*, 23:844, 1935. 8, 39

[Sch09] Thomas Scheidl. *A fundamental test and an application of quantum entanglement*. PhD thesis, University of Vienna, 2009. 61

[SD82] Marlan O. Scully and Kai Drühl. Quantum eraser: A proposed photon correlation experiment concerning observation and "delayed choice" in quantum mechanics. *Phys. Rev. A*, 25(4):2208–2213, Apr 1982. i, 17, 31, 33, 43

[SEW91] Marian O. Scully, Berthold-Georg Englert, and Herbert Walther. Quantum optical tests of complementarity. *Nature*, 351(6322):111–116, May 1991. i, 5, 31, 34, 37, 43

[SI03] Christoph Simon and William T. M. Irvine. Robust long-distance entanglement and a loophole-free bell test with ions and photons. *Phys. Rev. Lett.*, 91(11):110405, Sep 2003. 95

[SKO+06] Jacob F. Sherson, Hanna Krauter, Rasmus K. Olsson, Brian Julsgaard, Klemens Hammerer, Ignacio Cirac, and Eugene S. Polzik. Quantum teleportation between light and matter. *Nature*, 443(7111):557–560, October 2006. 113

[SPS+96] D. V. Strekalov, T. B. Pittman, A. V. Sergienko, Y. H. Shih, and P. G. Kwiat. Postselection-free energy-time entanglement. *Phys. Rev. A*, 54(1):R1–R4, Jul 1996. 46

[ST91] B. E. A. Saleh and M. C. Teich. *Fundamentals of Photonics*. John Wiley & Sons, Inc., 1991. 119, 120

[SW07] Jeffrey H. Shapiro and Franco N. Wong. On-demand single-photon generation using a modular array of parametric down-converters with electro-optic polarization controls. *Opt. Lett.*, 32(18):2698–2700, 2007. 77, 113

[Tan99] S. M. Tan. A computational toolbox for quantum and atomic optics. *Journal of Optics B: Quantum and Semiclassical Optics*, 1(4):424, 1999. 106

[UJA+04] Rupert Ursin, Thomas Jennewein, Markus Aspelmeyer, Rainer Kaltenbaek, Michael Lindenthal, Philip Walther, and Anton Zeilinger. Quantum teleportation across the danube. *Nature*, 430(7002):849–849, 2004. 113

[UTSM+07] R. Ursin, F. Tiefenbacher, T. Schmitt-Manderbach, H. Weier, T. Scheidl, M. Lindenthal, B. Blauensteiner, T. Jennewein, J. Perdigues, P. Trojek, B. Ömer, M. Fürst, M. Meyenburg, J. Rarity, Z. Sodnik, C. Barbieri, H. Weinfurter, and A. Zeilinger. Entanglement-based quantum communication over 144 km. *Nature Physics*, 3(7):481–486, 2007. 39, 95

[VPM+07] Giuseppe Vallone, Enrico Pomarico, Paolo Mataloni, Francesco De Martini, and Vincenzo Berardi. Realization and characterization of a two-photon four-qubit linear cluster state. *Physical Review Letters*, 98(18):180502, 2007. 46

[Wei31] K. F. v. Weizsäcker. Ortsbestimmung eines elektrons durch ein mikroskop. *Zeitschrift für Physik A Hadrons and Nuclei*, 70(1):114–130, 1931. 30

[Wei41] C. F. v. Weizsäcker. Zur deutung der quantenmechanik. *Zeitschrift für Physik A Hadrons and Nuclei*, 118(9):489, 1941. 30

[Wei99] Gregor Weihs. *Ein Experiment Zum Test der Bellschen Ungleichung unter Einsteinscher Lokalitaet.* PhD thesis, Universitaet Wien, 1999. 61, 116, 117

[Wer89] Reinhard F. Werner. Quantum states with einstein-podolsky-rosen correlations admitting a hidden-variable model. *Phys. Rev. A*, 40(8):4277–4281, Oct 1989. 10

[Whe84] J. A. Wheeler. In J. A. Wheeler and W. H. Zurek, editors, *Quantum Theory and Measurement*. Princeton University Press, 1984. i, ii, 17, 18, 19, 20, 39, 95

[WJS+98] Gregor Weihs, Thomas Jennewein, Christoph Simon, Harald Weinfurter, and Anton Zeilinger. Violation of bell's inequality under strict einstein locality conditions. *Phys. Rev. Lett.*, 81(23):5039–5043, Dec 1998. 10, 64

[WTCPM02] S. P. Walborn, M. O. Terra Cunha, S. Pádua, and C. H. Monken. Double-slit quantum eraser. *Phys. Rev. A*, 65(3):033818, Feb 2002. 36

[WZ82] W. K. Wootters and W. H. Zurek. A single quantum cannot be cloned. *Nature*, 299(5886):802–803, October 1982. 11

[YCZ+08] Zhen-Sheng Yuan, Yu-Ao Chen, Bo Zhao, Shuai Chen, Jorg Schmiedmayer, and Jian-Wei Pan. Experimental demonstration of a bdcz quantum repeater node. *Nature*, 454(7208):1098–1101, August 2008. 95

[Zei81] A. Zeilinger. General properties of lossless beam splitters in interferometry. *American Journal of Physics*, 49(9):882–883, 1981. 5

[Zei99] Anton Zeilinger. Experiment and the foundations of quantum physics. *Rev. Mod. Phys.*, 71(2):S288–S297, Mar 1999. 7, 36, 54

[ZGS+88] Anton Zeilinger, Roland Gähler, C. G. Shull, Wolfgang Treimer, and Walter Mampe. Single- and double-slit diffraction of neutrons. *Rev. Mod. Phys.*, 60(4):1067–1073, Oct 1988. 7

[ZGW+06] Qiang Zhang, Alexander Goebel, Claudia Wagenknecht, Yu-Ao Chen, Bo Zhao, Tao Yang, Alois Mair, Jorg Schmiedmayer, and Jian-Wei Pan. Experimental quantum teleportation of a two-qubit composite system. *Nat Phys*, 2(10):678–682, October 2006. 11

[Zot09] Stefan Zotter. Entangled photon experiments with a fast interferometric switchable beam splitter. Master's thesis, Universitaet Wien, 2009. 121, 124, 125

[ZP88] Marek Zukowski and Jaroslaw Pykacz. Bell's theorem: Proposition of realizable experiment using linear momenta. *Physics Letters A*, 127(1):1 – 4, 1988. 10, 46

[ZWJA05] Anton Zeilinger, Gregor Weihs, Thomas Jennewein, and Markus Aspelmeyer. Happy centenary, photon. *Nature*, 433(7023):230–238, 2005. 36

[ZZ91] Marek Zukowski and Anton Zeilinger. Test of the bell inequality based on phase and linear momentum as well as spin. *Physics Letters A*, 155(2-3):69 – 72, 1991. 45

[ZZHE93] M. Zukowski, A. Zeilinger, M. A. Horne, and A. K. Ekert. Event-ready-detectors bell experiment via entanglement swapping. *Phys. Rev. Lett.*, 71(26):4287–4290, Dec 1993. 14, 39, 78, 95

[ZZZ+05] Zhi Zhao, An-Ning Zhang, Xiao-Qi Zhou, Yu-Ao Chen, Chao-Yang Lu, Anders Karlsson, and Jian-Wei Pan. Experimental realization of optimal asymmetric cloning and telecloning via partial teleportation. *Physical Review Letters*, 95(3):030502, 2005. 78

B. Acknowledgments

During my PhD study I was very lucky to work with a number of gifted people. Without them this thesis would not have been possible. Let me take this opportunity to thank them for their continuing support and assistance.

First of all, I would like to thank Prof. Anton Zeilinger for supervising and supporting me over many years. It has been a privilege for me to study and work in his group. His guidance enabled and facilitated many of the experiments in this thesis. Although everyday work can be stressful at times, the reward of work in the highly interesting and fascinating field is more than enough to compensate this.

I would like to thank Thomas Jennewein for supervising and helping me with so many problems in the lab. His priceless ideas and tremendous inputs helped me to finish the experiments.

I have to express my gratitude to my lab mate Stefan Zotter and William Naylor during the delayed-choice entanglement-swapping experiment, and Angie Qarry and Nuray Tetik during the non-local quantum eraser experiment. They have been very supportive to me and provided a nice working climate. Many of the experiments reported in this thesis have been performed in close cooperation with theoreticians. I would like to thank all of them and especially Johannes Kofler, who is always very careful when revising papers and patient with the my questions.

I also want to thank the senior scientists of our group: Rupert Ursin, Markus Aspelmeyer, Philip Walther, Caslav Brukner and Nathan Langford for their help, advices and many encouraging discussions.

My fellow PhD colleagues shall also be thanked: Thomas Scheidl and Thomas Herbst for the Canary Islands experiment and the fun we had there, Sven Ramelow, for all those stimulating discussions and fancy optical mounts, Robert Prevedel, for his willingness to help and lend stuff, Alessandro Fedrizzi, for sharing his insights on the Sagnac source and Simon Gröblacher, for his help in electronics. I want to thank Stefanie Barz, Borivoje Dakic, Radoslaw Lapkiewicz, Alexandra Mech, Christoph Schäff, Alexander Treiber, Bernhard Wittmann, Peizhe Li and Fabian-Oliver Steinlechner for all the funny and/or stimulating discussions during coffee and lunch breaks. I would like to thank the whole quantum team and molecule team for the amazing atmosphere.

I thank William Naylor, Thomas Jennewein, Johannes Kofler, Richard Healey and Stefan Zotter for commenting on my thesis and helping me to improve it.

But most of all I am grateful to my family. My parents, Shaohua and Xiaobin, for their invaluable support and encouragement.

Finally, a special thank you goes to my girlfriend Zhihui for her love, understanding, patience and her never ending support.

C. Curriculum Vitae

Personal Data

Name: Xiaosong Ma

Born: 25.12.1980 Sichuan, China

Parents: Shaohua Ma and Xiaobin Cao

Chronology

1987-1993: Primary School, Wuxi, China

1993-1999: Highschool, Wuxi, China

1999-2003: Undergraduate, Nanjing, China

09.2003-08.2005: Master, Leiden, the Netherlands

08.2005-10.2005: internships in Philips Research, Eindhoven, the Netherlands

11.2005-now: Ph. D in Experimental Physics and Researcher at the Institute for Quantum Optics and Quantum Information, Austrian Academy of Science